

HYDROGEN GENERATION FROM CONVENTIONAL FUELS OVER  
MESOPOROUS MIXED OXIDE CATALYSTS UNDER TIME  
INTERRUPTED REACTION CONDITIONS

A THESIS SUBMITTED TO  
THE GRADUATE SCHOOL OF NATURAL AND APPLIED SCIENCES  
OF  
MIDDLE EAST TECHNICAL UNIVERSITY

BY

MUKADDES CAN

IN PARTIAL FULFILLMENT OF THE REQUIREMENTS  
FOR  
THE DEGREE OF DOCTOR OF PHILOSOPHY  
IN  
CHEMICAL ENGINEERING

APRIL 2011

Approval of the Thesis

**“HYDROGEN GENERATION FROM CONVENTIONAL FUELS OVER  
MESOPOROUS MIXED OXIDE CATALYSTS UNDER TIME  
INTERRUPTED REACTION CONDITIONS”**

submitted by **MUKADDES CAN** in partial fulfillment of the requirements for the degree of **Doctor of Philosophy in Chemical Engineering Department, Middle East Technical University** by,

Prof. Dr. Canan Özgen  
Dean, Graduate School of **Natural and Applied Sciences** \_\_\_\_\_

Prof. Dr. Deniz Üner  
Head of Department, **Chemical Engineering** \_\_\_\_\_

Prof. Dr. Deniz Üner  
Supervisor, **Chemical Engineering Dept., METU** \_\_\_\_\_

Assoc. Prof. Dr. Ayşen Yılmaz  
Co-supervisor, **Chemistry Dept., METU** \_\_\_\_\_

**Examining Committee Members:**

Prof. Dr. Gülşen Doğu  
Chemical Engineering Dept., Gazi University \_\_\_\_\_

Prof. Dr. Deniz Üner  
Chemical Engineering Dept., METU \_\_\_\_\_

Prof. Dr. Hayrettin Yücel  
Chemical Engineering Dept., METU \_\_\_\_\_

Prof. Dr. Gürkan Karakaş  
Chemical Engineering Dept., METU \_\_\_\_\_

Assist. Prof. Dr. Görkem Külah  
Chemical Engineering Dept., METU \_\_\_\_\_

**Date** \_\_\_\_\_

**I hereby declare that all information in this document has been obtained and presented in accordance with academic rules and ethical conduct. I also declare that, as required by these rules and conduct, I have fully cited and referenced all material and results that are not original to this work.**

Name, Last name:

Signature:

# ABSTRACT

## HYDROGEN GENERATION OF CONVENTIONAL FUELS OVER MESOPOROUS MIXED OXIDE CATALYSTS UNDER TIME INTERRUPTED REACTION CONDITIONS

Can, Mukaddes

Ph.D., Department of Chemical Engineering

Supervisor : Prof. Dr. Deniz Üner

Co-supervisor : Assoc. Prof. Dr. Ayşen Yılmaz

April 2011, 125 pages

In this study, catalytic activity of the Co and/or Pb-SBA-15 mesoporous catalysts in methane partial oxidation reaction was investigated. By using sol-gel, incipient wetness impregnation and post grafting method, SBA-15 samples are incorporated with Co and/or Pb at different weight loadings to provide a controlled geometry in nanometer scale. The characterization of the synthesized samples was done by XRD, N<sub>2</sub> adsorption isotherms, FTIR, TEM images, Raman and XPS analysis. In the present study also, gas phase methane partial oxidation modeling and the synthesizing of mesoporous SBA-15 silica with different pore sizes were investigated.

For the samples prepared by sol-gel method, XRD analysis showed that cobalt exists in the form of Co<sub>3</sub>O<sub>4</sub> and Pb exist in the form of PbO. BET surface areas of the Co loaded catalysts are in the range of 479.5-640.1 m<sup>2</sup>/g. However, in Pb loaded samples, higher metal loading decrease the surface area up to 4.63 m<sup>2</sup>/g.

Considering the both Co and Pb containing bi-metallic samples, TEM and BET results revealed that the ordered hexagonal mesostructure was fully destroyed.

The samples prepared by incipient wetness impregnation and post grafting method characterized by using BET, TEM, Raman and XPS analysis. According to the BET results all the samples show ordered mesostructure in agreement with TEM results for all Co and/or SBA-15 mesoporous samples. TEM results also revealed that, the Co(5%) Pb(5%)-SBA-15 catalyst prepared by incipient wetness impregnation method possess big cobalt and lead oxide crystallines on the mesoporous structure. Raman analysis results indicated that cobalt exist in  $\text{Co}_3\text{O}_4$  form. According to XPS results all samples containing cobalt include  $\text{Co}_3\text{O}_4$ .

The partial oxidation of methane was carried out in a fixed bed flow-type reactor in a temperature range of 50–850°C under atmospheric pressure. According to the reaction test results, the 0.5%Rh-Co-SBA15 catalyst shows the highest methane conversion (82%) and  $\text{H}_2$  selectivity. The non-precious metal show lower reactivities, addition of Pb to the Co-SBA-15 catalyst increases the catalytic activity and decrease the  $\text{H}_2$  production temperature.

Keywords: Methane, Partial Oxidation, Cobalt, Lead, SBA-15

# ÖZ

## ZAMAN KESİKLİ REAKSİYON KOŞULLARINDA MEZOPOROZ OKSİT KATALİZÖRLERİ KULLANILARAK HİDROKARBONLARDAN HİDROJEN ÜRETİMİ

Can, Mukaddes

Doktora, Kimya Mühendisliği Bölümü

Tez Yöneticisi : Prof. Dr. Deniz Üner

Ortak Tez Yöneticisi : Doç. Dr. Ayşen Yılmaz

Nisan 2011, 125 sayfa

Bu çalışmada Co ve Pb içeren mezo gözenekli katalizörlerin metan kısmi oksidasyon reaksiyonundaki aktiviteleri incelenmiştir. Sol-gel, emdirmeli yükleme ve post grafting yöntemleri kullanılarak farklı yüzdelerde Co ve/veya Pb içeren mezo gözenekli SBA-15 katalizörleri sentezlenmiştir. Sentezlenen katalizörlerin karakterizasyonu XRD, BET, FTIR, TEM, Raman karakterizasyon metotları kullanılarak yapılmıştır. Bu çalışma kapsamında ayrıca gaz faz metan oksidasyonunun modellenmesi ve değişik gözenek boyutuna sahip mezo gözenekli malzemelerin sentezlenmesi çalışması da gerçekleştirilmiştir.

Sol-gel metodu ile hazırlanan örneklerin XRD analizi kobaltın  $Co_3O_4$  formunda kurşunun ise PbO formunda olduğunu göstermiştir. Kobalt yüklü örneklerin BET analizi örneklerin yüzey alanının 479,5-640,1  $m^2/g$  aralığında olduğunu göstermiştir. Ancak Pb yüklü örneklerde yüzey alanı yükleme miktarının artışı ile birlikte 4.63  $m^2/g$  değerine kadar düşmüştür. TEM ve BET sonuçlarına göre hem kobalt hem de kurşun içeren örneklerin düzenli yapısının tamamen kaybolduğu gözlenmiştir.

Islaklık başlangıcı ile emdirme ve post grafting yöntemi ile hazırlanan örneklerin karakterizasyonu ise BET, TEM, Raman ve XPS analiz yöntemleri kullanılarak yapılmıştır. Hem BET hem de TEM sonuçlarına göre tüm örnekler düzenli mezogözenek yapısına sahiptir. TEM sonuçları ayrıca göstermiştir ki, ıslaklık başlangıcı ile emdirme yöntemi ile hazırlanan Co(5%) Pb(5%)-SBA-15 örneğinde büyük kobalt ve kurşun oksit kristalleri oluşmuştur. Raman analiz sonuçları cobaltın  $Co_3O_4$  formunda olduğunu göstermiştir. XPS sonuçlarına göre tüm cobalt içeren örnekler  $Co_3O_4$  içermektedir.

Metan kısmı oksidasyonu reaksiyonu sabit yatak reaktöründe 50-850°C sıcaklık aralığında atmosferik basınç altında yapılmıştır. Reaksiyon testi sonuçlarına göre, 0.5%Rh-Co-SBA-15 katalizör örneğien yüksek katalitik aktivite (82%) ve en yüksek  $H_2$  seçiciliğini göstermiştir. Değerli metal içermeyen örnekler daha düşük katalitik aktivite göstermiştir. Ancak kobalt içeren örneklere kurşun eklenmesi ile katalitik aktivite artmış ve  $H_2$  üretim sıcaklığı daha düşük sıcaklıklara kaymıştır.

Anahtar kelimeler: Metan, Kısmi Oksidasyon, Kobalt, Kurşun, SBA-15.

*To my family*



## ACKNOWLEDGEMENTS

I would like to express my thanks to every person who has encouraged and supported me throughout the research. Firstly, I want to express my deep and sincere gratitude to my supervisor Prof. Dr. Deniz Üner for her supervision during my PhD study. She has guided me patiently, supported and encouraged me whenever I face difficulties through the study. One more person whom I want to thank is my co-advisor, Assoc. Prof. Dr. Ayşen Yılmaz for supervision, comments, criticism, encouragement during my PhD study. I am also very grateful to Ayşen Yılmaz's friendly attitude and enthusiasm. The members of the thesis supervision committee, Prof. Dr. Gülşen Doğu and Assist. Prof. Dr. Görkem Kùlah are gratefully acknowledged for their positive attitude and constructive comments.

Selçuk University is gratefully acknowledged for providing opportunity to the author to conduct PhD in METU by OYP program. The author is thankful for financial support by METU Research Fund Projects (BAP-08-11-DPT.2002K120510).

I also want to express my gratitude to Gülten Orakçı, from Chemical Engineering Department for their technical support in BET measurements.

I also would like to thank Burcu Akça for her contributions and support during my research. I'm also grateful to Semih Seyyidođlu, Mustafa Fatih Genişel from METU Chemistry Department and Selda Keskin from METU Central Laboratory for their technical assistance.

The author is thankful to Prof. Dr. Hans J. Kleebe from Technical University of Darmstadt for providing the TEM images of the catalysts.

I would like thank to Prof. Dr. Christian Hess for providing me research opportunities in his laboratory in Technical University of Darmstadt (Germany). I am also thankful to Sandra Sanze, Jörg Thielemann for their friendly attitudes.

I would also like to express my appreciation to whole ‘‘Cactus Research Group’’ (Hilal Demir Kıvrak, Hale Ay, Arzu Kanca, Orçun Ergün, Mert Mehmet Oymak, Başar Çağlar, Bahar İpek, Volkan Değirmenci, Ebru Erünel, Özge Güner, Hakan Ö. Olcay, Özlem Özcan, Volkan E. Genç, Bora Atalık, Atalay Çalışan, Güvenç Oğulğönen, Mustafa Yasin Aslan, İbrahim Bayar, and other members) and others whom I forgot to mention.

# TABLE OF CONTENTS

ABSTRACT .....	IV
ÖZ.....	VI
ACKNOWLEDGEMENTS .....	IX
TABLE OF CONTENTS .....	XI
LIST OF TABLES .....	XIV
LIST OF FIGURES .....	XV
CHAPTERS	
1. INTRODUCTION AND SCOPE.....	1
1.1 METHANE PARTIAL OXIDATION.....	1
1.2 MESOPOROUS MATERIALS AS SUPPORT .....	2
1.3 SCOPE OF THESIS .....	4
2. SBA-15 (SANTA BARBARA NO:15).....	6
2.1 INTRODUCTION .....	6
2.2 SYNTHESIS MECHANISM OF SBA-15.....	8
2.3 SURFACE CHEMISTRY OF MESOPOROUS SILICA.....	10
3. METHANE PARTIAL OXIDATION OVER METAL OXIDES.....	12
3.1 METHANE PARTIAL OXIDATION.....	12
3.2 PARTIAL OXIDATION OVER METAL OXIDES .....	17
3.3 SOLID OXIDE FUEL CELLS USING Co and Pb OXIDES.....	21
4. MODELING HOMOGENEOUS PARTIAL OXIDATION .....	26
4.1 INTRODUCTION.....	26
4.2 RESULTS AND DISCUSSION .....	27
4.2.1 The Effect of Temperature .....	27

4.2.2 Effect of residence time.....	29
4.2.2 Effect of pressure.....	29
4.2.4 Effect of initial O <sub>2</sub> /CH <sub>4</sub> ratio .....	30
5. SYNTHESIS OF CO AND/ORPB-SBA-15 CATALYSTS: DIRECT SYNTHESIS METHOD .....	32
5.1 EXPERIMENTAL .....	32
5.1.1 Synthesis of Mesoporous Co and/or Pb SBA-15 Materials by using direct synthesis method .....	32
5.2 CATALYST CHARACTERIZATION.....	33
5.3 RESULTS AND DISCUSSION.....	33
5.3.1 N <sub>2</sub> ADSORPTION.....	33
5.3.2 X-Ray Diffraction (XRD) .....	35
6. SYNTHESIS OF CO AND/OR PB/SBA-15 MATERIALS: INCIPIENT WETNESS IMPREGNATION AND POST GRAFTING METHODS .....	39
6.1 INTRODUCTION.....	39
6.2 EXPERIMENTAL .....	40
6.2.1 Synthesis of Pure SBA-15 .....	40
6.2.2 Synthesis of Amino Functionalized SBA-15 via Post-Synthesis grafting Method.....	41
6.2.3 Synthesis of Co and/or Pb-SBA15 materials by incipient wetness impregnation method.....	41
6.3 CHARACTERIZATION OF THE CATALYSTS.....	42
6.4 RESULTS AND DISCUSSION.....	42
6.4.1 N <sub>2</sub> Adsorption.....	42
6.4.2 Transmission Electron Microscopy .....	45
6.4.3 X-Ray Photoelectron Spectroscopy.....	47
6.4.4 Raman Spectroscopy .....	52
7. SYNTHESIS OF SBA-15 WITH DIFFERENT PORE SIZES .....	57
7.1 INTRODUCTION.....	57
7.2 EXPERIMENTAL .....	58

7.1.1 Synthesis of SBA-15 materials.....	58
7.1.2 Synthesis of 1%Pt-SBA15 material by using incipient wetness impregnation method.....	59
7.3 CATALYST CHARACTERIZATION.....	59
7.4 RESULTS AND DISCUSSION .....	60
7.4.1 N <sub>2</sub> ADSORPTION.....	60
7.4.2 X-Ray Diffraction (XRD) .....	62
7.4.3 FTIR Analysis .....	65
8. METHANE PARTIAL OXIDATION OVER MESOPOROUS CO AND/OR PB-SBA-15 CATALYSTS.....	67
8.1 INTRODUCTION.....	67
8.2 EXPERIMENTAL.....	67
8.2.1 Reaction Tests .....	67
8.2.2 Heat and Mass Transfer Limitations in Mesoporous Materials .....	69
8.2.3 Stop-Effect (Time Interrupted Reaction Conditions).....	70
8.3 RESULTS AND DISCUSSION.....	71
8.3.1 Reaction Tests.....	71
9. CONCLUSIONS .....	80
REFERENCES .....	83
APPENDICES	
CHEMKIN GRI 3.0 MECHANISM PARAMETERS.....	98
XPS AND RAMAN FIGURES .....	107
BET FIGURES .....	113
CURRICULUM VITAE .....	122

## LIST OF TABLES

Table 3.1 Literature Survey Results for Partial Oxidation .....	15
Table 3.2 Syngas Reactions [Rostrup-Nielsen et.al, 2000] .....	16
Table 3.3 Hydrocarbon selectivities over different PbO catalysts [Baerns and Ross, 1989] .....	19
Table 5.1 The mixed oxide catalyst compositions and surface areas .....	34
Table 6.1 The mixed oxide catalyst compositions and surface areas (Incipient Wetness Impregnation Method: Cobalt Chloride based) .....	43
Table 6.2 The mixed oxide catalyst compositions and surface areas (Functionalized SBA-15 samples) .....	44
Table 6.3 Co 2p binding energy values of different samples .....	48
Table 6.4 Co 2p binding energy values of Co-SBA-15 catalysts (Incipient Wetness Impregnation Method) .....	50
Table 6.5 Co 2p binding energy values of Co-SBA-15 catalysts (Post Grafting Method) .....	52
Table 7.1 Synthesis conditions and paramaters of SBA-15 materials .....	60

## LIST OF FIGURES

Figure 1.1 Structures of mesoporous M41S materials: a) MCM-41 (2Dhexagonal), b) MCM-48 (cubic),and c) MCM-50 (lamellar) [Hoffmann et al.,2006].....	3
Figure 2.1 Schematic Illustration of the formation of the triblock copolymer/mesostructured silica hybrid and mesoporous silica SBA-15[Xi and Tang, 2005]. .....	7
Figure 2.2 Surfactant-directed synthesis of mesoporous materials from inorganic, organic or hybrid building blocks [Lu, 2006]. .....	9
Figure 2.3 Representation of the silanol groups on the silica surfaces[Giraldo et al., 2007].....	11
Figure 4.1 Effect of temperature on H <sub>2</sub> yield .....	28
Figure 4.2 Effect of temperature on CO yield.....	28
Figure 4.3 Effect of the temperature on C <sub>2</sub> H <sub>2</sub> , C <sub>2</sub> H <sub>4</sub> , C <sub>2</sub> H <sub>6</sub> , C <sub>3</sub> H <sub>8</sub> yields .....	29
Figure 4.5 Effect of pressure on H <sub>2</sub> yield.....	30
Figure 4.6 Effect of initial O <sub>2</sub> /CH <sub>4</sub> ratio on H <sub>2</sub> yield. ....	31
Figure 5.1 High angle XRD patterns of different Co/SBA-15 materials .....	35
Figure 5.2 Low angle XRD patterns of different Co/SBA-15 materials.....	36
Figure 5.3 High angle XRD patterns of different Pb/SBA-15 materials.....	37

Figure 5.4 Low angle XRD patterns of different Pb/SBA-15 materials .....	37
Figure 5.5 High angle XRD patterns of different Co-Pb/SBA-15 materials.....	38
Figure 5.6 Low angle XRD patterns of different Co-Pb/SBA-15 materials .....	38
Figure 6.1 Schematic of post synthesis grafting to functionalize silica surface with amine group [Chew et al., 2010].....	40
Figure 6.2 Nitrogen adsorption-desorption isotherms of pure SBA-15. ....	45
Figure 6.3 TEM images of pure SBA-15 .....	45
Figure 6.4 TEM images of pure %5Co-%5 Pb impregnated SBA-15 sample .....	46
Figure 6.5 TEM images of pure %10Co functionalized SBA-15 sample.....	46
Figure 6.6 TEM images of %5Co%5 Pb functionalized SBA-15 sample.....	47
Figure 6.7 XPS spectra of the Co 2p level for Co impregnated mesoporous silica samples .....	49
Figure 6.8 XPS spectra of the Co 2p level for Co and Pb impregnated mesoporous silica samples. ....	49
Figure 6.9 XPS spectra of the Co 2p level for Co functionalized mesoporous silica samples .....	51
Figure 6.10 XPS spectra of the Co 2p level for Co and Pb functionalized mesoporous silica sample.....	51



Figure 6.11 Raman Shift of pure SBA-15 .....	53
Figure 6.12 Raman Shift of Co and/or Pb impregnated SBA-15 samples. ....	54
Figure 6.13 Raman Shift of Co funct-SBA15 sample.....	55
Figure 6.14 Raman spectra of Pb impregnated-SBA15 sample.....	56
Figure 7.1 N <sub>2</sub> adsorption-desorption isotherms of P123/CTAB ratio 1/4sample ..	61
Figure 7.2 N <sub>2</sub> adsorption-desorption isotherm of P123/CTAB ratio 1/5 sample ..	61
Figure 7.3 Low angle XRD patterns of different SBA-15 materials (P123/CTAB=1:4).....	62
Figure 7.4 Low angle XRD patterns of different SBA-15 materials (P123/CTAB=1:5).....	63
Figure 7.5 Low angle XRD pattern of 1%Pt/SBA-15 catalyst prepared by incipient wetness impregnation method at different pore diameter. ....	64
Figure 7.6 High angle XRD pattern of 1%Pt/SBA-15 catalyst prepared by incipient wetness impregnation method at different pore diameters.....	64
Figure 7.7 FTIR spectra of the SBA15 samples (For P123/CTAB:1/4 and different KCl amounts). ....	65
Figure 7.8 FTIR spectra of the SBA15 samples (For P123/CTAB:1/5 and different KCl amounts). ....	66
Figure 7.9 FTIR spectra of the 1%Pt/SBA15 samples (For P123/CTAB).....	66

Figure 8.1 Schematic diagram of the experimental set-up. ....	68
Figure 8.2 Methane conversion (a) and H <sub>2</sub> , CO <sub>2</sub> and CO production (b) over Co(5)-SBA15 catalyst (Incipient Wetness Impregnation Method) as a function of temperature. ....	72
Figure 8.3 H <sub>2</sub> yield of Co(5)-SBA15 as a function of temperature.....	72
Figure 8.4 Methane conversion (a) and H <sub>2</sub> , CO <sub>2</sub> and CO production (b) over Co(5)-Pb(5)-SBA15 catalyst (Incipient Wetness Impregnation Method) as a function of temperature. ....	73
Figure 8.5 H <sub>2</sub> yield of Co(5)-Pb(5)-SBA15 as a function of temperature.....	74
Figure 8.6 Methane conversion (a) and H <sub>2</sub> , CO <sub>2</sub> and CO production (b) over Co(5)-Pb(10)-SBA15 catalyst (Incipient Wetness Impregnation Method) as a function of temperature. ....	75
Figure 8.7 H <sub>2</sub> yield of Co(5)-Pb(10)-SBA15 catalyst as a function of temperature. ....	75
Figure 8.8 Methane conversion (a) and H <sub>2</sub> , CO <sub>2</sub> and CO production (b) over Co(5)-SBA15 catalyst (Post Grafting Method) catalyst as a function of temperature. ....	76
Figure 8.9 H <sub>2</sub> yield of Co(5)-SBA15 catalyst (post grafting method) as a function of temperature.....	77

Figure 8.10 Methane conversion (a) and H <sub>2</sub> , CO <sub>2</sub> and CO production (b) over Co(5) Pb(5)-SBA15 catalyst (Post Grafting Method) as a function of temperature. ....	77
Figure 8.11 H <sub>2</sub> yield of Co(5)-Pb(5)-SBA15 catalyst (post grafting method) as a function of temperature. ....	78
Figure 8.12 Methane conversion (a) and H <sub>2</sub> , CO <sub>2</sub> and CO production (b) over 0.5%RhCo(5) SBA-15 catalyst as a function of temperature. ....	79
Figure 8.13 H <sub>2</sub> yield of 0,5%RhCo(5)- SBA15 catalyst (incipient wetness impregnation method) as a function of temperature. ....	79
Figure B.1XPS spectra of the O 1s level for Co impregnated mesoporous silica sample 107	
Figure B.2XPS spectra of the O 1s level for Co impregnated mesoporous silica sample.....	107
Figure B.3XPS spectra of the Si 2p level for Co impregnated mesoporous silica sample.....	108
Figure B.4XPS spectra of the Si 2p level for Co impregnated mesoporous silica sample.....	108
Figure B.5XPS spectra of the O 1s level for Co functionalized mesoporous silica sample.....	109
Figure B.6XPS spectra of the O 1s level for Co functionalized mesoporous silica sample.....	109

Figure B.7 XPS spectra of the Si 2p level for Co functionalized mesoporous silica sample.....	110
Figure B.8 XPS spectra of the Si 2p level for Co functionalized mesoporous silica sample.....	110
Figure B.9 XPS spectra of the Pb 4f level for Co and Pb impregnated mesoporous silica sample. ....	111
Figure B.10 XPS spectra of the Pb 4f level for Co and Pb impregnated mesoporous silica sample. ....	111
Figure B.11 XPS spectra of the Pb 4f level for Co and Pb impregnated mesoporous silica sample. ....	112
Figure B.12 Raman spectra of 5%Pb-SBA-15 catalyst.....	112
Figure C.1 Nitrogen adsorption isotherm of Co(5% wt)-impregnated SBA-15 ..	113
Figure C.2 Nitrogen adsorption isotherm of Co(10% wt) impregnated SBA-15.	114
Figure C.3 Nitrogen adsorption isotherm of Co(5% wt)-Pb(10% wt)-impregnated SBA-15 .....	114
Figure C.4 Nitrogen adsorption isotherm of Co(5% wt)-functionalized SBA-15	115
Figure C.5 Nitrogen adsorption isotherm of Co(10% wt)-functionalized SBA-15 .....	115
Figure C.6 Nitrogen adsorption isotherm of Co(5% wt)-Pb(5% wt)-functionalized SBA-15 .....	116

Figure C.7 Nitrogen adsorption isotherm of Pb (10% wt)-functionalized SBA-15 .....	116
Figure C.8 Nitrogen adsorption isotherm of Pb (5% wt)- impregnated SBA-15.	117
Figure C.9 BJH adsorption pore size distribution of Pure SBA-15 .....	117
Figure C.10 BJH adsorption pore size distribution of Co(5%wt-impregnated SBA-15).....	118
Figure C.11 BJH adsorption pore size distribution of Co (10%wt-impregnated-SBA-15).....	118
Figure C.12 BJH adsorption pore size distribution of Co(5%wt)-Pb(5%wt)-impregnatedSBA-15 .....	119
Figure C.13 BJH adsorption pore size distribution of Co(5%)wt-functionalized-SBA-15 .....	119
Figure C.14 BJH adsorption pore size distribution of Co(10%wt functionalized )-SBA-15 .....	120
Figure C.15 BJH adsorption pore size distribution of Co(10%wt functionalized )-SBA-15 .....	120
Figure C.16 BJH adsorption pore size distribution of Pb(%5wt-functionalized SBA-15 .....	121
Figure C.17 BJH adsorption pore size distribution of Pb5%wt-impregnated.....	121

## LIST OF SYMBOLS

Å	Angstrom, length unit
AFC	Alkaline fuel cell
APTMS	3-Aminopropyltrimethoxysilane
a.u.	Arbitrary Unit
BET	Brunauer-Emmett-Teller
BJH	Barrett-Joyner-Halenda
CMK-1	Carbon Mesostructures from Korea
CTAB	Cetyltrimethylammonium Bromide
cc	Cubic Centimeters (cm <sup>3</sup> )
E	Activation Energy, cal/mol
FT-IR	Fourier Transform Infrared
GRI	The Gas Research Institute
$\Delta H_{0rxn}$	Enthalpy Change on Reaction at STP, kJ/mol
HMS	Hexagonal Mesoporous Silica
ID	Internal Diameter, mm
IUPAC	The International Union of Pure and Applied Chemistry
M41S	Mesoporous silica by Mobil Corporation
MCFC	Molten Carbonate Fuel cell
MCM-41	Mobil Composition of Matter No 41
MCM-48	M41S Type Mesoporous Silica (Cubic)
MCM-50	M41S Type Mesoporous Silica (Lamellar)
MSU	Michigan State University
NMR	Nuclear Magnetic Resonance
OMMs	Ordered Mesoporous Materials
OSC	Oxygen Storage Compound
P123	Triblock co-polymer, EO <sub>20</sub> PO <sub>70</sub> EO <sub>20</sub>
PAFC	Phosphoric Acid Fuel Cell
PEMFC	Proton Exchange Membrane Fuel Cell

POM	Partial Oxidation of Methane
R	Universal Gas Constant
SBA-15	Santa Barbara Number 15
SOFC	Solid Oxide Fuel Cell
Syn-gas	Synthesis Gas, H <sub>2</sub> /CO mixtures
T	Temperature, K
TCD	Thermal Conductivity Detector
TEM	Transmission Electron Microscopy
$\theta$	Angle (°)
wt %	Weight percent

# CHAPTER 1

## INTRODUCTION AND SCOPE

### 1.1 METHANE PARTIAL OXIDATION

Energy is very crucial for human life and providing a secure and accessible supply of energy is important for the sustainability of modern societies. The global energy requirement is rapidly rising as the human population, urbanization and modernization increase. Depletion of the fossil fuel reserves and the environmental problems have led to people to seek energy sources via alternative energy conversion methods [Luo et al., 2007; Asif and Muneer, 2007].

Hydrogen energy seems to be a long term solution to the worldwide increase in energy demands. Since it can be used as clean fuel in various energy end-use sectors involving the conversion to electricity without CO<sub>2</sub> emission, and also can be stored and transported over long distance with lower loss compared to electricity, it is expected that its demand will increase significantly in the near future [Yamawaki et al., 2007; Koh et al., 2007].

A variety of methods are available to produce hydrogen, including the reforming of hydrocarbons (via steam reforming, partial oxidation or autothermal reforming), gasification of coal or biomass, and the electrolysis or thermochemical decomposition of water. Hydrocarbon reforming methods generate a gaseous mixture of hydrogen, carbon monoxide, carbon dioxide and water. The produced hydrogen can be used separately or combining with carbon monoxide as synthesis gas for the upstream production of chemicals and fuels.



The studies have shown that as the H/C ratios decrease, the thermal efficiency of reforming processes decrease. So, using methane rather than larger hydrocarbons is more advantageous. Methane is the main component of natural gas, which is an abundant natural resource and could thus serve as a valuable feedstock for the production of hydrogen and valuable chemicals [Koh et al., 2007].

Compared with other reforming processes such as steam and CO<sub>2</sub> reforming, partial oxidation of methane (POM) has attracted considerable attention since this reaction is energy saving and the produced syn-gas has a H<sub>2</sub>/CO ratio of 2, which is desirable for use in production of methanol and synthetic fuels [Gao et al., 2008].

## **1.2 MESOPOROUS MATERIALS AS SUPPORT**

Heterogeneous catalysts are extensively studied due to their high efficiency and reusability. Adjustment of the surface properties and structure of a catalyst enable to design catalysts which have desired catalytic activity. It is demanded that any active catalyst possesses high surface areas on which active phases are well dispersed and pore size providing fast mass transfer of the reactants and products to and from the catalytic sites [Zhu et al., 2009; Trong On et al., 2001].

Porous materials have been widely used as catalysts and catalyst supports. The International Union of Pure and Applied Chemistry (IUPAC) divide nanoporous materials into three groups based on their pore diameter ( $d$ ): microporous,  $d < 2.0$  nm; mesoporous,  $2 \leq d \leq 50$  nm; macroporous,  $d > 50$  nm [Taguchi and Schüth, 2001]. Among the microporous materials, zeolites are best known and widely studied porous materials [Meynen et al., 2009]. They possess high surface area and uniform, molecular sized micropores [Meynen et al., 2007]. They attracted much interest as both catalysts and supports. However, their small pore channels (<2 nm) cause severe limitations when large reactant molecules are processed [Zhu et

al., 2009; Taguchi and Schüth, 2001]. Therefore, a great number of studies has focused on development of mesoporous materials with pores ranging from 2 nm to 50 nm [Meynen et al., 2007].

The first successful synthesis of ordered mesoporous silica was achieved by Mobil scientists in 1992 [Marquez-Alvarez et al., 2008; Taguchi and Schüth, 2001]. The mesoporous (M41S) silica materials including hexagonal-MCM-41, cubic-MCM-48 and lamellar-MCM-50 (Fig.1.1) have been synthesized by using alkyl trimethyl ammonium halides as the structure-directing surfactants under basic conditions. These materials have large uniform pore structures, high specific surface areas and specific pore volumes [Oye et al., 2001; Vinu et al., 2006].

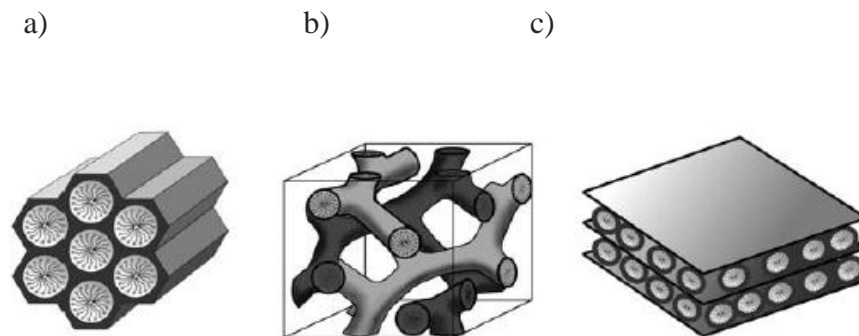


Figure 1.1 Structures of mesoporous M41S materials: a) MCM-41 (2D hexagonal), b) MCM-48 (cubic), and c) MCM-50 (lamellar) [Hoffmann et al., 2006].

Since the synthesis of the M41S silica materials, a great number of new ordered mesoporous silica materials having different pore sizes, composition and morphology were also discovered including SBA-15 (P6 mm), CMK-1, MSU-n, HMS, etc. [Shylesh et al., 2008; Wang et al., 2005].

These ordered mesoporous materials with high surface areas (800–2000 m<sup>2</sup>/g), large pore volumes, tunable uniform pore sizes have received considerable interest

due to their practical applications in catalysis, separation, and adsorption [Yang and Zhao, 2005; Ponvel et al., 2010]. SBA-15 (Santa Barbara No:15) mesoporous silica (Specific surface area = 600–1000 m<sup>2</sup>/g) is among the most considerably studied ordered mesoporous materials [Sayari and Yang, 2005 ; Laugel et al., 2008]. Its thicker walls (3–6 nm) provide a higher thermal and hydrothermal stability than thinner-walled MCM-41 [Laugel et al., 2008]. Since it generally possesses larger pores (in the range of 5 to 30 nm) than MCM-41 and higher pore volumes, SBA-15 is one of the most suitable silica material for incorporating metal and metal oxide nanoparticles [Muresanu et al., 2008 ; Laugel et al., 2008].

### **1.3 SCOPE OF THESIS**

For the catalytic application of nanostructured materials, tunable pore size and high surface area are demanded. Mesoporous materials with high surface area and pore volume fulfill these requirements. In addition, owing to their thermal and hydrothermal stabilities, they can be used high temperature required reactions. Depending on these advantages, Co and Pb incorporated SBA-15 samples which has high surface areas were synthesized.

The partial oxidation reactions over metal oxides are an interesting alternative method to produce syngas. The metal oxide is an oxygen-transfer agent in these reactions. Ceria and the oxide materials containing ceria have attracted much interest as oxidation catalysts due to their high activity in the redox reactions and high oxygen storage capacity. As another alternative to Ce, Co and Pb metal oxides which have high oxygen release ability provide potential materials for oxidation reactions. Due to these advantages, Co and Pb mixed oxide catalysts were used in this study.

In this thesis, Co and /or Pb containing mesoporous SBA-15 materials were synthesized by using different synthesis techniques such as direct synthesis

methods, incipient wetness impregnation, post grafting methods and methane partial oxidation reaction were carried out over these catalysts. The main objective of this thesis is to synthesize SBA-15 mesoporous materials having well dispersed Co and/or Pb and to test the activity of these catalysts in methane partial oxidation reaction.

In Chapter 4, gas phase methane partial oxidation reaction were modeled to understand the kinetic behavior of CH<sub>4</sub> partial oxidation by using CHEMKIN GRI 3.0 mechanism. The characterization of the Co and/or Pb-SBA-15 catalysts were obtained by using different techniques, namely XRD, XPS, TEM, BET, Raman, FT-IR, for which the details are reported in Chapter 5, 6. In addition to these, SBA-15 samples with different pore sizes were also synthesized and characterized to observe the tuning features of SBA-15 mesoporous materials. The results are given in Chapter 7. Catalytic Methane partial oxidation reaction results obtained over these mesoporous Co and/or Pb-SBA-15 catalysts are presented in Chapter 8.

## CHAPTER 2

### SBA-15 (SANTA BARBARA NO:15)

#### 2.1 INTRODUCTION

In the last years, a great number of research have been devoted to the synthesis and applications of ordered mesoporous materials [Sayari and Yang, 2005]. SBA-15 mesoporous silica, first synthesized by Zhou et al. in 1998, is one of the most extensively investigated ordered mesoporous sieve. It can be easily synthesized by using a variety of poly(ethylene oxide)–poly(propylene oxide)–poly(ethylene oxide) triblock copolymers ( $\text{EO}_x\text{PO}_y\text{EO}_x$ ) as templates, as can be shown in Fig. 2.1 [Xi and Tang, 2005].

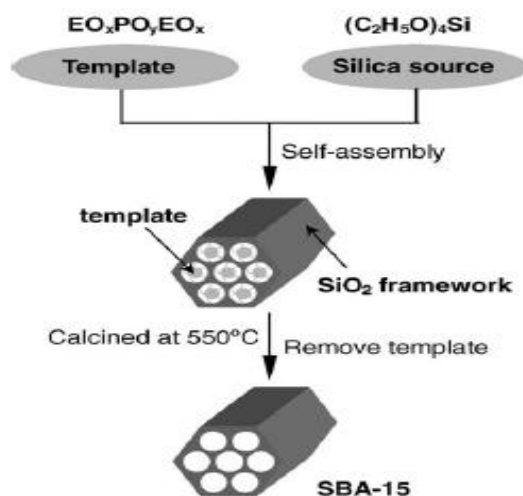


Figure 2.1 Schematic Illustration of the formation of the triblock copolymer/mesoporous silica hybrid and mesoporous silica SBA-15[Xi and Tang, 2005].

The following features of SBA-15 make it a promising catalyst support: (i) it can be easily and reproducibly synthesized within a wide range of temperatures (35-130°C) using sodium silicate, alkoxydes like tetra ethyl ortho silicate (TEOS) and tetramethylortosilicate (TMOS) as silica sources; (ii) it is a hexagonally ordered silica material and it has tailorable uniform mesopores [4-15 nm] and micropores in the mesopore walls; (iii) it has thick pore walls (2-6 nm), which provide thermal and hydrothermal stability; and (iv) depending on the synthesis conditions, it may present a large variety of morphologies [Sayari and Yang, 2005; Giraldo et al, 2007].

These mesoporous materials have a great importance in various applications such as catalysis, adsorption. Nonetheless, the frameworks of mesoporous silica materials are rather inactive and the applicability is restricted [Chino and Okubo, 2005]. So, active sites must be incorporated to the mesoporous silica according to requirements [Shylesh et al, 2008 ; Martin-Aranda and Cejka, 2010]. Up to now, much research has focused to functionalize the surfaces of these materials.

Stabilizing highly metals and oxides in uniform porous matrices, nanoparticles can be confined in the cavities of mesoporous silicates. It has been shown that the metal particles can be incorporated into mesopore channels and their size is controlled by the mesopore diameter [Yuranov et al., 2004]. Incorporation of the metals inside the pore channels of mesoporous silica can be achieved via direct synthesis (one step synthesis) method or post-synthesis treatment. In direct synthesis method, active phases are added to reaction mixture during the synthesis of the mesoporous silica materials. The post-synthesis metal deposition was performed over a calcined mesoporous support using wetness impregnation, ion-exchange, in situ reduction, and vapor-phase deposition techniques [Wang et al., 2009; Martin-Aranda and Cejka, 2010].

## **2.2 SYNTHESIS MECHANISM OF SBA-15**

Surfactant templated self-assembly is one of the most favourable ways for synthesizing of mesoporous materials. Non-covalent weak interactions such as hydrogen bonding, van der Waals forces, and electrostatic interaction between the surfactants or their supermolecular structures and the building blocks drive the self-assembly. It is reported that amphiphilic molecules can self-organize into a various supermolecular structures containing spherical micelles, hexagonal rods, lamellar liquid crystals and other assemblies. These structures can be used as templates to adjust pore structure and size [Yang et al.,2009].

Non-covalent interactions between the surfactant and the building blocks enable the organization of building blocks around the surfactant structures resulting the mesostructured composites including surfactant. After the surfactant removed by calcination or extraction with solvents, mesoporous materials can be produced as can be seen in Figure 2.2 [Yang et al.,2009; Lu, 2006].

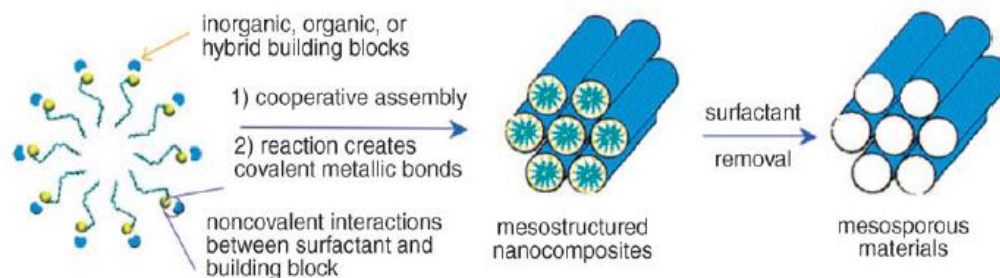
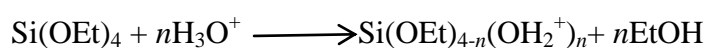


Figure 2.2 Surfactant-directed synthesis of mesoporous materials from inorganic, organic or hybrid building blocks [Lu, 2006].

The interaction between the silica and the surfactant has been investigated in several studies. Different assembly mechanisms have been introduced. Huo et al. [1994] presented four different synthesis mechanisms which are based on electrostatic interactions between the silica and surfactant including  $(S^+I^-)$ ,  $(S^-I^+)$ ,  $(S^-X^+I^-)$  and  $(S^-M^+I^-)$ , where S surfactant (+ cationic, - anionic), I soluble inorganic (silica), X halogen ion, and M metal cation. Obtaining these conditions require that the reaction must be conducted at very low pH, if the silica surface is positively charged, or at  $pH = 7-10$ , where the surface is negatively charged [Berggren et al., 2005].

In the synthesis of the SBA-15 mesoporous silica, amphilic block co-polymers are used as structure directing agent. So, regarding the nonionic alkyl-ethylene oxide surfactants or poly(alkylene oxide) triblock copolymer species in acid conditions,  $(S^0H^+)(X^-I^+)$  formation mechanism has been proposed [Zhao et al., 1998; Berggren et al., 2005].

Firstly, alkoxy silane species are hydrolyzed,





Partial oligomerization of the silica follow the hydrolization step. The EO moieties of the surfactant associate with hydronium ions in strong acidic medium.



It is proposed that the cationic silica species and charge-associated EO units are assembled together through a combination of electrostatic, hydrogen bonding, and van der Waals interactions forming  $\text{REO}_{m-y}[(\text{EO})\cdot\text{H}_3\text{O}^+]_y \dots y\text{X}^- \dots \text{I}^+$  which can be described as  $(\text{S}^0\text{H}^+)(\text{X}\text{T}^+)$  mechanism [Zhao et al., 1998].

### 2.3 SURFACE CHEMISTRY OF MESOPOROUS SILICA

The mesoporous silicas consist of pore walls which are crystallographically amorphous. Due to their amorphous pore walls, mesoporous silicas can be modified via post-synthesis methods which can be carried out size control, framework stabilisation, compositional modifications or the formation of mesoporous/zeolite composite materials [Xia and Mokaya, 2003].

The silica materials can be considered as tetraesters of silicic acid,  $\text{Si}(\text{OH})_4$  [Berggren et al., 2005]. The surface of these materials contains silanol groups,  $(\text{Si}-\text{OH})$  in high concentrations. These silanol groups are convenient anchoring points for organic functionalization reactions [Shyles et al., 2008]. Three types of silanol groups are present on the silica surface including (a) isolated (free) (b) hydrogen-bonded (vicinal) and (c) geminal as can be seen in Figure 2.3 [Giraldo et al., 2007; Vansant et al., 1995; Shyles et al., 2008]. Silylation, generally occurs on free  $(\text{Si}-\text{OH})$  and geminal silanol  $[=\text{Si}(\text{OH})_2]$  groups, while hydrogen-bonded silanol groups are less accessible to modification because they form hydrophilic networks among themselves [Shyles et al., 2008].

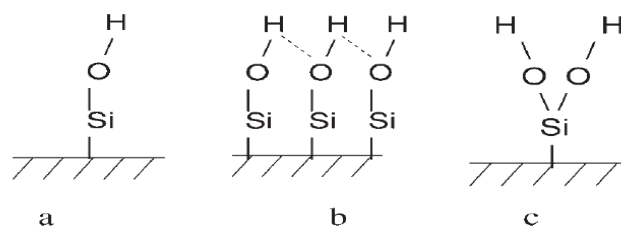


Figure 2.3 Representation of the silanol groups on the silica surfaces[Giraldo et al., 2007]

The content of the silanol groups can be changed depending on the surfactant removal procedure and they can be modified by using postsynthesis treatments. Quantification of the silanol groups can be made by using Fourier Transform Infrared analysis (FTIR), Nuclear Magnetic Resonance (NMR) and Temperature programmed desorption (TPD) techniques [Giraldo et al., 2007].

## CHAPTER 3

# METHANE PARTIAL OXIDATION OVER METAL OXIDES

### 3.1 METHANE PARTIAL OXIDATION

In the recent decades, the conversion of methane to value-added products such as liquid hydrocarbons and oxygenates has received considerable attention. The availability of large amount of natural gas and the decreasing supply of world petroleum reserves had made methane important raw material for synthesis of clean fuels and chemicals [Choudhary and Goodman, 2000; Holmen, 2009; Salazar-Villalpando, 2008].

Methane ( $\text{CH}_4$ ) is the main constituent of natural gas, which is an abundant worldwide and relatively clean energy sources [Tsai et al, 2004; Lyubovsky et al, 2003]. It is very stable and symmetrical molecule with a C-H bond dissociation energy of 104 kcal/mol. Since it has strong C-H bonds which must be broken, methane activation is a big challenge for researchers all over the world. [Choudhary and Goodman, 2000; Li et al, 1999; Holmen, 2009]. Several promising process are proposed to convert  $\text{CH}_4$  directly into more valuable compounds, such as synthesis gas, (syngas,  $\text{CO} + \text{H}_2$ ), ethylene, methanol ( $\text{CH}_3\text{OH}$ ), and formaldehyde ( $\text{CH}_2\text{O}$ ) [Tsai et al, 2004].

In last years, synthesis gas production from alkanes has attracted great interest due to the necessity of the high-content hydrogen streams for fuel cells applications

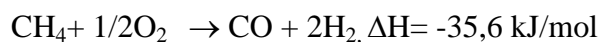
and internal combustion engines [Schmidt et al., 2003]. The production of syngas is a very important process to the petrochemical industry since syngas is an important chemical feedstock for producing many chemicals involving methanol, higher hydrocarbons via Fischer-Tropsch chemistry, and acetic acid [Hohn and Schmidt, 2001 ; Marschal and Mlecko, 1999].

Industrially, synthesis gas is mostly generated via natural gas steam reforming process. It is a very expensive process because of the high heat requirement [Larentis et al., 2001].



Since this reaction is highly endothermic, large furnaces are used to supply the necessary energy [Hohn and Schmidt, 2001].

Much research has been proposed to generating syngas via alternate processes, the catalytic partial oxidation of methane has been extensively investigated as an alternative process to other reforming processes [Ferreira 2010 ; Hohn and Schmidt, 2001].



In this reaction, methane reacts with oxygen to form a mixture of H<sub>2</sub> and CO which is called synthesis gas. Temperatures [Moon, 2008]. It is commonly run at high temperatures around 1500–1600 K [Song and Guo, 2006].

It has been observed that methane may be partially oxidized generating H<sub>2</sub> and CO as the main products at millisecond contact times [Hickman and Schmidt, 1993; Joensen and Rostrup-Nielsen, 2002]. Table 3.1 shows a brief literature survey results for partial oxidation of hydrocarbons over different catalysts. This reaction has been studied in different types of reactors, and high syngas yields

have been obtained. It can be executed as non-catalytic combining with steam reforming which is called autothermal reforming or without using steam by catalytic partial oxidation [Hohn and Schmidt, 2001].

Table 3.1 Literature Survey Results for Partial Oxidation

Catalyst	Fuel	(CH <sub>4</sub> /O <sub>2</sub> )	Contact time	Fuel conversion (%)	Selectivity H <sub>2</sub> (%)	Ref.
Noncatalytic	methane	1	NA	80.1	92.6	[Tsai et.al, 2004]
Rhodium coated alumina monoliths	Methane, butane, cyclohexane, n-hexane	2	1-10 ms	~100	>70	[Schmidt et.al, 2003]
Rhodium monolith	methane	2	1.2-6 ms	78	88	[Hohn and Schmidt, 2003]
Rhodium coated monolith	n-hexane	2	2-20 ms	~100	99	[Connor et.al, 2000]
Rh/γ-Al <sub>2</sub> O <sub>3</sub>	methane	1.8	NA	55	NA	[Burke and Trimm, 2006]
Rh/Al <sub>2</sub> O <sub>3</sub>	propane	(C/O) 0.8	0.075	NA	72	[Silberova et.al, 2005]
Rhodium coated monolith	n-decane	(C/O) 0.8	12 ms	99	86	[Krummenacher et.al, 2003]
Rhodium washcoated metallic monolith	methane	1.43	1.5 min	98.9	77.6	[Jung et.al, 2003]
Pt/Rh gauze	methane	1.25	0.00021-0.00033 s	60	NA	[Fathi et al., 1998]
Ni/α-Al <sub>2</sub> O <sub>3</sub>	methane	2	NA	92	97	[Marschall and Mleczko, 1999]
Ce <sub>1-x</sub> Ni <sub>x</sub> O <sub>y</sub>	methane	2	3 s	NA	80	[Shan et.al,2006]
Ni/SiC	methane	2	NA	75	NA	[Sun et.al, 2005]
LaNiO <sub>x</sub> /CeO <sub>2</sub> -ZrO <sub>2</sub> /α-Al <sub>2</sub> O <sub>3</sub> monolith	methane	2	5.9 ms	~90	NA	[Pavlova et.al,2005]
Ni/MgO	methane	2	NA	93.7	94	[Requies et.al, 2005]
Ru/TiO <sub>2</sub>	methane	2	NA	44.9	54.7	[Perkas et.al, 2005]

When it is compared with steam reforming, the slight exothermicity is the major advantage of the partial oxidation reaction. This allow autothermal reforming operation and decrease the investment cost and emissions of CO<sub>2</sub> and NO<sub>x</sub>. The CO/H<sub>2</sub> ratio of about 2 obtained by this process is ideal for methanol production and in Fischer-Tropsch synthesis. Table 3.1 shows syngas reactions, and relevant thermodynamic data [Marschall and Mleczko, 1999; Fangli et al., 2007].

Table 3.2 Syngas Reactions [Rostrup-Nielsen et.al, 2000].

	$-\Delta H^{\circ}_{298}(\text{kJ/mol})$
<b>Steam Reforming</b>	
$\text{CH}_4 + \text{H}_2\text{O} = \text{CO} + 3\text{H}_2$	
$\text{C}_n\text{H}_m + n\text{H}_2\text{O} = n\text{CO} + (n+1/2 m)\text{H}_2$	-206
$\text{CO} + \text{H}_2 = \text{CO}_2 + \text{H}_2$	-1175
	41
<b>CO<sub>2</sub> Reforming</b>	
$\text{CH}_4 + \text{CO}_2 = \text{CO} + 2 \text{H}_2\text{O}$	
	-247
<b>Autothermal Reforming</b>	
$\text{CH}_4 + 3/2 \text{O}_2 = \text{CO} + 2 \text{H}_2\text{O}$	520
$\text{H}_2\text{O} + \text{CH}_4 = \text{CO} + 3\text{H}_2$	-206
$\text{CO} + \text{H}_2\text{O} = \text{CO} + \text{H}_2$	41
<b>Catalytic Partial Oxidation</b>	38
$\text{CH}_4 + 1/2 \text{O}_2 = \text{CO} + 2\text{H}_2$	

### 3.2 PARTIAL OXIDATION OVER METAL OXIDES

Catalytic partial oxidation of methane (POM) has been extensively studied for synthesis gas production. However, this technology is limited as an industrial process because of some problems such as the rapid temperature increase of the catalyst and the risk of explosion. To eliminate these disadvantages, a new two-step process was proposed by some researchers for the production of synthesis gas from methane in the absence of gaseous oxidant. This technology provides better product selectivity and reduces the process cost since it does not require pure oxygen for the oxidation reaction. Two interconnected reactors can be used to carry out this process. Firstly, within the fuel reactor, methane is oxidized by the lattice oxygen of metal oxide to generate CO and H<sub>2</sub>, and then, reduced metal oxide is moved to the regeneration reactor and re-oxidized by air by producing water and carbon dioxide. The synthesis gas with a H<sub>2</sub>/CO ratio of 2 can be produced. Since fuel does not react directly with gas phase oxygen, explosion risk can be eliminated. In addition, by using air rather than pure oxygen can reduce the cost of partial oxidation reaction [Kongzhai et al., 2008 ; Li et al., 2010].

Converting the methane to synthesis gas by using lattice oxygen of oxygen storage compound (OSC) is an attractive way for natural gas applications. The metal oxide is used as an oxygen transfer agent in these reactions. This idea is not new. Methane oxidation over iron and nickel cerium oxides have been well studied previously [Gorshkov et al., 2001]. Due to their high oxygen storage capacity, ceria and metal oxides containing ceria has received great attention. It also exhibits high catalytic activity in the redox reactions. It is observed that the redox properties and the lattice oxygen mobility of CeO<sub>2</sub> can be improved, when ceria is used with other metal oxides as a complex [Li et al., 2010].

Recently, the gas–solid reaction between methane and lattice oxygen of Cerium oxides (equation 3.1-3.3) to give synthesis gas was reported by Otsuka et al. [1998].





Li et al. [1998] studied the direct conversion of methane to synthesis gas using lattice oxygen of  $\text{CeO}_2\text{-Fe}_2\text{O}_3$  complex oxides ( $\text{CeO}_2\text{-Fe}_2\text{O}_3$ ,  $\text{CeO}_2\text{-ZrO}_2$  and  $\text{ZrO}_2\text{-Fe}_2\text{O}_3$ ) complex oxides were synthesized and tested in methane oxidation reaction in the absence of gaseous oxidant. The results indicated that reaction temperature strongly affect the methane conversion and CO and  $\text{H}_2$  selectivities. As the reaction temperature increase, they also increase rapidly. This is probably due to the high rate of lattice oxygen migration under high temperature. The isothermal reactions at  $800^\circ\text{C}$  show that the selective oxidation of methane over metal oxides is affected by the following factors: features of activated oxygen species (i.e., lattice oxygen), the route of methane activation (i.e., onreduced Fe species), and the lattice oxygen mobility. The results obtained over  $\text{ZrO}_2\text{-Fe}_2\text{O}_3$  sample indicates that it is appropriate for methane combustion reaction. In addition, the methane conversion is improved by the reduced Fe species which has a catalytic performance for methane decomposition.

Although  $\text{CeO}_2\text{-ZrO}_2$  complex oxides present a high activity for methane oxidation, it shows the low synthesis gas selectivity because of the surface defects on Ce-Zr-O surface. However,  $\text{CeO}_2\text{-Fe}_2\text{O}_3$  sample exhibits high activity and selectivity for the synthesis gas production.

As another alternative to iron, ceria, nickel oxides, lead oxide is proposed. Due to the corrosive effect of lead oxide melt on reactor system and the difficulties in experiments using lead, methane oxidation over lead oxide has not been studied much upto now [Gorshkov et al., 2001]. Addition to methane partial oxidation, oxidative coupling of methane over metal oxides have also been extensively

studied. Oxidative coupling reaction can be accomplished via the REDOX method and methane reacts with a reducible metal oxide (reagent) then the reduced metal oxide is subsequently reoxidized by gas phase oxygen [Baerns and Ross, 1989].

There are some studies about methane partial oxidation and oxidative coupling over PbO catalysts.

Baerns and Ross [1989] studied oxidative coupling reaction over PbO catalysts using supports which have different acidity/basicity. Results are given in Table 3.3.

Table 3.3 Hydrocarbon selectivities over different PbO catalysts [Baerns and Ross, 1989]

Catalysts	Selectivities		
	C2	C3	C4
PbO (20) /Al <sub>2</sub> O <sub>3</sub> .xSiO <sub>2</sub>	20	-	-
PbO (31)/ γ-Al <sub>2</sub> O <sub>3</sub>	53	1	-
PbO(05) / γ-Al <sub>2</sub> O <sub>3</sub>	56	2	1
PbO(08) /SiO <sub>2</sub>	56	9	-
PbO (31)/MgO	65	3	1

The results revealed that C<sub>2+</sub> selectivity was increased as the the surface acidity was decreased. It was stated that reducing of surface acidity is probably due to alkali metal addition or increasing lead oxide ratio in the catalyst which cause covering the acidic sites of an alumina-silicate support.

Gorshkov et al. [2001] studied high temperature oxidation of methane by supported lead oxide. The samples were prepared by the impregnation of alumina (γ or α-Al<sub>2</sub>O<sub>3</sub>). The methane oxidation experiments over PbO/Al<sub>2</sub>O<sub>3</sub> which is used

as an oxidant were performed in a cyclic mode (incomplete reduction–complete oxidation by the O<sub>2</sub>–He mixture). Firstly, reduction period was done. Methane oxidation was done through a separate pulses. After the pulses product gas mixture was analyzed. Then, the sample was oxidized. The lead oxide reduction amount in the reaction was not higher than 5–10%. The experiments showed that the selectivity of the methane oxidation extremely changes as the extent of reduction of PbO increases. The samples which its composition close to PbO, the only oxidation product is CO<sub>2</sub>, however, the PbO sample where most part of it is reduced, CO is the main gas product. The extent of PbO reduction greatly affect the selectivity of methane oxidation. So, the experiments indicates that methane oxidation rate of PbO which is reduced previously higher than the rate of PbO reduction by methane. In several different studies, methane converted into CO and CO<sub>2</sub> over metal oxides previously, However, a rigorous change in the selectivity of methane oxidation at ~50% extent of PbO reduction is an interesting result. It can be supposed that if oxygen is not enough on the surface, the steps of adsorbed intermediate oxidation do not appear. But, the selectivity should be affected slowly as oxygen is deficient on the surface. So, in this system, a drastic change in the selectivity is possibly due to the change in the structure of the dominant surface intermediate when oxygen is deficient.

Nozaki et al. [1993] studied several investigations of oxidative coupling of methane over lead oxide catalysts. In one study, they have performed oxidative coupling of methane by using membrane reactors. They have used nonporous membrane film that contains PbO modified by alkali-metal or alkaline earth compound. Modified PbO membrane film was coated on a porous tube (type I- MgO/Al<sub>2</sub>O<sub>3</sub> or SiO<sub>2</sub>-Al<sub>2</sub>O<sub>3</sub>) or nonporous tube (type II- ZrO<sub>2</sub> stabilized by CaO, MgO, or Y<sub>2</sub>O<sub>3</sub>). The membrane support tube coated with lead oxide layer was inserted in an alumina tube. While methane at a flow rate of 90 mL/min of was supplied into annular space between the outer tube and inner tube, air was supplied to the inside of the inner tube at 60 mL/min. The product gas mixture was analyzed by using gas chromatography. A flame ionization detector with a

methanator and Porapak- N column were used to measure the Carbon oxides and C<sub>2</sub> hydrocarbons. The results obtained indicated that oxide ion was moved from the oxygen (air) side to the methane side via PbO film. C<sub>2</sub> hydrocarbons were produced with high selectivity (>90%), however, both the supports on which the membrane was formed and alkali-metal compounds affected the activity. When the type II membrane were used, it was observed that oxide ions was transported from support tube to PbO membrane. This is explained by determining the amount of consumed oxygen from PbO/YSZ (yttria-stabilized zirconia) catalyst in a methane stream. It was shown that oxygen transportation controled the reaction rate when CSZ (calcia-stabilized zirconia) and MSZ (magnesia-stabilized zirconia) were used as the supports. On the other hand, the reaction rate was affected by the surface reaction of methane with PbO when porous material or YSZ (yttria-stabilized zirconia) was used as the support.

### **3.3 SOLID OXIDE FUEL CELLS USING Co and Pb OXIDES**

Fuel cells are devices producing electricity, heat and water by combining the hydrogen-rich fuel with oxygen. solid oxide [Lin and Beale, 2006]. Due to high energy efficiency and low environmental pollution, fuel cells become a promising alternative to conventional power generation systems [Han et al., 2008 ; Wang et al., 2011].

The fuel cell assembly consist of a solid or liquid electrolyte layer and two electrodes [Kirubakaran et al., 2009]. At the anode (positively charged electrode) the fuel is turned into positively charged ion and a negatively charged electron [Fuel Cell Technology Review]. The positive ions are transported through the electrolyte from anode to cathode side. Since the electrolyte do not permit flow the electrons to the cathode side, electrons move to the cathode via an external electrical circuit generating the power that drives the motor [Fuel Cell Technology Review ; Kirubakaran et al., 2009 ; Green Car Congress]. Positive and negative

ions are returned at the cathode and react with oxidant to produce water and carbon dioxide.

Classification of the fuel cells can be made according to the type of electrolyte and fuel. Moreover, depending on the operating temperature, they can be further classified. PEMFC (Proton exchange membrane fuel cell), AFC (Alkaline fuel cell) and PAFC (Phosphoric acid fuel cell) work at 50–250°C. However, MCFC (Molten carbonate fuel cell) and SOFC (Solid oxide fuel cell) operate at high temperature which is in the range of 650–1000 °C [Kirubakaran et al., 2009].

Comparing the other fuel cell systems such as PEM fuel cell, SOFCs have some advantages such as very high electrical efficiency, fuel flexibility and tolerance to fuel pollutants [Salogni and Colonna, 2010]. Because of the gas insensitivity, SOFCs allow using unconventional fuels such as biomass and coal gas. fuel cell review. Since SOFCs operate at high temperatures, internal reforming can be accomplished. This means that the SOFC can convert the natural gas or petroleum to hydrogen within the fuel cell structure [Fuel Cell Technology Review].

SOFCs comprise a solid electrolyte layer which is generally Yttria Stabilized Zirconia (YSZ), and two electrodes [Salogni and Colonna, 2010]. Oxygen ions are transferred through the solid electrolyte from cathode to anode side where they oxidize the fuel to produce electrons, water and carbon monoxide. The electrons at the anode side move via the external circuit to the cathode. By reducing the oxygen at the cathode, the cycle is completed [Fuel Cell Technology Review].

In recent years, fuel cells which are using coal to generate power have attracted considerable interest. In such fuel cells, much higher electrical efficiency can be generated than traditional carbon combustion processes. In most cases, the fuel cell convert the coal to the syngas by steam reforming process. Then, this gas mixture can be used by the cell. However, using the carbon directly could be favorable for the process. Utilization of solid oxide fuel cells (SOFC) with molten metal oxide

is an interesting approach for the improvement of the direct-carbon fuel cells(DCFC). In this procedure, through equation 3.4, oxygen from electrolyte are moved to the molten metal to produce metal oxide. After that, the metal oxide are combine with fuel and reduced in the anode. Metal oxide can be also separated and reduced in a different reactor [Jayakumar et al., 2010].



Jayakumar et al. [2010] studied molten-metal anodes: In, Pb, and Sb in solid oxide fuel cells (SOFC). The cell was operated between 973 and 1173 K. The melting temperatures of In, Pb, and Sb are 430, 601, and 904 K, respectively. The impedance of molten-metal electrodes are affected by oxide formation between the electrode-electrolyte interface. By operating the cell at temperatures above the melting temperatures of both the metal and its oxide, electrode performance can be increased. The study focused on Pb and Sb molten metal anodes since their oxides have relatively low melting temperatures, 1161 K for PbO and 929 K for Sb<sub>2</sub>O<sub>3</sub>. When Sn and In were used in the cell, at all temperatures cell impedances increased. Pb molten metal anode used 973 and 1073 K exhibit the similar results. However, the cell impedance at 1173 K remained low since this temperature is above the melting temperature of PbO. The impedances of molten Sb electrodes at 973 K were low and current flow do not change the impedance due to the low melting temperature of Sb<sub>2</sub>O<sub>3</sub>.

Regarding the molten metal anode solid oxide fuel cells, there are some studies about Pb and Co mixed metal oxides.

Several methods have been regarded to improve the lead alloy anodes properties. Addition of cobalt (in one form or another) to the lead alloy or to the electrolyte is the most promising observed effect. The first study explaining the effect of cobalt

was reported in 1938. The results obtained indicates that cobalt ions (0–67.5mg/L) in an electrolyte promote the evolution of oxygen and reduce the anode potential. It was discussed that porosity of the  $\text{PbO}_2$  film and its surface characteristics were affected by cobalt. Additionally, it raised the moving of the electric current through the pores to the underlying metallic lead [Nikoloski and Nicol, 2010].

It is presented that the monitored effect due to the one or more of the following causes: (a) decomposition of lead persulfates (the hydrolysis product of which is  $\text{PbO}_2$  via cobalt) (b) easier discharge of the sulfate ion through cobalt, possibly by  $\text{Co}_2\text{O}_3$  precipitated on the anode acting as an “oxygen carrier” and (c) with addition of cobalt ions, formation of an unknown impermeable film on the anode [Nikoloski and Nicol and reference therein, 2010]

Anodic oxidation of  $\text{Pb}^{2+}$  and  $\text{Co}^{2+}$  in a sulphamate bath involving suspended  $\text{Co}_3\text{O}_4$  (or  $\text{NiCo}_2\text{O}_4$ ) particles has been investigated by Cattarin et al. [2001]. By using this method, composite oxides were prepared containing particles dispersed in a matrix. Matrix material comprise of  $\text{PbO}_2$  and hydrous Co oxides,  $\text{CoO}_x$  with  $x < 2$ . The results indicates that the electrolysis of  $\text{Co}_3\text{O}_4$  or  $\text{NiCo}_2\text{O}_4$  particles in sulphamate electrolytes having in it  $\text{Pb}^{2+}$  and  $\text{Co}^{2+}$  result in the anodic deposition of composite materials. Co concentration ( $X_{\text{Co}}$ ) within these deposits approaches 0.5. The samples prepared by incorporation of particles shows higher initial catalytic activity than either  $\text{PbO}_2 + \text{Co}_3\text{O}_4$  or  $\text{PbO}_2 + \text{CoO}_x$  anodes. The results obtained also indicates that the potential required to evolve oxygen changes linearly with  $X_{\text{Co}}$ .

It is reported that any insoluble anode material used for zinc electrowinning from sulphate solutions should have some important properties such as high electrical conductivity, good electrocatalytical capabilities (for oxygen evolution), good stability (corrosion resistance), and high mechanical strength. Using only pure Pb as a anode material does not sufficient to obtain these properties. So, its alloying with other metals is generally used. It is previously indicated that

addition of Co to Pb, in a concentration of 0.02–0.1%, significantly decrease the oxygen over potential and corrosion rate of Pb. It has also been verified that Pb–Co alloy anodes possess better properties compared with Co–Ag anodes used in industry [Rashkov and reference therein, 1999].

Rashkov et al. [1999] prepared an anodic lead–cobalt (Pb–Co) 0.5–6% alloy for electrowinning of zinc from sulphuric acid electrolytes. They used Co as an alternative to Ag. The results obtained compared with commercial Pb–Ag anode with 1% Ag. Effect of Co content on corrosion resistance of Co–Pb alloy anode and changing of over potential as a function of time were studied. It is determined that the corrosion resistance of the Co–Pb anodes is better when Co content is above 0.5%. Additionally, the anodic overpotential of Co–Pb containing 3% Co is nearly 0.08–0.1 V lower than Pb–Ag alloy.

Considering these studies about the Pb and Co oxides, the prepared Co–Pb mixed oxide samples can be used in solid oxide anode fuel cell applications.



## CHAPTER 4

# MODELLING HOMOGENEOUS PARTIAL OXIDATION

### 4.1 INTRODUCTION

It is known for several decades that the importance of the heterogeneous (that is, catalytic) and homogeneous (that is, gas-phase) reactions and the interaction between these reactions is especially for high-temperature catalytic reactions. Since first determining the role of these reactions in catalytic oxidations, the importance of coupled heterogeneous-homogeneous reactions in a various reactions systems such as catalytic combustion, partial oxidation of small alkanes, and oxidative coupling of methane were also determined.

Since these reaction system occur at high temperatures, paralleling to catalytic surface reactions, noncatalytic (that is, homogeneous) gas-phase reactions also appear. Although gas-phase reactions are accepted to be the product-forming reactions, the occurrence of homogeneous reactions is an undesired feature in catalysis cause the selectivity losses. Because of the uncontrolled process temperatures, safety hazards can arise. So, for a well-controlled and safe chemical process, the reaction mechanism and the major effects of the operating parameters on the ignition behavior must be well understood [Chattopadhyay et.al, 2006].

Detailed chemical mechanisms defining the oxidation of methane are possibly the most investigated chemical kinetic models. The Gas Research Institute (GRI) mechanisms present the most popular kinetic model owing to the easy of

access in a number of electronic versions (GRI-Mech1.2, 2.11 and 3.0). GRI-Mech 3.0 involve 325 elementary chemical reactions for the 53 species which is optimized to carry out over the ranges 1000–2500 K, 1.0–1000 kPa [Chattopadhyay and Veser, 2006; Zhu et al., 2001].

In this part of the thesis, a kinetic study of partial oxidation of CH<sub>4</sub> for synthetic-gas production is presented. The effects of the initial O<sub>2</sub>/CH<sub>4</sub> ratio, reaction temperature and pressure and residence time on the product yields are investigated. A plug flow reaction system with a length of 30 cm is simulated using CHEMKIN package incorporating the GRI 3.0 mechanism [GRI 3.0 Mechanism Parameters]. CHEMKIN GRI 3.0 mechanism parameters are given in Appendix C.

## **4.2 RESULTS AND DISCUSSION**

A kinetic analysis is carried out to determine the kinetic behaviour of the CH<sub>4</sub> partial oxidation by using the CHEMKIN package incorporating the GRI 3.0 mechanism. The model is regarded as a plug flow reaction system with a length of 30 cm. Reactor diameter is 1 inch and flow rate is 300 cm<sup>3</sup>/sec. Simulations were performed over a temperature range of 800–3000 K with a 100 K interval.

### **4.2.1 The Effect of Temperature**

Temperature has an important effect on product yields. Above the temperatures 2000 K, CH<sub>4</sub> is completely consumed at the reactor exit. Maximum H<sub>2</sub> mole fraction is obtained at 2200 K (mole fraction is 0.66). Above this temperature, H<sub>2</sub> amount begins to decrease. Maximum CO mole fraction is obtained at 2300 K. CO mole fraction is 0.33 at this point. Other hydrocarbons such as C<sub>2</sub>H<sub>2</sub>, C<sub>2</sub>H<sub>4</sub>, C<sub>2</sub>H<sub>6</sub>, C<sub>3</sub>H<sub>8</sub> can also be produced in partial oxidation of CH<sub>4</sub>, although in

considerably low amounts. The yields of these products change with the temperature. Maximum  $C_2H_2$  is obtained at 1600 K, with mole fraction of 0.087. Figure 4.1, 4.2 and 4.3 show the effect of temperature on  $H_2$ , CO, and other hydrocarbons yields respectively.

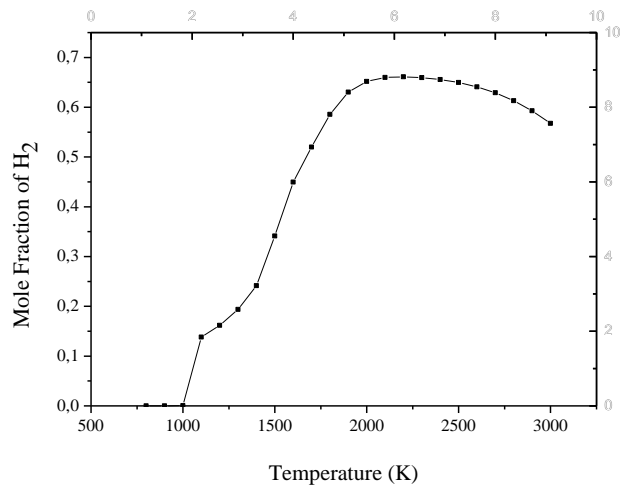


Figure 4.1 Effect of temperature on  $H_2$  yield

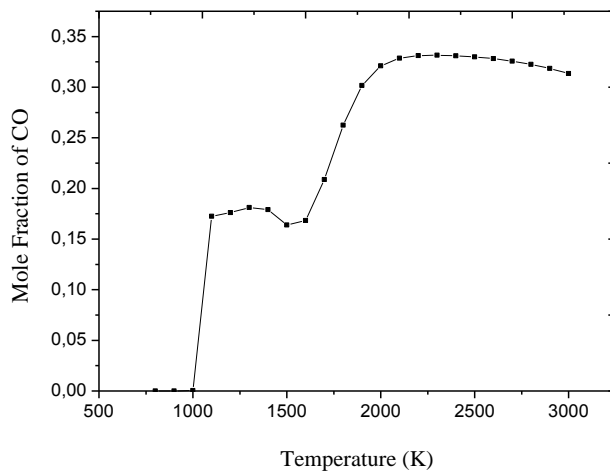


Figure 4.2 Effect of temperature on CO yield

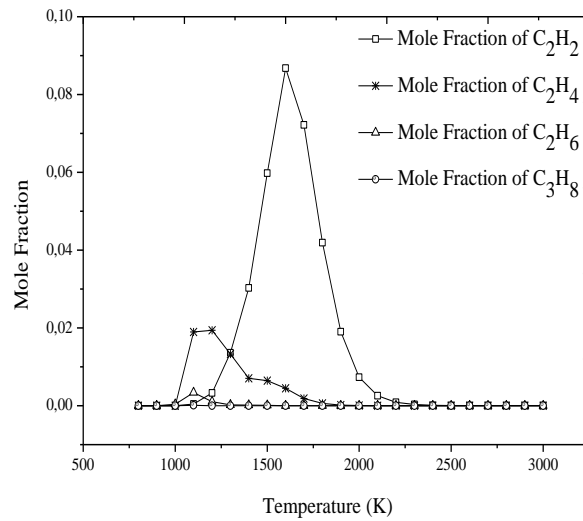


Figure 4.3 Effect of the temperature on C<sub>2</sub>H<sub>2</sub>, C<sub>2</sub>H<sub>4</sub>, C<sub>2</sub>H<sub>6</sub>, C<sub>3</sub>H<sub>8</sub> yields

#### 4.2.2 Effect of residence time

At millisecond contact times, methane is partially oxidized forming H<sub>2</sub> and CO as the main products. As the residence time increases, CO, H<sub>2</sub>, CH<sub>4</sub> and O<sub>2</sub> amounts do not change after ~0.004 s. Figure 4.4 shows effect of residence time on CO and H<sub>2</sub> amounts.

#### 4.2.2 Effect of pressure

Figure 4.5 shows the effect of pressure on H<sub>2</sub> yield. When the temperature below the 1200 K at 1 atm or higher than 2000 K pressure do not have much effect on the synthesis gas production. Pressure significantly affect the syngas production in the temperature range of 1200 K-2000 K. As the pressure increase, H<sub>2</sub> yield decrease.

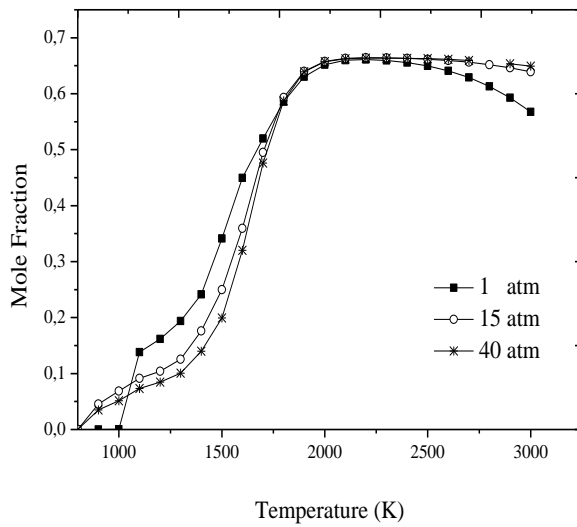


Figure 4.4 Effect of pressure on H<sub>2</sub> yield.

#### 4.2.4 Effect of initial O<sub>2</sub>/CH<sub>4</sub> ratio

When the O<sub>2</sub>/CH<sub>4</sub> is less than 0.5, the equilibrium products contain CO and H<sub>2</sub>. There are no CO<sub>2</sub> and H<sub>2</sub>O. However, as the O<sub>2</sub>/CH<sub>4</sub> is increased from 0.5, partial oxidation and full combustion occur parallel and products consist of a mixture of CO, H<sub>2</sub>, CO<sub>2</sub> and H<sub>2</sub>O. Since the oxidation properties of hydrogen are more than CO, when the initial O<sub>2</sub>/CH<sub>4</sub> ratio exceeds the 0.5, CH<sub>4</sub> is rapidly oxidized and its amount decreases drastically. Figure 4.6 shows changing of major product yields, for different initial O<sub>2</sub>/CH<sub>4</sub> ratios.

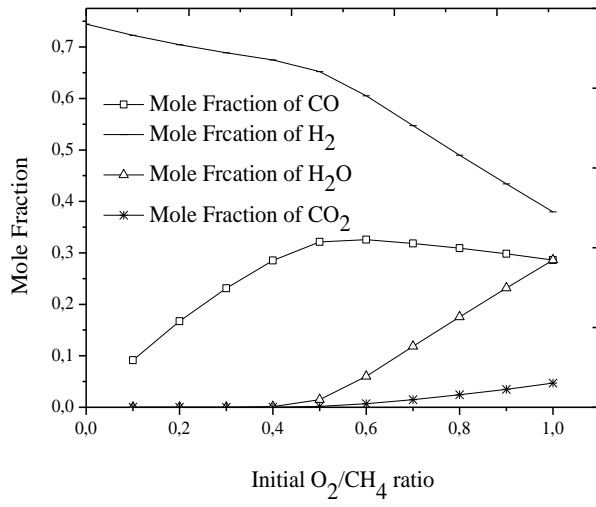


Figure 4.5 Effect of initial  $O_2/CH_4$  ratio on  $H_2$  yield.

## CHAPTER 5

### SYNTHESIS OF Co AND/OR Pb-SBA-15 CATALYSTS: DIRECT SYNTHESIS METHOD

#### 5.1 EXPERIMENTAL

##### 5.1.1 Synthesis of Mesoporous Co and/or Pb SBA-15 Materials by using direct synthesis method

SBA-15 type catalysts were prepared according to the literature [Zhao et al., 1998-a]. In order to synthesize pure SBA15 molecular sieve, 9 ml of tetraethoxy orthosilicate (TEOS) was added to 150 ml of 1.6 M HCl solution containing 4 g triblock poly(ethylene oxide)–poly(propylene oxide)–poly(ethylene oxide) (EO<sub>20</sub>-PO<sub>70</sub>EO<sub>20</sub>, Aldrich). The mixture was stirred for 24 h at 40°C and was allowed to react at 100°C overnight in Teflon bottles. The solid material obtained after filtering was finally calcined in air flow at 500 °C for 5h. In the preparation of the cobalt modified SBA15, an appropriate amount of cobalt was introduced simultaneously with TEOS in the form of cobalt chloride (CoCl<sub>2</sub>·6H<sub>2</sub>O, Merck). Pb modified catalyst was prepared similarly introducing lead in the form of lead acetate ((CH<sub>3</sub>COO)<sub>2</sub>Pb·3H<sub>2</sub>O, Riedel-de Haen) simultaneously with TEOS. Different loadings of catalysts were prepared with respect to content of SiO<sub>2</sub>.

## 5.2 CATALYST CHARACTERIZATION

XRD patterns were measured on a Rigaku-Miniflex diffractometer using Cu K $\alpha$ -ray radiation ( $\lambda=1.5405 \text{ \AA}$ ) operating at 30 kV and 15mA. XRD patterns were recorded between  $2\theta = 1.0\text{--}3.0^\circ$  with  $0.005^\circ$  intervals,  $0.2^\circ$  data collection velocity in one minute; and  $2\theta = 5.0\text{--}75.0^\circ$  with  $0.05^\circ$  intervals,  $1^\circ$  data collection velocity in one minute.

Surface area of the prepared materials were determined by Brunauer, Emet and Teller (BET) method by N<sub>2</sub> adsorption-desorption measured at 77 K on a micromeritics ASAP 2000 volumetric system. The samples were outgassed for 8 h at 363 K in vacuum prior to the nitrogen adsorption measurements at 77 K.

## 5.3 RESULTS AND DISCUSSION

### 5.3.1 N<sub>2</sub> Adsorption

Surface areas were calculated by BET (Brunauer-Emmett-Teller) method. The increase of the metal loading into SBA-15 lead to a decrease in the surface area due to the substitution of pores with metal atoms (Table 5.1). The bimetallic CoPb-SBA15 sample exhibit a drastically low surface area while Co loaded SBA-15 samples show quite high BET surface areas. Increasing of Pb/Si ratio up to 0.15 caused a drastic decrease in the surface area.

Figure 5.1 shows the estimated textural parameters such as BET surface area, adsorption average pore diameter, and cumulative adsorption pore volumes for different samples.



Table 5.1 The mixed oxide catalyst compositions and surface areas

<b>Sample</b>	<b>Co/Si Atomic Ratio</b>	<b>Pb/Si Atomic Ratio</b>	<b>wt %Co</b>	<b>wt %Pb</b>	<b>BET surface area (m<sup>2</sup>/g)</b>
SBA-15	-	-			772.5
Co/SBA-15	0.01	-	0.95		640.1
	0.03	-	2.63		723.1
	0.05	-	4.09		799.3
	0.1	-	7.03		778.5
	0.15	-	9.23		653.5
	0.20	-	10.96		785.8
	0.25	-	12.33		636.7
	0.3	-	13.45		479.5
Pb/SBA-15	-	0.01		3.24	670.2
	-	0.03		8.7	546.7
	-	0.05		13.11	501.8
	-	0.1		21.15	189.6
	-	0.15		26.58	8.14
	-	0.20		30.50	7.54
	-	0.25		33.45	4.63
Co-Pb/SBA-15	0.1	0.1	4.84	17.02	11.4
	0.1	0.3	2.98	31.45	4.2
	0.15	0.1	6.61	15.50	10.3

### 5.3.2 X-Ray Diffraction (XRD)

The wide angle XRD patterns of Co/SBA-15, consisting of different Co/Si ratios, are presented in Fig. 5.1. In the XRD patterns at high diffraction angles ( $2\theta = 5-75^\circ$ ), no characteristic peaks of metal oxide was observed up to Co/Si ratio=0.1 in SBA-15 sample, indicating that Co well dispersed on the surface of the sample or incorporated in the pore walls of silica framework. However, appreciable characteristic peaks are shown for the samples having bigger Co/Si atomic ratio, indicating presence of crystallites of cobalt oxide existing on the surface of silica or within the pores of silica. The peaks observed at  $2\theta \approx 35-40^\circ$  demonstrate that cobalt exists in the form of  $\text{Co}_3\text{O}_4$ .

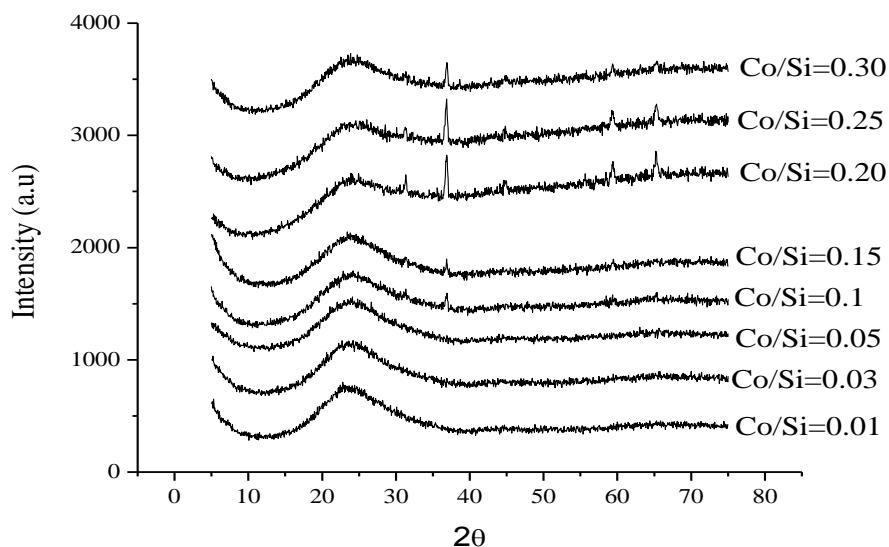


Figure 5.1 High angle XRD patterns of different Co/SBA-15 materials

The ordered hexagonal structure of SBA-15 was observed for first four samples (Co/Si=0.01,0.03,0.05,0.1) via the small angle XRD pattern as it can be seen in Fig. 5.2. For these samples, the hexagonal structure of SBA-15 was confirmed by

a typical XRD pattern consisting of weak two peaks (at  $2\theta$  around  $1.6^\circ$  and  $1.8^\circ$ ). The strong peak at  $2\theta$  around  $0.8^\circ$  could not be observed due to the instrumental limitation. In cobalt incorporated catalysts, the long range order was lost as the Co/Si ratio is increased.

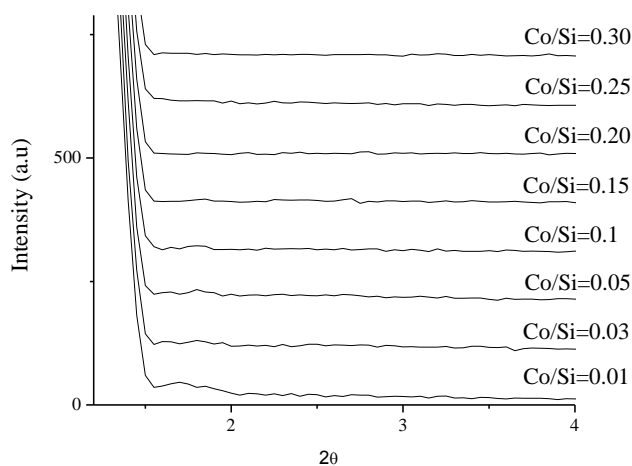


Figure 5.2 Low angle XRD patterns of different Co/SBA-15 materials

The presence of intense characteristic peaks of Pb in the wide angle XRD indicate the formation of crystallites as it can be seen in Fig. 5.3. In contrast to the cobalt loading the addition of Pb cause crystallization at Pb/Si=0.15. The peaks observed at  $2\theta \approx 30-35^\circ$  indicates that lead exist in the form of PbO metal oxide structure. Moreover, the peaks observed at  $2\theta \approx 20-25^\circ$  were assigned to the presence of  $\text{SiO}_2$ .

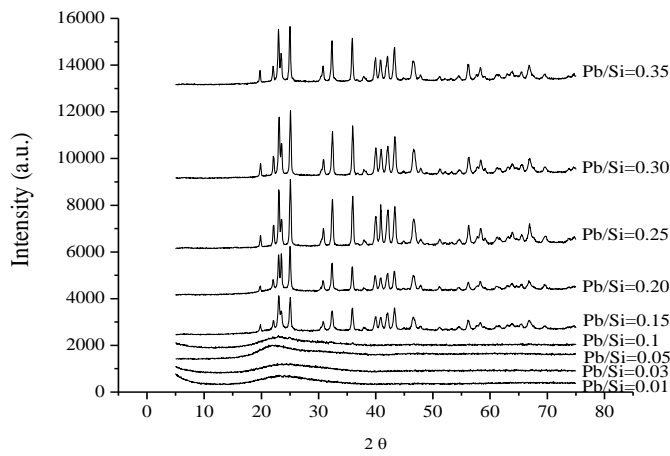


Figure 5.3 High angle XRD patterns of different Pb/SBA-15 materials

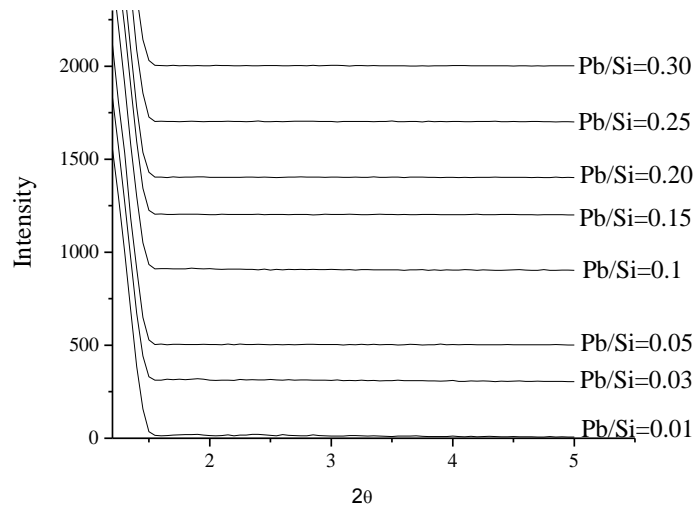


Figure 5.4 Low angle XRD patterns of different Pb/SBA-15 materials

As shown in Fig. 5.5, the XRD patterns at high diffraction angles were obtained by incorporating different amount of Co and Pb into SBA-15. The presence of highly intense characteristic peaks of Co and Pb in the pattern shows that the formation of crystallites increased by the addition of cobalt and lead. The long

range order was lost in the both Pb and Co metal loading to SBA-15 which is observed in Fig.5.6.

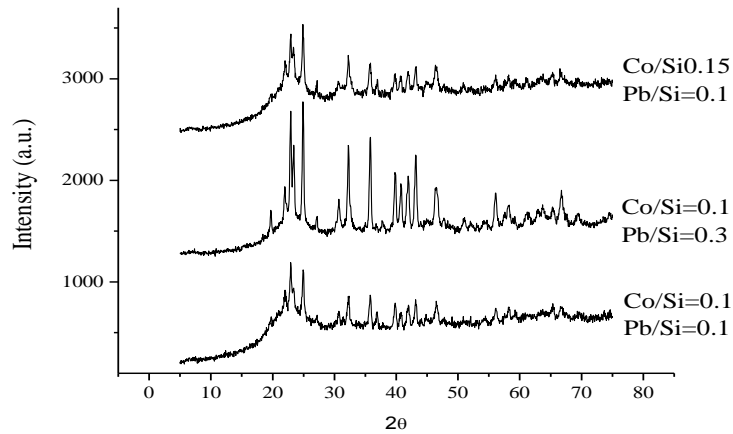


Figure 5.5 High angle XRD patterns of different Co-Pb/SBA-15 materials

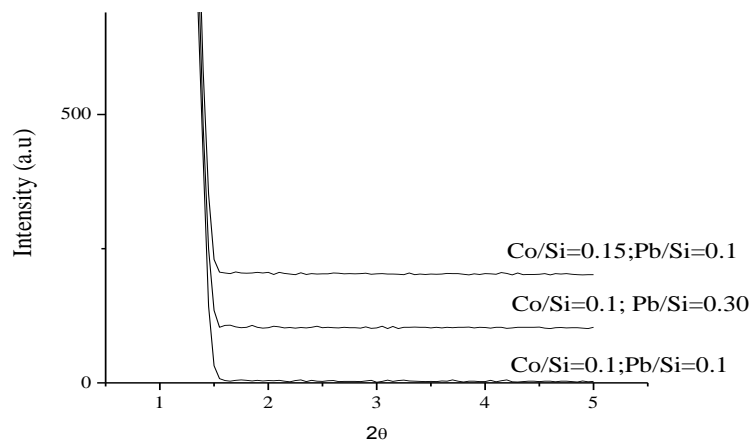


Figure 5.6 Low angle XRD patterns of different Co-Pb/SBA-15 materials

## CHAPTER 6

# SYNTHESIS OF Co and/or Pb/SBA-15 MATERIALS: INCIPIENT WETNESS IMPREGNATION and POST GRAFTING METHODS

### 6.1 INTRODUCTION

The functionalization of mesoporous silica has received notable interest, owing to potential application of these mesoporous materials in catalysis, drug delivery, and adsorption. There are two common methods to functionalization of mesoporous silica: postsynthesis method and co-condensation (one-pot or direct synthesis) method [Brühwiler, 2010]. A great number of metals, metal oxides (sulfides), acid groups and organic functionalities can be incorporated to the mesoporous silica by applying these techniques [Wang et al., 2004].

In postsynthetic methods, which is often called as grafting, functional groups are introduced to the mesoporous silica after the surfactant (structure directing agent) removal. Specific parts of the mesoporous silica surface such as external surface, pore surface, pore entrances can be functionalized without changing the mesostructure [Brühwiler, 2010].

Post synthesis grafting is generally carried out by stirring of mesoporous silica and silane- or polymer-containing amino groups in solvent (e.g. toluene). This method takes advantage of the abundant silanol groups which are available on the mesoporous silica surface. Surface hydroxyl groups (on silanol groups) on the

mesoporous silicas reacts with the alkoxy ligands of the silane forming covalent Si–O–Si bonds. Figure 6.1 represents the surface modification of hydroxyl groups with alkoxy silane via post-synthesis method [Chew et al., 2010 ;Brühwiler, 2010].

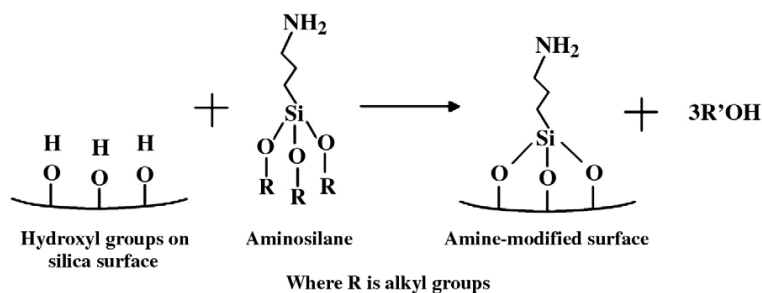


Figure 6.1 Schematic of post synthesis grafting to functionalize silica surface with amine group [Chew et al., 2010].

In this part of the thesis, Co and/or Pb are loaded to as synthesized SBA-15 mesoporous silica by using incipient wetness impregnation method and loaded to NH<sub>2</sub> functionalized SBA-15 prepared by post grafting method. Characterization of the samples were done by BET, XPS, TEM and Raman techniques.

## 6.2 EXPERIMENTAL

### 6.2.1 Synthesis of Pure SBA-15

Pure SBA-15 sample was synthesized according to Zhao et al. [1998-b]. 4.07 g Pluronic P123 (BASF) were dissolved in 150 ml 1.6 molar HCl in a closed PE bottle standing in an oil bath of 35°C. After the mixture was stirred about 1h, 9 ml tetraethoxysilane (TEOS, 99+%, Alfa Aesar) were added to this solution. Stirring was continued for 20 h at 35 °C. After aging for 24 h at 85 °C, the suspension was filtered and washed over a nutsch filter (frit with porosity 4) and a vacuum flask.

For the washing procedure, distilled water and ethanol were used. The resultant material was calcined for 12 h at 550°C.

### **6.2.2 Synthesis of Amino Functionalized SBA-15 via Post-Synthesis grafting Method**

6.4 ml of 3-aminopropyltrimethoxysilane (APTMS, 97%, Aldrich) was added to a stirred suspension of 2.5 g SBA-15 in 100 ml toluene at 65°C under reflux. The suspension was stirred for 12 h at this temperature, then it was filtered and washed with toluene in order to remove all free amine. Washing procedure was performed 5 times over a Nutsche filter (frit with porosity 4) and a vacuum flask. A new amount of toluene was not used until the former was eliminated of [Hess et al., 2004].

For incorporation of the metals (cobalt and lead), the amino-functionalized SBA-15 samples treated with defined amount solution of  $\text{CoCl}_2 \cdot 6\text{H}_2\text{O}$  and  $(\text{CH}_3\text{COO})_2\text{Pb} \cdot 3\text{H}_2\text{O}$  for 4 h at room temperature. After that, the powder was collected by filtration and dried at room temperature overnight. The calcination was done at 550 °C for 12 h [Yokoi et al., 2004].

### **6.2.3 Synthesis of Co and/or Pb-SBA15 materials by incipient wetness impregnation method**

The impregnation solution was prepared by dissolving an appropriate amount of cobalt and lead salts in distilled water. Approximately 2.5 ml of solution per gram of support was needed to bring about incipient wetness. The slurries obtained after impregnation were dried at 120°C for 12 hours. After that, the catalyst prepared was calcined in air at 500 °C for 5 h [Xiong et al., 2008].



### **6.3 CHARACTERIZATION OF THE CATALYSTS**

Surface characterization of catalysts for quantification of surface composition, X-ray Photoelectron Spectroscopy (XPS) was performed. The method reveals which chemical elements are present at the surface. The X-ray photoelectron spectra were obtained using Mg K $\alpha$  ( $h\nu=1253.6$  eV) unmonochromatized radiation with SPECS spectrometer. The charging effects were corrected by using the C1s peak, as reference for all samples at a binding energy BEof 284.6 eV.

Surface areas of the synthesized catalysts were determined by Brunauer, Emet and Teller (BET) method by N<sub>2</sub> adsorption-desorption measured at 77 K on a micromeritics ASAP 2000 volumetric system. The samples were outgassed for 8 h at 363 K in vacuum prior to the nitrogen adsorption measurements at 77 K. Raman spectra were measured at room temperature with an excitation wavelength of 514 nm and a power of 10 mW (measured with Ophir P/N 1J06013 Laser power/energy monitor).

### **6.4 RESULTS AND DISCUSSION**

#### **6.4.1 N<sub>2</sub> Adsorption**

Surface areas were calculated by BET (Brunauer-Emmett-Teller) method and pore size distributions were determined using the BJH (Barrett-Joyner-Halenda) method. The estimated textural parameters such BET surface area, adsorption average pore diameter, and cumulative adsorption pore volumes for different weight loaded Co and or Pb SBA-15 catalysts are shown in Table 6.1 and 6.2.

Pure SBA-15 BET surface area is 658,52m<sup>2</sup>/g. This confirm the highly ordered mesostructure in good agreement with the TEM result. Co and Pb loaded catalysts have lower surface areas than pure SBA-15.

The average pore diameter of SBA-15 is 65.9 Å and by the introduction of Co or Pb into SBA-15 pore diameter does not change drastically. However, pore volume decrease with the addition of the Co and Pb. The increase in the metal loadings of metals in SBA-15 result in a decrease in the surface area due to the blocking of pores with metal atoms. The decrease in the pore volume by metal loading is in consistent with the surface area measurements.

Table 6.1 The mixed oxide catalyst compositions and surface areas (Incipient Wetness Impregnation Method: Cobalt Chloride based)

Sample	Co wt%	Pb wt%	BET surface area (m <sup>2</sup> /g)	D <sub>BJH</sub> (Å)	V <sub>BJH</sub> (cm <sup>3</sup> /g)
SBA-15	-	-	658,5	65,9	0,56
Co/SBA-15	5	-	449,1	69,4	0,51
	10	-	411,2	62,8	0,46
	20	-	254,6	69,4	0,40
Pb/SBA-15	-	5	482,8	65,8	0,55
	-	10	456,0	63,6	0,50
	-	20	318,8	62,6	0,43
Co-Pb/SBA-15	5	5	439,0	65,9	0,53
	5	10	305,0	69,3	0,54

Table 6.2 The mixed oxide catalyst compositions and surface areas (Functionalized SBA-15 samples)

Sample	Co wt%	Pb wt%	BET surface area (m <sup>2</sup> /g)	D <sub>BJH</sub> (Å)	V <sub>BJH</sub> (cm <sup>3</sup> /g)
SBA-15	-	-	658,5	65,9	0,56
Co/SBA-15	5	-	395,6	62,5	0,43
	10	-	502,9	65,9	0,56
Pb/SBA-15	-	5	333,3	62,9	0,42
	-	10	310,8	51,8	0,46
Co-Pb/SBA-15	5	5	420,3	62,6	0,51

Figure 6.2 shows N<sub>2</sub> adsorption desorption isotherm of the of SBA-15. The nitrogen adsorption-desorption isotherms of the all the catalysts were given in Appendix B. All the catalysts exhibit type IV adsorption isotherms. Type H1 hysteresis loop was observed for all catalysts samples, which is a characteristic of mesoporous silica solids. The TEM images indicated that SBA-15 has more ordered structure than cobalt and lead loaded catalyst.

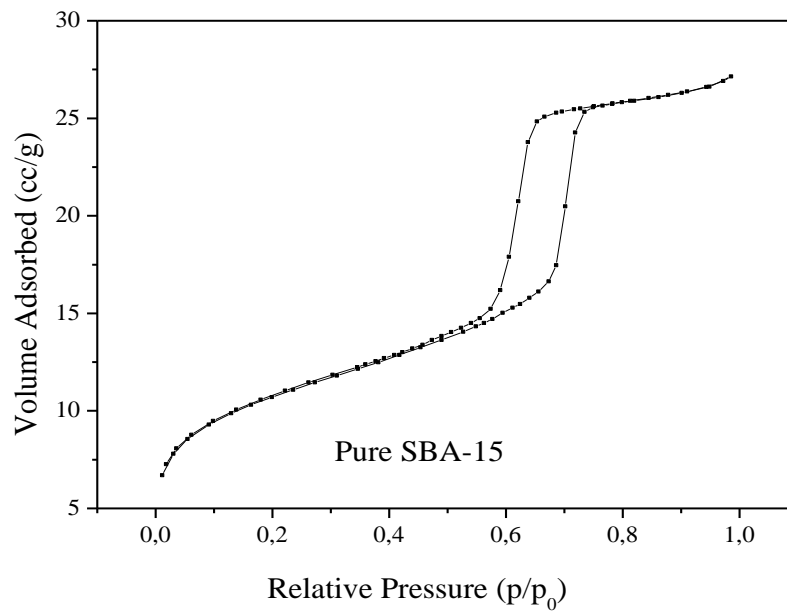


Figure 6.2 Nitrogen adsorption-desorption isotherms of pure SBA-15.

#### 6.4.2 Transmission Electron Microscopy

The TEM images of pure SBA-15 confirm the ordered structure of the material, and shows the cylindrical pores are arranged in an ordered hexagonal array. The TEM image of pure SBA-15 are given in Fig. 6.3.

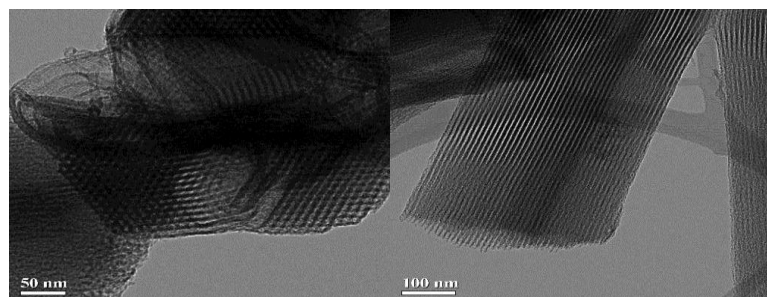


Figure 6.3 TEM images of pure SBA-15

As it can be seen in Fig. 6.4 %5wt %5Pb loaded SBA-15, when cobalt and lead was incorporated to the SBA-15 structure, the mesostructure was retained. The catalyst possesses the typical two-dimensional hexagonal structure of SBA-15. Also there are big Co and Pb oxide particules are available on the SBA-15 structure.

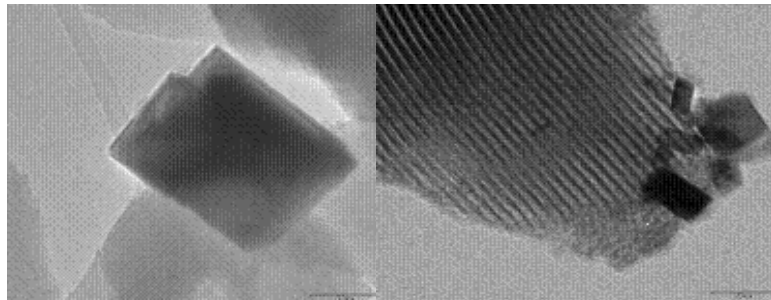


Figure 6.4 TEM images of pure %5Co-%5 Pb impregnated SBA-15 sample

TEM images of 10%Co functionalized SBA-15 sample and%5wtCo%5wtPb functionalized SBA-15 sample (fig. 6.5 and 6.6 show thatnanoparticles are well and periodically located within mesochannels of SBA-15 materials, there is no indication of nano particules on the surface of SBA-15 structure. Cobalt and or lead could not be distinguished in the TEM images at this loading, which indicates a high dispersion of cobalt and lead in the mesostructure.

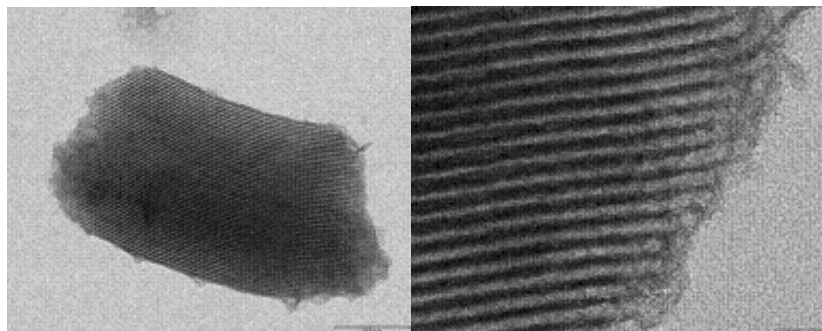


Figure 6.5 TEM images of pure %10Co functionalized SBA-15 sample

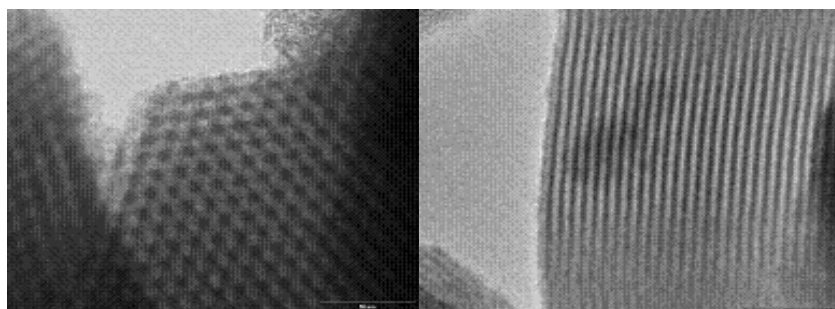


Figure 6.6 TEM images of %5Co%5 Pb functionalized SBA-15 sample

### 6.4.3 X-Ray Photoelectron Spectroscopy

Surface characterization of Pb and Co was performed by XPS for revealing the oxidation states of the species. Table 6.3 show Co 2p binding energy values of some Co containing catalyst materials.

Table 6.3 Co 2p binding energy values of different samples.

Sample	Co 2p <sub>3/2</sub>	Co 2p <sub>1/2</sub>	Ref.
CoO	780.9	795.7	[Christoskova et.al, 1999]
Co/Al <sub>2</sub> O <sub>3</sub>	781.4	796.2	[Mendes et.al, 2006]
Co/5%Nb <sub>2</sub> O <sub>5</sub> /Al <sub>2</sub> O <sub>3</sub>	781.2	796.2	[Mendes et.al, 2006]
Co/Nb <sub>2</sub> O <sub>5</sub>	780	795.4	[Mendes et.al, 2006]
CuCo/SiO <sub>2</sub>	782.6	-	[Llorca et.al, 1999]
Co <sub>43</sub> Al <sub>18</sub> O <sub>39</sub>	781.5	-	[Asami et.al, 1999]
Cu-Co/SiO <sub>2</sub>	778.1	793.2	[Cesar et.al, 2001]
%5CoO <sub>x</sub> /TiO <sub>2</sub>	781.3	-	[Kim, 2005]
Co/Al <sub>2</sub> O <sub>3</sub>	779.8	-	[Xiong et.al, 2005]
Co/Zr/Al <sub>2</sub> O <sub>3</sub>	780	-	[Xiong et.al, 2005]
Co/SiO <sub>2</sub>	780.5	-	[Zhou et.al, 2006]
Co/Zn/SiO <sub>2</sub>	781	-	[Nobuntu et.al, 2007]
25%Co/SiO <sub>2</sub>	779.7	-	[Ernst et.al, 1998]
Co/SBA-15	781.7	-	[Khodokov et.al, 2002]
Co-HMS	781.7	797.9	[Bhoware et.al, 2006]

Figure 6.7 and 6.8 show XPS spectra of the Co 2p level for Co and/or Pb impregnated SBA-15 mesoporous silica samples.

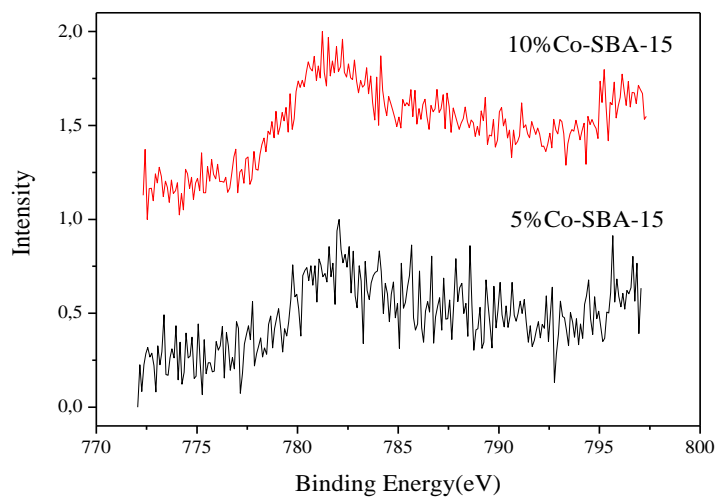


Figure 6.7 XPS spectra of the Co 2p level for Co impregnated mesoporous silica samples

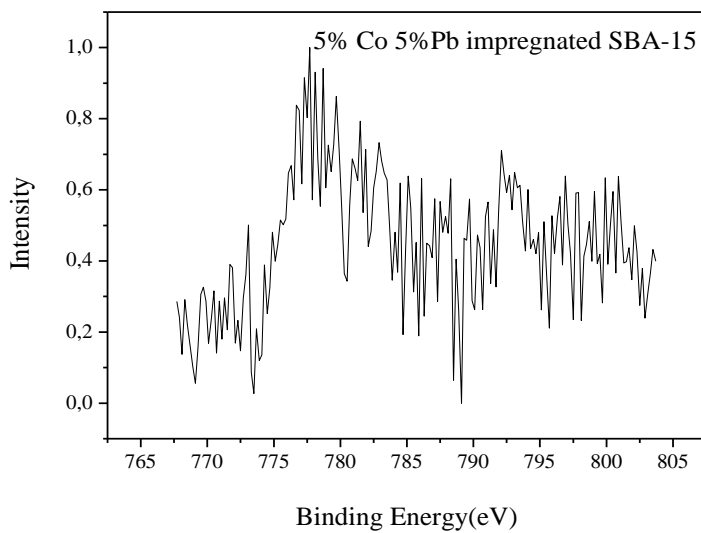


Figure 6.8 XPS spectra of the Co 2p level for Co and Pb impregnated mesoporous silica samples.



Table 6.4 Co 2p binding energy values of Co-SBA-15 catalysts (Incipient Wetness Impregnation Method)

Sample	Co 2p <sub>3/2</sub> (e V)	Co 2p <sub>1/2</sub> (e V)
5%Co-SBA-15	781,90	
10%Co-SBA-15	781,65	796,5
5%Co-10%Pb-SBA-15	780,30	796,05

Co<sub>3</sub>O<sub>4</sub> which is an spinel oxide phase of cobalt exhibit two oxidation states: Co<sup>3+</sup> is in octahedral symmetry and Co<sup>2+</sup> is in tetrahedral symmetry. Co<sup>3+</sup>/Co<sup>2+</sup> ratio is 2:1 in Co<sub>3</sub>O<sub>4</sub> cobalt oxide phase. As it can be seen in Table 6.4, Binding energy value of Co 2p<sub>3/2</sub> for 5%Co-10%Pb-SBA-15 sample shows typical Co<sup>2+</sup>/Co<sup>3+</sup> ions in the Co<sub>3</sub>O<sub>4</sub> spinel phase. In the case of 5%Co-SBA-15 and 10%Co-SBA-15 catalysts, the Co 2p<sub>3/2</sub> peak binding energies was shifted to higher energies (BE 781,6 and 781,9 Ev, respectively) [Zhou et.al, 2006].

In the literature it has been announced that cobalt series occupy the identical binding energy region belonging to Co 2p<sub>3/2</sub> and Co 2p<sub>1/2</sub> electrons, however, since the chemical shift of main peaks in XPS spectra of Co 2p electrons in Co<sup>2+</sup> and Co<sup>3+</sup> is not obvious enough, the distinction among the cobalt compound is still unclear. So, it is difficult to distinguish the monoxide and the spinel of the cobalt compounds only by the main peak position in XPS spectra. However, distinguishing the monoxide and spinel of the cobalt compounds. the satellite structures of the main peaks and the intensity ratio of the Co 2p<sub>1/2</sub> satellite to its to main peak have been used. Considering this information, It can be said that 5%Co-SBA-15 and 10%Co-SBA-15 samples also contain Co<sub>3</sub>O<sub>4</sub> [Khadokov et.al, 2002 ; Martinez et al., 2003]. The Raman analysis also show that in these catalysts Co is in the form of Co<sub>3</sub>O<sub>4</sub>.

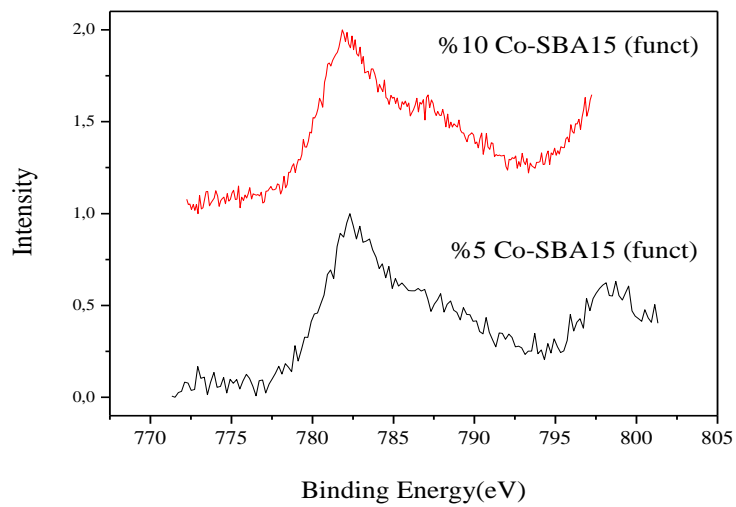


Figure 6.9 XPS spectra of the Co 2p level for Co functionalized mesoporous silica samples

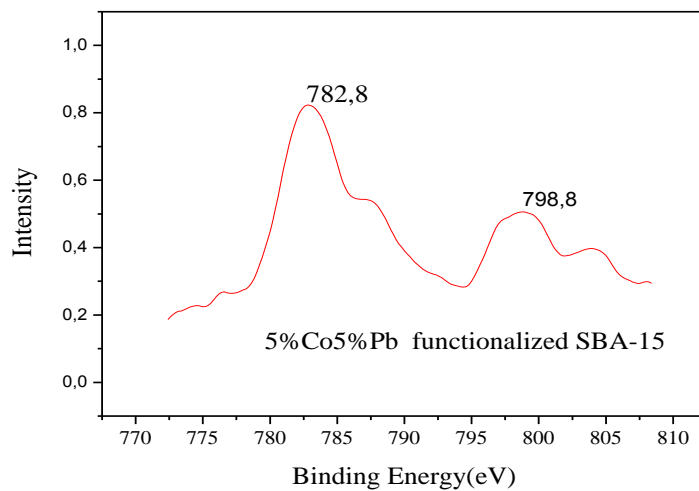


Figure 6.10 XPS spectra of the Co 2p level for Co and Pb functionalized mesoporous silica sample.

Figure 6.9 and 6.10 show that XPS spectra of the Co 2p level for Co functionalized mesoporous silica samples. Co 2p<sub>3/2</sub> binding energy values for the Co-SBA-15 (functionalized) materials can be seen in Table 6.5. Regarding the information reported above, it can be said that functionalized samples also include Co<sub>3</sub>O<sub>4</sub> forms of the cobalt.

Table 6.5 Co 2p binding energy values of Co-SBA-15 catalysts (Post Grafting Method)

Sample	Co 2p <sub>3/2</sub>	Co 2p <sub>1/2</sub>
5%Co-SBA-15 (funct)	782,3	798,3
10%Co-SBA-15 (funct)	781,9	
5%Co-5%Pb-SBA-15 (funct)	782,8	798,8

According to the XPS results, the O1s binding energy around 533 eV exhibit characteristic oxygen in SiO<sub>2</sub> [Khakadov et al., 2002].

#### 6.4.1 Raman Spectroscopy

Raman spectra of the catalysts samples were measured at room temperature with an excitation wavelength of 514 nm and a power of 10 mW (measured with Ophir P/N 1J06013 Laser power/energy monitor).

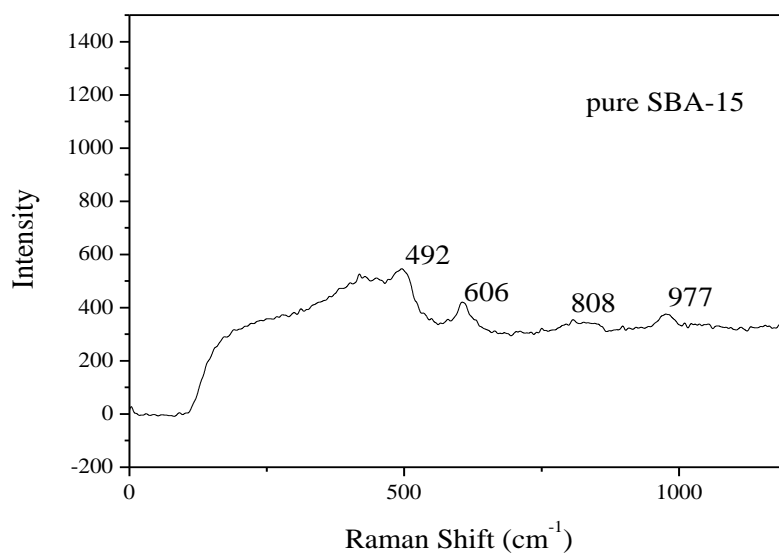


Figure 6.11 Raman Spectra of pure SBA-15

Figure 6.11 shows the Raman spectrum of pure SBA-15 sample. The 492 cm<sup>-1</sup> band can be attributed to cyclic tetrasiloxane rings of the silica support. Raman bands at 604, 808, 977 are assigned to cyclic trisiloxane, the symmetrical Si-O-Si stretching mode and Si-OH stretch of surface hydroxyl groups, respectively [Hess et.al, 2007].

The results of the Raman analysis of the Co impregnated and Co and Pb impregnated SBA-15 samples shows the typical characteristic peaks of the Co<sub>3</sub>O<sub>4</sub> oxidation state. Figure 6.12 shows the Raman Shift of these samples.

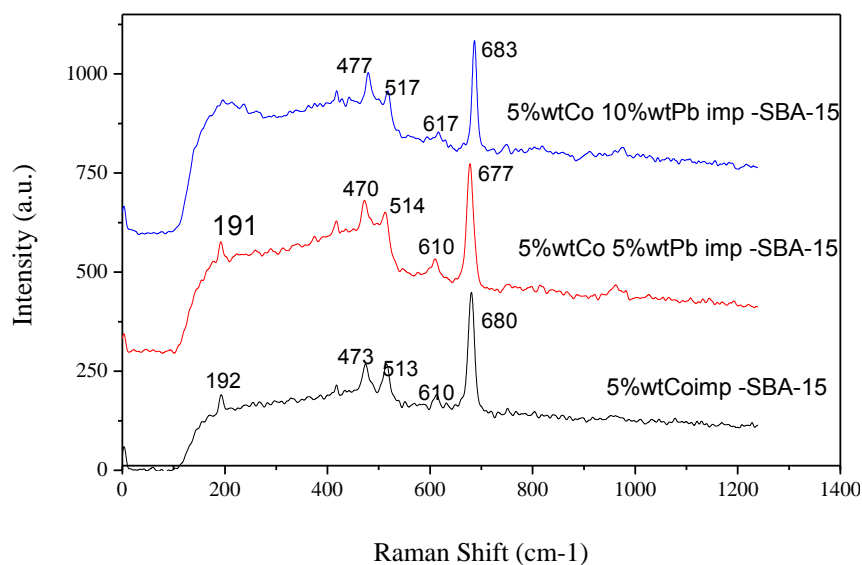


Figure 6.12 Raman Spectra of Co and/or Pb impregnated SBA-15 samples.

Raman spectra of the Co and/or Pb-SBA-15 samples exhibit five Raman peaks (Figure 6.12) located at around 192, 475, 516, 615 and 680  $\text{cm}^{-1}$ , which correspond to all the five Raman-active modes ( $A_{1g}$ ,  $E_g$  and  $3F_{2g}$ ) of  $\text{Co}_3\text{O}_4$  [Zhou et al., 2007 ; Yung et al., 2007]. These samples do not show any Pb oxide crystallites. One reason may be the high metal loading. Higher loaded samples tend to agglomeration of deposited oxides. Addition to loading effects another possible reason may be that in case of Co oxides the presence of crystallites dominates whereas in case of Pb oxides more amorphous phases form. As crystallites give stronger Raman signals they may dominate over amorphous phases.

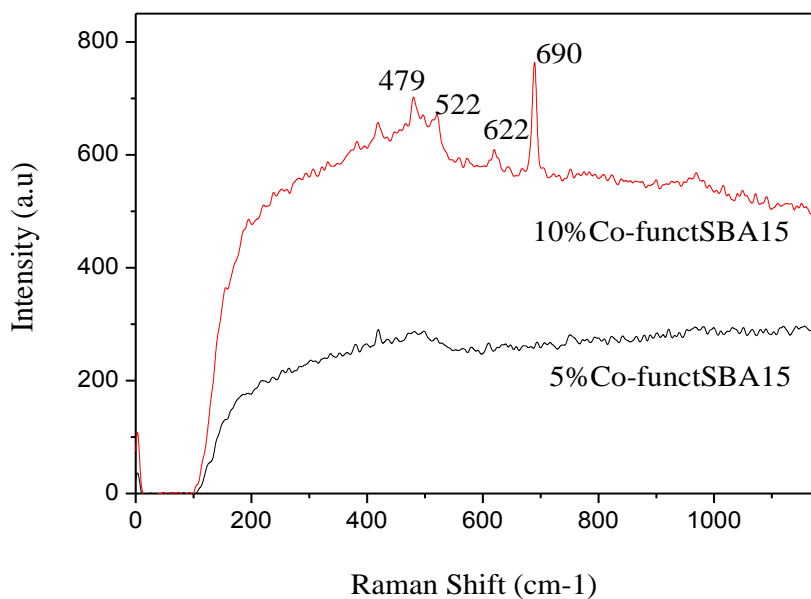


Figure 6.13 Raman Spectra of Co funct-SBA15 sample.

Figure 6.13 shows the Raman Shift of Co-funct SBA-15 samples. As in impregnated samples also, Co functionalized SBA-15 samples (10%Co funct SBA-15) show the  $\text{Co}_3\text{O}_4$  oxidation state.

Only Pb impregnated SBA-15 samples did not show any oxide of Pb Raman peak. As can be seen in Figure 6.14, The Raman spectrum of 10%Pb-SBA-15 sample shows only typical SBA-15 Raman bands at 491, 605, 808 and  $977\text{ cm}^{-1}$ . However, The Raman spectrum of SBA-15 catalyst containing 5%wt Pb present cyclic tetrasiloxane rings of the silica support.

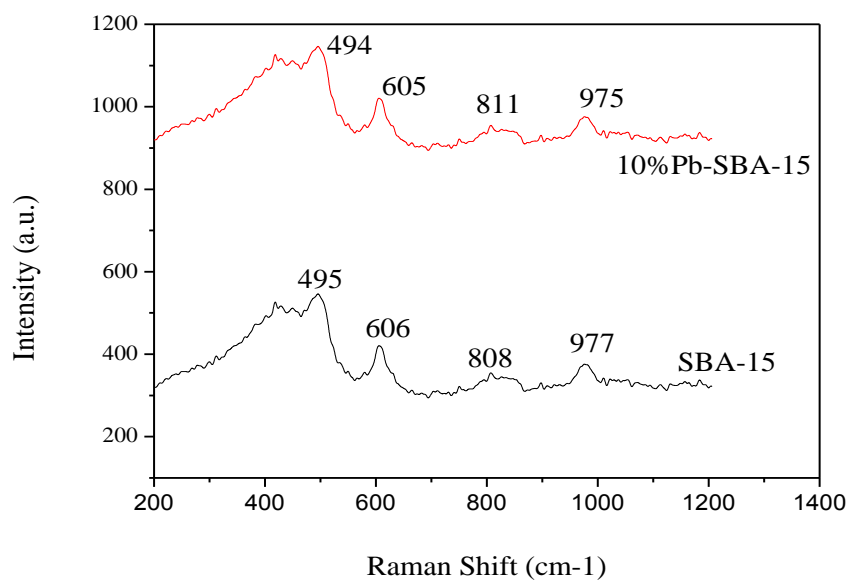


Figure 6.14 Raman Spectra of Pb impregnated-SBA15 sample.

## CHAPTER 7

# SYNTHESIS OF SBA-15 WITH DIFFERENT PORE SIZES

### 7.1 INTRODUCTION

The pore size is a critical physical parameter for OMMs and, can be adjusted depending on their applications. The studies revealed that controlling of the mesopore diameter can be accomplished by using surfactants with various tail lengths, polymer as templates, by adding organic additives, such as 1,3,5-trimethylbenzene, triisopropylbenzene, alkanes, amines and tetraalkylammonium cations, and also by the hydrothermal post-synthesis treatment. Nonetheless, the addition of organic auxiliary chemical during the hydrothermal synthesis process is one of the most efficient approaches to synthesize mesoporous material with larger pore diameter. In recent years, it has been observed that, using of 1,3,5-trimethylbenzene and/or 1,3,5-triisopropylbenzene as auxiliary chemical(s) during the synthesis increased the pore size of the MCM-41 material drastically [Zang et al., 2006 ; Jana et al., 2004].

Although to enlarge and to decrease the pore size morphology are the two main feature to manipulate the pore size of OMMs, the studies have generally been focused on the enlargement of the pore size, while very few on the decrease of the pore morphology. By using short double chain surfactants as templates, MCM-41-type materials with the pore size near the region between micropores and mesopores have recently been synthesized.



It is reported that the addition of CTAB as co-structure-directing agents to the solution could be decreased the main pore sizes of SBA-15 materials continuously by controlling the micelle properties of P123. In addition, inorganic salts such as KCl,  $\text{NH}_4\text{F}$  or  $\text{NaSO}_4$  have important effects on the micelle properties [Zang et al., 2006].

In this chapter of the thesis, pure SBA-15 silica materials were synthesized by using both cationic surfactant (CTAB) and inorganic salt (KCl) to tailor the pore size of the materials. 1%Pt-SBA-15 materials were the materials. The characterization of the samples were done by using XRD, BET and FTIR characterization techniques.

## **7.2 EXPERIMENTAL**

### **7.2.1 Synthesis of SBA-15 materials**

Two type of samples were synthesized to investigate the pore size change :a) Different amounts of CTAB (cetyltrimethylammonium bromide) was added into the solution of P123 ( $\text{EO}_{20}\text{PO}_{70}\text{EO}_{20}$ ) at a constant concentration, b) Different amounts of KCl were added into the solution of P123 and CTAB at a constant ratio and concentration. In the synthesis process, Firstly, 2 g of P123 was dissolved completely in 75 ml of 1.6 M HCl. After that, a calculated amount of CTAB dissolved into this solution. Then 3.3 g TEOS ( $\text{C}_8\text{H}_{20}\text{O}_4\text{Si}$ ) was added to this mixture under rigorous stirring. The mixture was stirred for about 20 h. All of the processes were kept at  $40^\circ\text{C}$ . The white material obtained was transfer into Teflon bottles and aged at  $100^\circ\text{C}$  for 24 h. After the white powders were recovered, washed and dried, the material was calcined at  $500^\circ\text{C}$  for 8 h. After the calcination, SBA-15 mesoporous samples were finally obtained [Zang et al., 2006].

### **7.2.2 Synthesis of 1%Pt-SBA15 material by using incipient wetness impregnation method.**

The impregnation solution was prepared by dissolving an appropriate amount of  $\text{PtCl}_2(\text{NH}_3)_4 \cdot \text{H}_2\text{O}$  salt in distilled water. Approximately 3.5 ml of solution per gram of support was needed to bring about incipient wetness. The slurries obtained after impregnation were dried overnight at room temperature and at  $150^\circ\text{C}$  for 2 h. After that, the catalyst prepared was calcined in air at  $410^\circ\text{C}$  [Uner and Uner, 2005].

### **7.3 CATALYST CHARACTERIZATION**

XRD patterns were measured on a Rigaku-Miniflex diffractometer using Cu  $K\alpha$ -ray radiation ( $\lambda=1.5405 \text{ \AA}$ ) operating at 30 kV and 15mA. XRD patterns were recorded between  $2\theta = 1.0\text{--}3.0^\circ$  with  $0.005^\circ$  intervals,  $0.2^\circ$  data collection velocity in one minute; and  $2\theta = 5.0\text{--}75.0^\circ$  with  $0.05^\circ$  intervals,  $1^\circ$  data collection velocity in one minute.

Surface area of the synthesized catalysts were determined by Brunauer, Emet and Teller (BET) method by  $\text{N}_2$  adsorption-desorption measured at 77 K on a micromeritics ASAP 2000 volumetric system. The samples were outgassed for 8 h at 363 K in vacuum prior to the nitrogen adsorption measurements at 77 K.

FTIR spectra were obtained using a Nicolet 510 Fourier Transformed Infrared Spectrometer at room temperature. Spectra were recorded by accumulating 20 scans and  $4 \text{ cm}^{-1}$  resolution. After the background KBr spectra were obtained, spectra originating from the samples were recorded in the mid-IR region ( $4000 - 400 \text{ cm}^{-1}$ ).

## 7.4 RESULTS AND DISCUSSION

### 7.4.1 N<sub>2</sub> Adsorption

Table 7.1 shows that BET surface area and pore diameter of materials having different P123/CTAB ratio. As can be seen in the table the increase in the second template (CTAB) in SBA-15 causes a decrease in the surface areas and pore diameters. When this ratio is kept at 1/4 and KCl (inorganic additives) amount is changed, both surface area and pore diameter decreases. However, increasing of KCl did not cause any significant effect while this ratio is constant as 1/5.

Table 7.1 Synthesis conditions and parameters of SBA-15 materials

Samples number	P123/CTAB (molar ratio)	KCl (gr)	BET surface area(m <sup>2</sup> /g)	D <sub>BJH</sub> pore diameter(Å)
1	1/4	0.11	591.9	47.1
2	1/4	0.21	594.5	48.2
3	1/4	5.62	559.5	43.0
4	1/4	11.24	367.4	43.3
5	1/5	0.11	650.6	47.0
6	1/5	0.21	586.5	51.0
7	1/5	5.62	492.6	46.2
8	1/5	11.24	387.9	48.4

N<sub>2</sub> adsorption-desorption isotherms of the samples can be seen in Figure 7.1 and 7.2. For samples prepared by using P123/CTAB=1:4 ratio, all samples showed type IV hysteresis loop indicating the mesoporous structure, and adding KCl did

not cause any effect. However, when the P123/CTAB ratio is 1/5, as the KCl amount increase it is seen that the adsorption and the desorption curves begin to approach each other. Sample 5 and 6 show  $H_1$  type hysteresis loops, while sample 7 and 8 show  $H_2$  type hysteresis loop, meaning that the pores of former 2 samples are open and cylindrical, the pores of the last 2 samples is somewhat blocked.

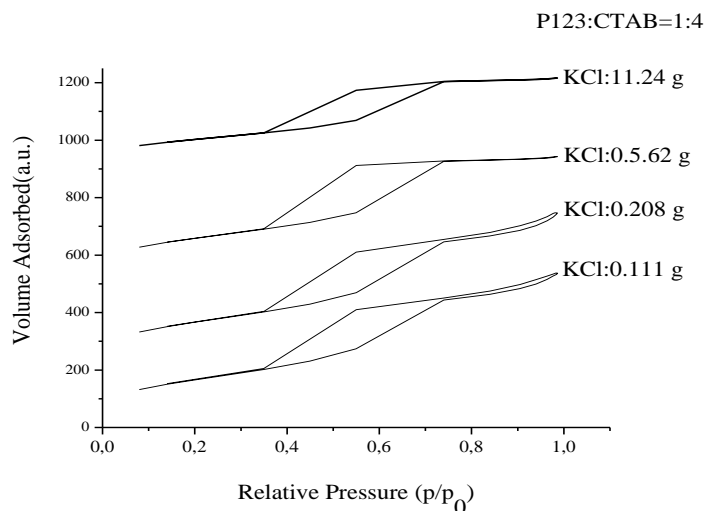


Figure 7.1  $N_2$  adsorption-desorption isotherms of P123/CTAB ratio 1/4 sample

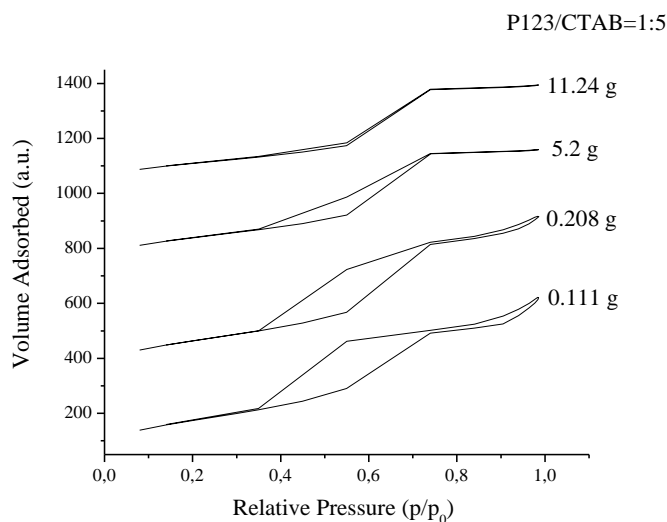


Figure 7.2  $N_2$  adsorption-desorption isotherm of P123/CTAB ratio 1/5 sample

#### 7.4.2 X-Ray Diffraction (XRD)

The ordered hexagonal structure of SBA-15 is confirmed by typical diffractions in all samples as it can be seen in Fig. 7.3 and 7.4. The strong peak at  $2\theta$  around  $0.8^\circ$  could not be observed due to the instrumental limitation. Two characteristic peaks of SBA-15 ( $2\theta=1.6, 1.8^\circ$ ) structure observed in the low-angle X-ray patterns for SBA-15 materials were shifted to right side for all samples. This confirms that pore size of these samples decreases since this two theta values inversely proportional to particle size. When P123/CTAB ratio is kept at 1/4 and KCl (inorganic additives) amount is increased, the orderness increases as it can be seen in Figure 7.3. But, this change is not clear in samples 5,6,7,8 (P123/CTAB=1/5) (fig. 7.4).

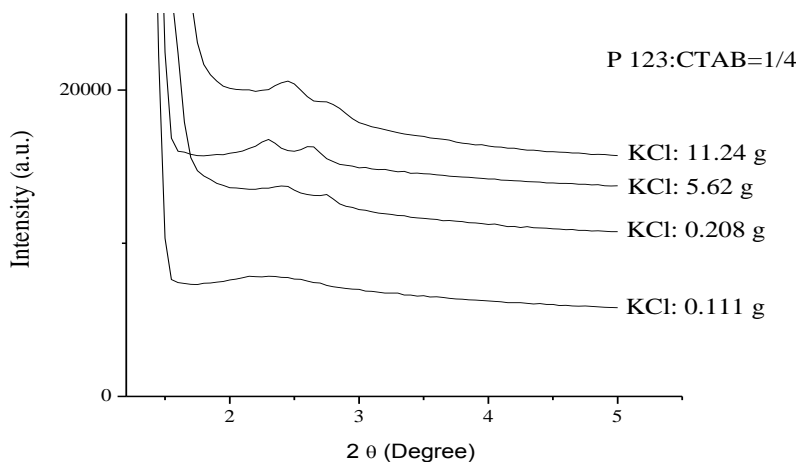


Figure 7.3 Low angle XRD patterns of different SBA-15 materials (P123/CTAB=1:4)

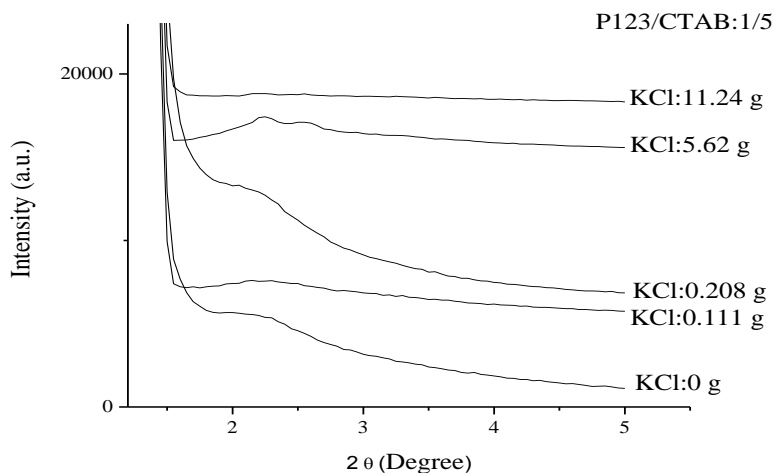


Figure 7.4 Low angle XRD patterns of different SBA-15 materials (P123/CTAB=1:5)

Figure 7.5 and 7.6 show that the low angle and high angle XRD pattern of 1%Pt-SBA15 (prepared by incipient wetness impregnation) catalysts, respectively. Low angle XRD pattern of 1%Pt-SBA15 catalysts shows that the ordered hexagonal structure of SBA-15 is confirmed by typical diffractions for all samples as can be seen in Fig. 5. However, the best ordered structures was obtained for samples (P123/CTAB=1/2) and (P123/CTAB=1/4). The high angle XRD patterns of 1%Pt/SBA-15 catalysts (prepared by incipient wetness impregnation method) indicated the presence of crystallinities of Pt.

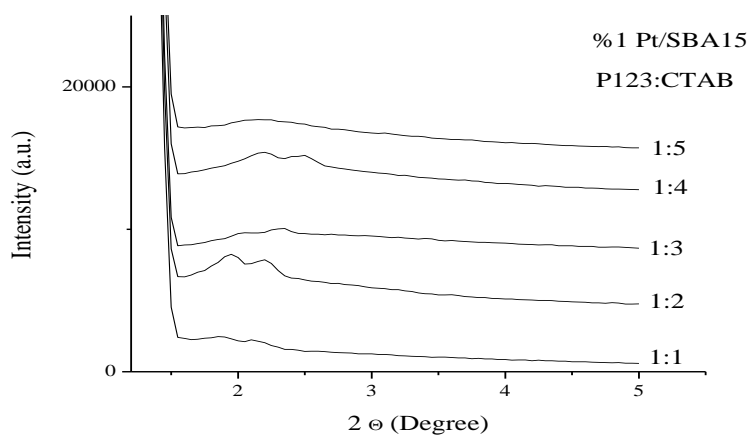


Figure 7.5 Low angle XRD pattern of 1%Pt/SBA-15 catalyst prepared by incipient wetness impregnation method at different pore diameter.

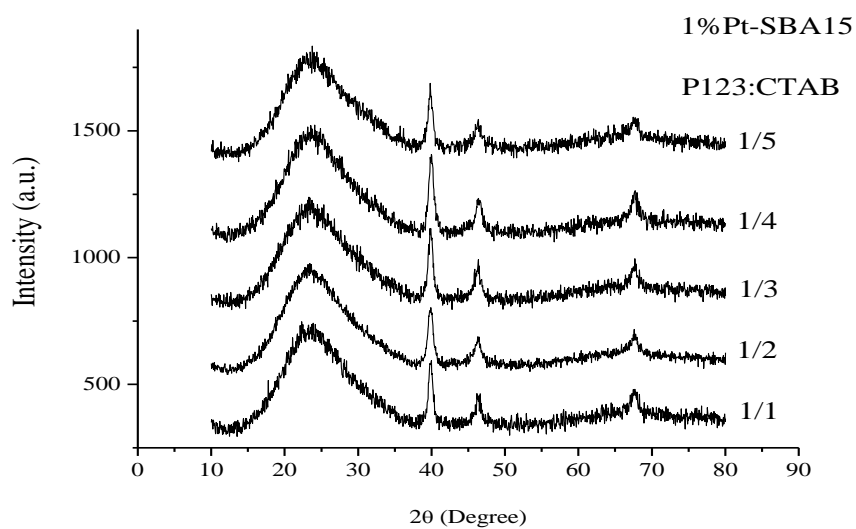


Figure 7.6 High angle XRD pattern of 1%Pt/SBA-15 catalyst prepared by incipient wetness impregnation method at different pore diameters.

### 7.4.3 FTIR Analysis

The FTIR spectra shows the functional groups vibration modes of the catalysts. The large band at  $3432\text{cm}^{-1}$  can be assigned to vibration absorption of the silanol groups ( $\nu_{\text{OH}}$  (Si-O-H)). Three main peaks observed at  $400$  and  $1600\text{ cm}^{-1}$ ,  $\sim 465\text{ cm}^{-1}$ ,  $\sim 800\text{ cm}^{-1}$ ,  $\sim 1090\text{ cm}^{-1}$ , are caused by tetrahedral oxygen atoms' vibration, asymmetric stretching movements exist in  $\text{SiO}_2$ . All the samples shows these bands (Fig 7.7, 7.8, 7.9). Absorption band observed at  $\sim 960\text{ cm}^{-1}$  due to the  $\nu_{\text{as}}$  (Si-OH) vibrations obtained by  $\text{Si-O}^- \text{R}^+$  groups form into  $\text{Si-O}^- \text{H}^+$  groups. The peak intensity at  $960\text{ cm}^{-1}$  decreases in some samples. This is because decreasing of the Si-O-R or Si-OH groups. This difference is shown easily in Pt containing samples but this discrimination not clear in SBA15 samples with no metal.

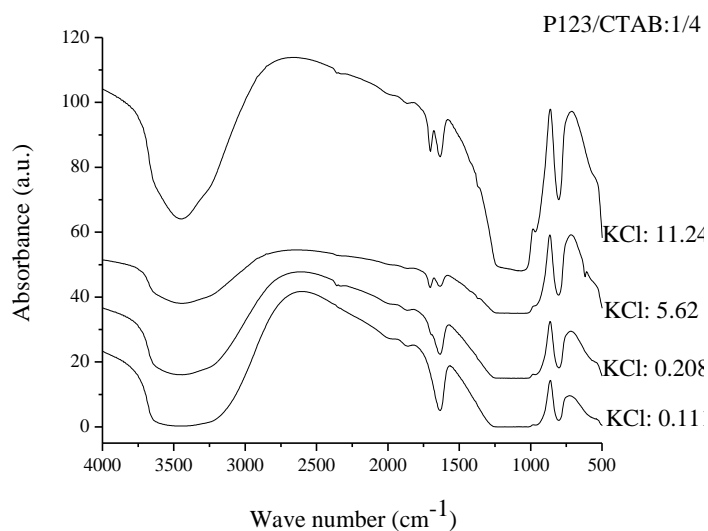


Figure 7.7 FTIR spectra of the SBA15 samples (For P123/CTAB:1/4 and different KCl amounts).



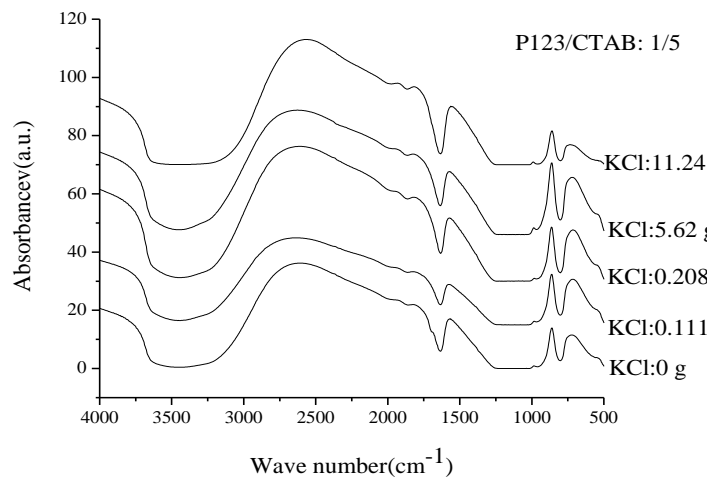


Figure 7.8 FTIR spectra of the SBA15 samples (For P123/CTAB:1/5 and different KCl amounts).

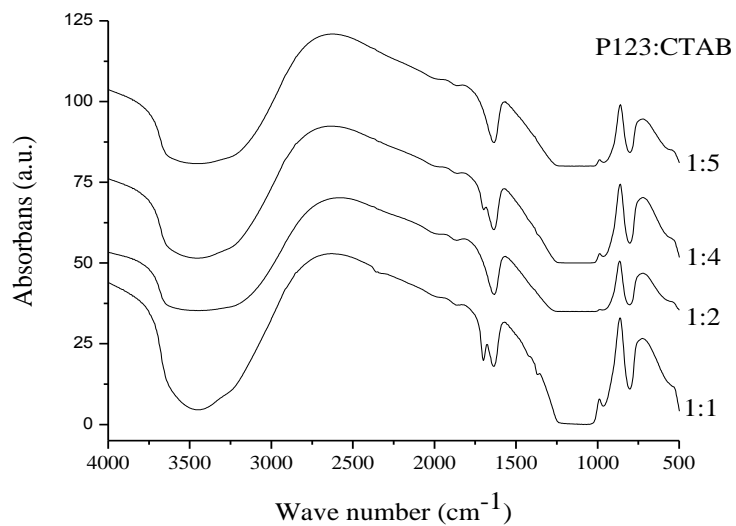


Figure 7.9 FTIR spectra of the 1%Pt/SBA15 samples (For P123/CTAB).

## CHAPTER 8

# METHANE PARTIAL OXIDATION OVER MESOPOROUS Co and/or Pb-SBA-15 CATALYSTS

### 8.1 INTRODUCTION

Catalysts used in the partial oxidation of methane to generate synthesis gas can be divided into two groups: noble metal-based catalysts and metal-based catalysts. It is reported that among the different noble metal catalysts Rh is the most active and stable catalyst toward deactivation. Since the costs of Rh-based catalysts are expensive, improvement of cheaper and alternative metal-based catalysts such as Fe-, Co-, and Ni-based ones would be promising [Kim et al., 2004].

In this part of the thesis, methane partial oxidation were investigated over 0.5%Rh-Co-SBA-15 and Co and/or Pb-SBA15 catalysts prepared by using different synthesis procedures. In addition, heat and mass transfer limitations in mesoporous materials and stop effect behavior were also discussed through the chapter.

### 8.2 EXPERIMENTAL

#### 8.2.1 Reaction Tests

The catalytic partial oxidation of methane was performed at atmospheric pressure in a continuous fixed bed flow-type reactor (4 mm i.d and 25 cm length, quartz) at a temperature range of 50–850°C. Schematic diagram of experimental set-up is

given figure 8.1. The hand-made furnace was equipped with a thermocouple to measure the reaction temperature. Mass flow controllers (Teledyne) were used to control the CH<sub>4</sub> (99.98 % pure) and O<sub>2</sub> flows.

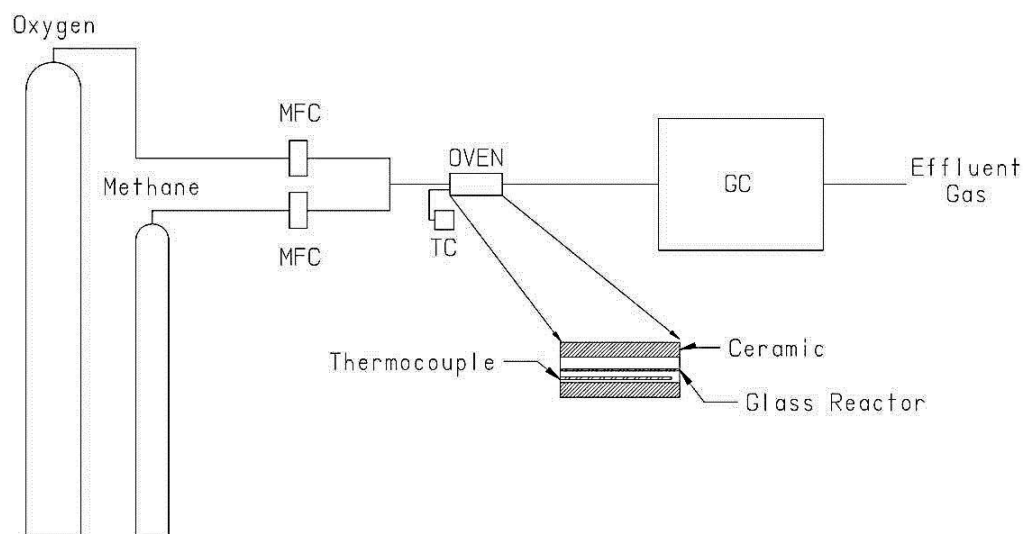


Figure 8.1 Schematic diagram of the experimental set-up.

The reactant gases were fed to the reactor at stoichiometric ratio ( $\text{CH}_4/\text{O}_2=2$ ) and at a total flow rate of 9 ml/min. In each experiment 0.05 g catalysts was loaded to reactor and supported with quartz wool.

Reactant and product components were analyzed by an on-line gas chromatograph (HP 4890 A) equipped with a Porapak Q Column and a thermal conductivity detector (TCD). The conversion was calculated as the amount of raw material transformed in reaction divided by the amount that was fed to the reactor.

### **8.2.2 Heat and Mass Transfer Limitations in Mesoporous Materials**

In heterogeneously catalyzed reactions, obtaining the true kinetic rate expressions for that reaction system, all heat and mass transfer limitations must be eliminated. Temperature and concentration gradients cause high deviations in a catalyst's activity or selectivity. Interphase gradients can exist between the bulk fluid and the external surface of the catalyst. Intraparticle gradients are confined inside the catalyst particles [Mears, 1971].

In gas solid catalytic reaction, before reacting at the catalyst surface, the gas reactant must be transported from bulk phase to the catalyst particle surface, then, it must diffuse into the pores of the catalyst which is porous material having active sites. For gas solid reactions, mass transfer within the pellet is more important from external mass transfer. However, external heat transfer is more important than internal heat transfer [Joshi and Doraiswamy, 2010].

The elimination of the external and internal transport limitations is a complicated problem. Up to now, many useful and interesting criteria have been presented to estimate the heat and mass transfer effects which is substantially changing the experimental results [Mears, 1971; Madon and Boudart, 1982]; Koros and Nowak 1967, Doraiswamy and Sharma (1984). These criteria can be empirical or analytical for evaluating the transport effect. Although the analytic criterias are useful, estimation of the parameters can be difficult [Mears, 1971; Joshi and Doraiswamy, 2010 ; Madon and Boudart, 1982].

Intraparticle gradient can be checked by changing the catalyst particle size. If the reaction rate is not depend on particle size, it can be considered that reaction is free from intraparticle gradients) [Mears, 1971]. Internal diffusional gradients can be eliminated by making the experiments with catalysts having different particle sizes at same reaction conditions and determining the particle size which decrease the conversion [Joshi and Doraiswamy, 2010].

The external heat and mass transfer limitations can be controlled by using different feed velocities at constant space velocity. If the conversion do not change as the feed flow rate is changed, it can be considered that external heat and mass transfer is negligible [Madon and Boudart, 1982]. So, for determining the minimum feed velocity in that reactor system, conversion levels should be noticed. If the reaction conversion do not change at that feed velocity, it can be used as minimum velocity for the reactor [Joshi and Doraiswamy, 2010].

SBA-15 is probably the most studied ordered mesoporous material. It is a hexagonally ordered silica material. It is not known whether if these hexagonal tubes prevent the reactant gas flow from the catalyst. When we use this mesoporous materials in the powder form, there may be pressure drop and heat and mass transfer limitations.

### **8.2.3 Stop-Effect (Time Interrupted Reaction Conditions)**

“The stop-effect which leads to increase of reaction rate under transient conditions was first defined by Koubek et al. This behavior was investigated for catalytic dehydration of alcohols and deamination of amines. In this phenomenon, when the reactant feed concentration switched to zero at constant total feed flow rate, the reaction rate increase drastically. Makarova et al. observed this effect in the dehydration of n-butanol on H-ZSM-5 and amorphous aluminosilicate. In addition, stop-effect was studied for ethanol dehydration on alumina by Moravek and Kraus” [Golay et al, 1997; Golay et al., 1998]. The dehydration of ethanol to ethylene on  $\gamma$ -alumina at 180-200 °C was performed by Golay et al. [1998] to investigate the stop-effect. A model were used to describe this behavior. According to the model, it is considered that two different sites exist on the catalyst surface,  $S_1$  (acidic) and  $S_2$  (basic). Ethanol can adsorb on one of these sites, and for the ethylene formation, a free basic site ( $S_2$ ) is needed [Golay et al, 1997; Golay et al, 1999].

In our experimental system, stop effect also can be applied to increase the reaction rate for the methane partial oxidation. By switching off one reactant: O<sub>2</sub> or CH<sub>4</sub> during the feed of reactant gas, selectivity of the CO or H<sub>2</sub> may be increased.

## **8.3 RESULTS AND DISCUSSION**

### **8.3.1 Reaction Tests**

Methane partial oxidation was carried out over different mesoporous catalysts which has prepared from different methods. The experiments were performed within the temperature interval of 50-850 °C under atmospheric pressure.

The results obtained over Co(5)-SBA-15 revealed that methane conversion is 22% on this catalyst (Fig. 8.2) The main products obtained from this reaction are H<sub>2</sub>, CO<sub>2</sub> and CO. H<sub>2</sub> production started nearly 650 °C. However, detectable amounts of CO were formed at 800°C. H<sub>2</sub> yield over Co(5)-SBA15 catalyst is shown in Figure 8.3. Only Co containing catalyst shows low H<sub>2</sub> production (%4) at 850°C.

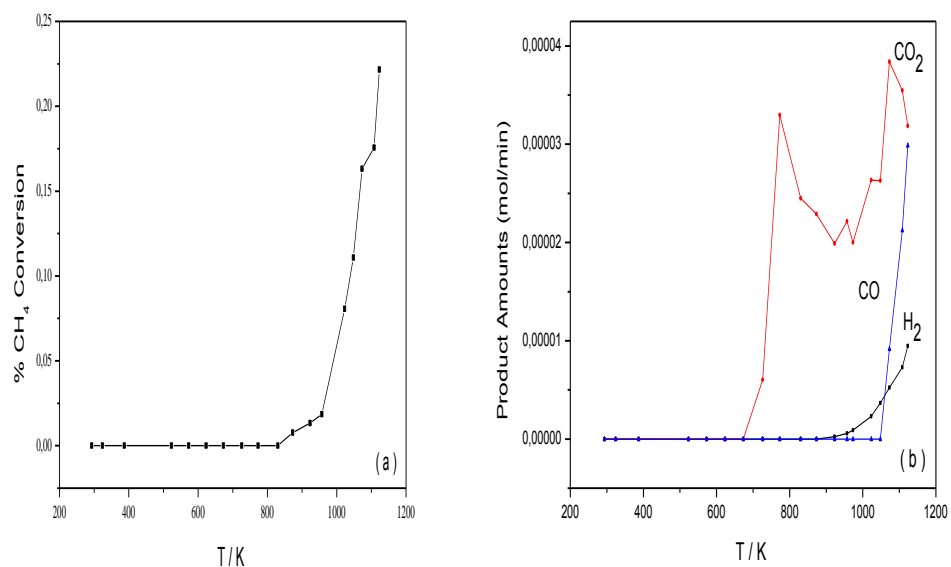


Figure 8.2 Methane conversion (a) and H<sub>2</sub>, CO<sub>2</sub> and CO production (b) over Co(5)-SBA15 catalyst (Incipient Wetness Impregnation Method) as a function of temperature.

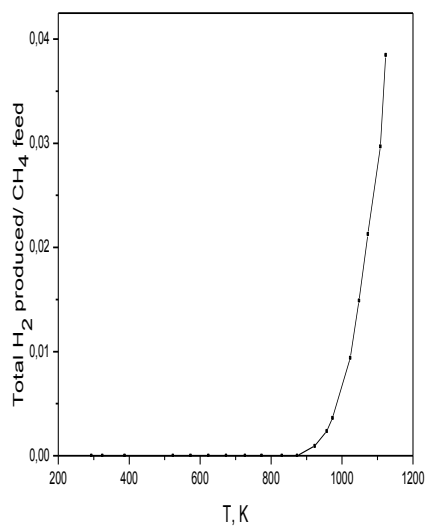


Figure 8.3 H<sub>2</sub> yield of Co(5)-SBA15 as a function of temperature.

When the activity tests are made over Co(5)-Pb(5)-SBA15 bi-metallic catalyst, methane conversion decreased to 16%. The reaction products are the same with

Co(5)-SBA15 sample but the H<sub>2</sub> formation starts at a lower temperature (475°C). H<sub>2</sub> yield also low (%4,5) for this catalyst like Co(5)-SBA15 sample. The main reason of low H<sub>2</sub> yield for this sample is probably the conversion of H<sub>2</sub> to H<sub>2</sub>O after 475°C.

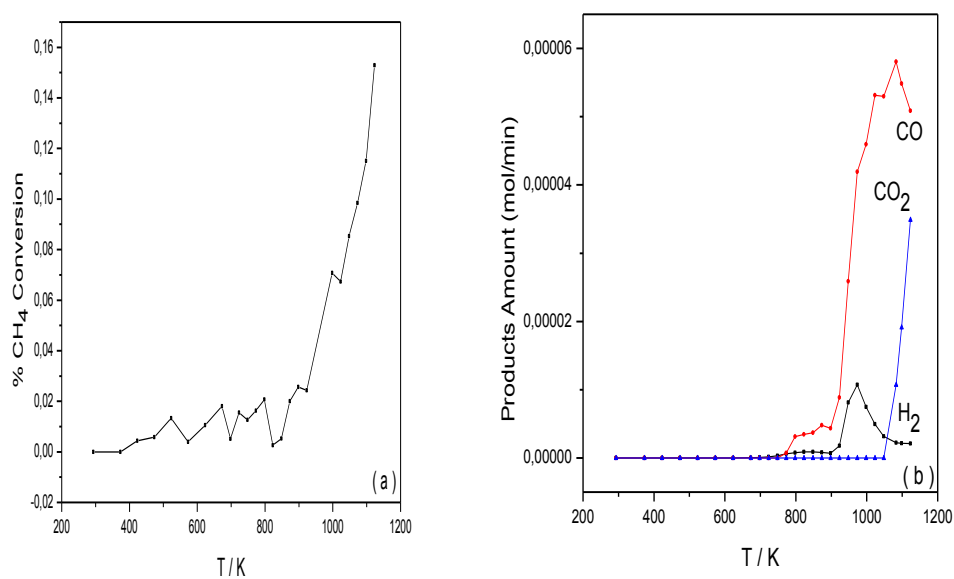


Figure 8.4 Methane conversion (a) and H<sub>2</sub>, CO<sub>2</sub> and CO production (b) over Co(5)-Pb(5)-SBA15 catalyst (Incipient Wetness Impregnation Method) as a function of temperature.



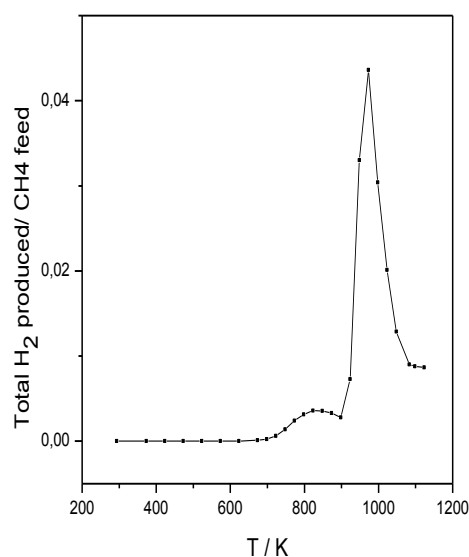


Figure 8.5 H<sub>2</sub> yield of Co(5)-Pb(5)-SBA15 as a function of temperature.

For the reaction over the bi-metallic catalyst –Co(5)-Pb(10)-SBA15, methane conversions were quite high (40%) as compared to Co(5)-Pb(5)-SBA15 catalyst at 850°C. In addition, H<sub>2</sub> formation started a very lower temperature at 400°C. Due to gas phase oxidation, H<sub>2</sub> production rate started to decrease after the 675 °C. The temperatures higher from 675 °C H<sub>2</sub> converted to H<sub>2</sub>O by total oxidation reaction like Co(5)-Pb(5)-SBA15 bi-metallic sample.

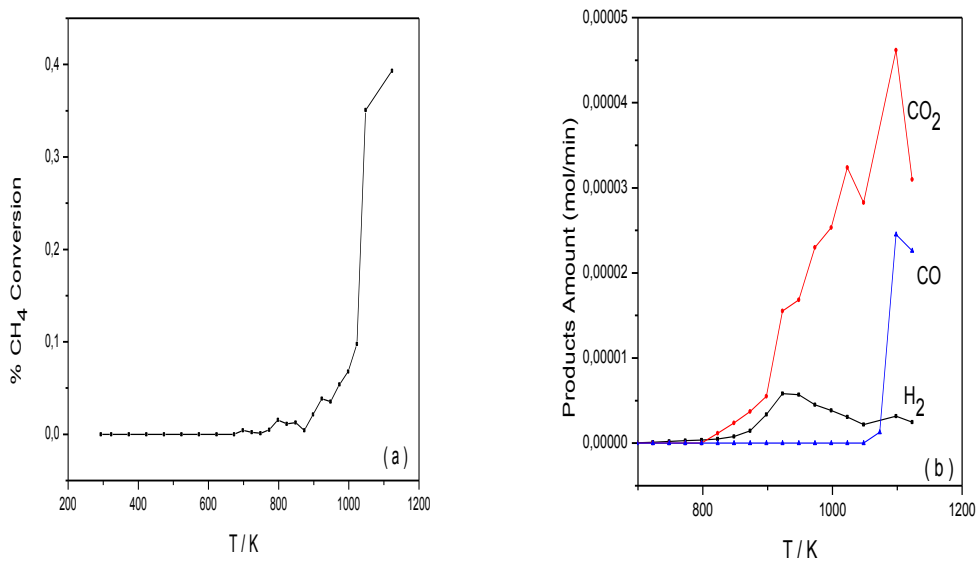


Figure 8.6 Methane conversion (a) and H<sub>2</sub>, CO<sub>2</sub> and CO production (b) over Co(5)-Pb(10)-SBA15 catalyst (Incipient Wetness Impregnation Method) as a function of temperature.

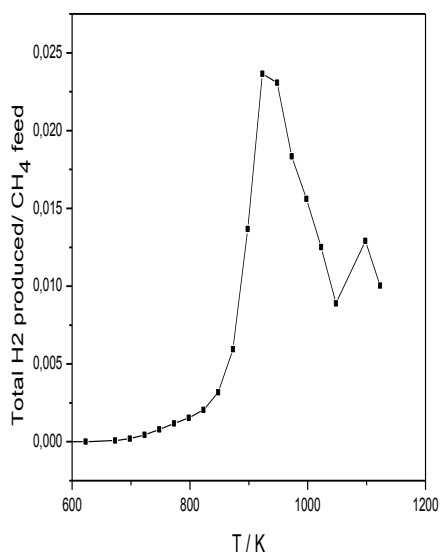


Figure 8.7 H<sub>2</sub> yield of Co(5)-Pb(10)-SBA15 catalyst as a function of temperature.

Figure 8.8 shows that reaction results over Co(5)-SBA-15 catalyst (post grafting method). Comparing the preparation method of the catalyst, methane conversion (16%) is very close to the catalyst with same metal content prepared by impregnation method. As it can be seen in Figure 8.8, H<sub>2</sub> production starts nearly the same temperature (650°C) like Co(5)-SBA-15(incipient wetness impregnation).

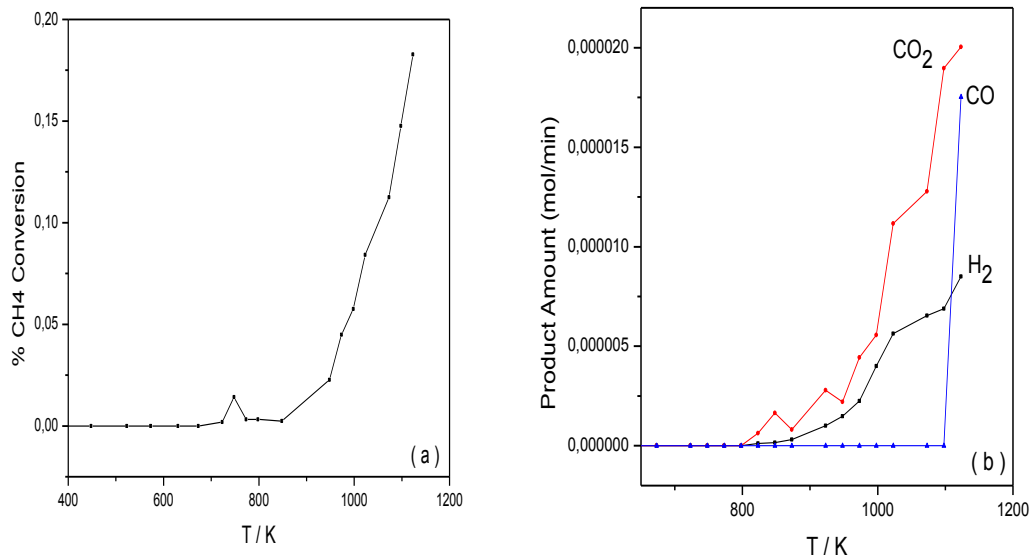


Figure 8.8 Methane conversion (a) and H<sub>2</sub>,CO<sub>2</sub> and CO production (b) over Co(5)-SBA15 catalyst (Post Grafting Method) catalyst as a function of temperature.

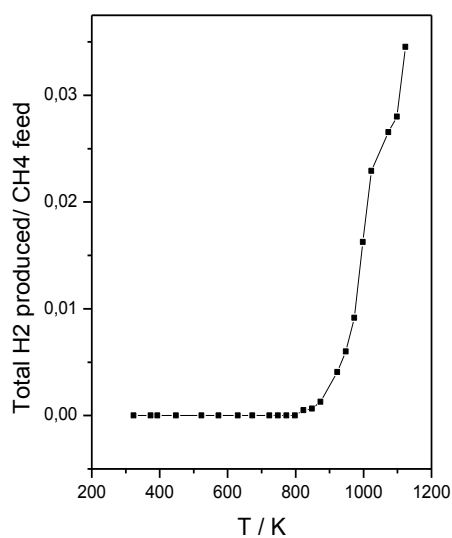


Figure 8.9 H<sub>2</sub> yield of Co(5)-SBA15 catalyst (post grafting method) as a function of temperature.

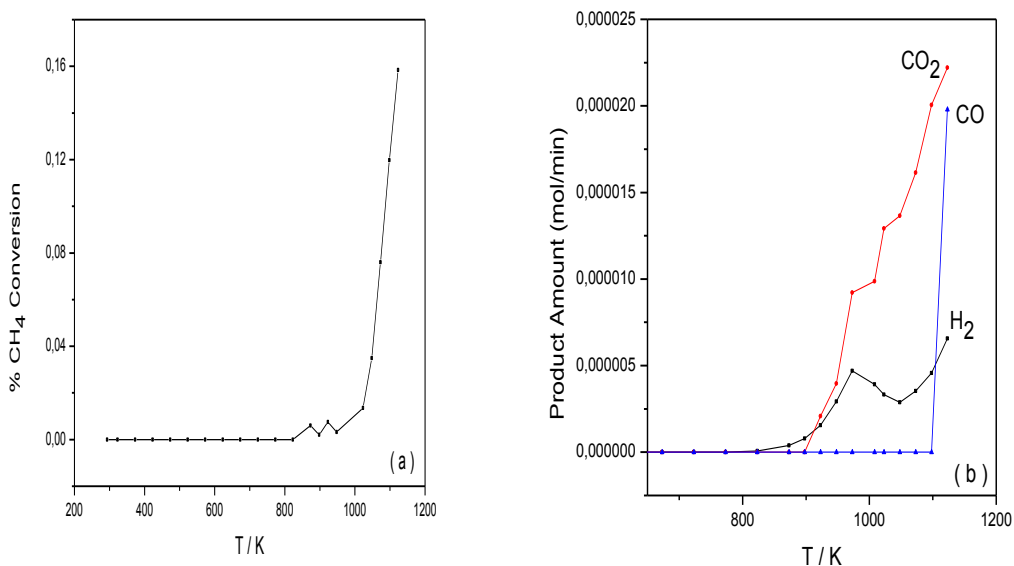


Figure 8.10 Methane conversion (a) and H<sub>2</sub>, CO<sub>2</sub> and CO production (b) over Co(5) Pb(5)-SBA15 catalyst (Post Grafting Method) as a function of temperature.

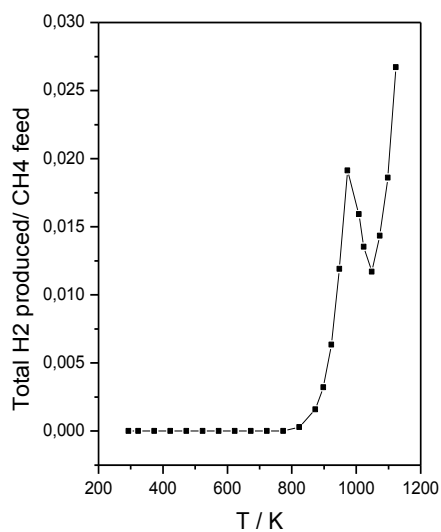


Figure 8.11 H<sub>2</sub> yield of Co(5)-Pb(5)-SBA15 catalyst (post grafting method) as a function of temperature.

Addition of Pb to the Co(5)-SBA15 sample decrease the H<sub>2</sub> production temperature to 500°C. As it can be seen in bi-metallic Co(5)-Pb(10)-SBA-15 sample synthesized by impregnation method, H<sub>2</sub> formation started to decrease at 675°C.

The highest methane conversion (82%) and H<sub>2</sub>yield(40%) wereobtained over 5%RhCo(5)SBA-15 sample (Figure 8.6) due to the lack of oxygen at high conversions. Figure 8.12 and 8.13 show that methane conversion; H<sub>2</sub>, CO<sub>2</sub> and CO production and H<sub>2</sub> yield, respectively.

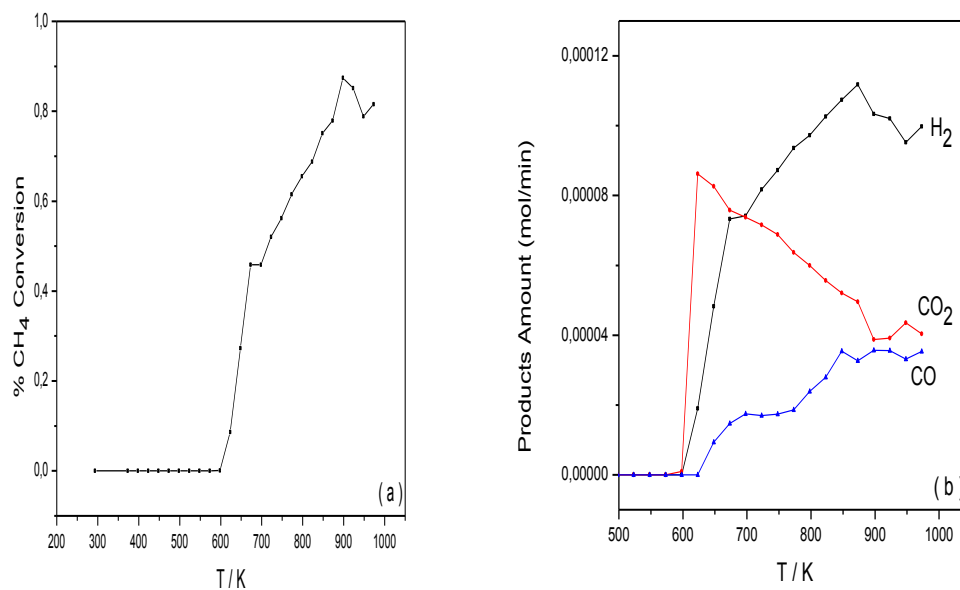


Figure 8.12 Methane conversion (a) and H<sub>2</sub>, CO<sub>2</sub> and CO production (b) over 0.5%RhCo(5) SBA-15 catalysts as a function of temperature.

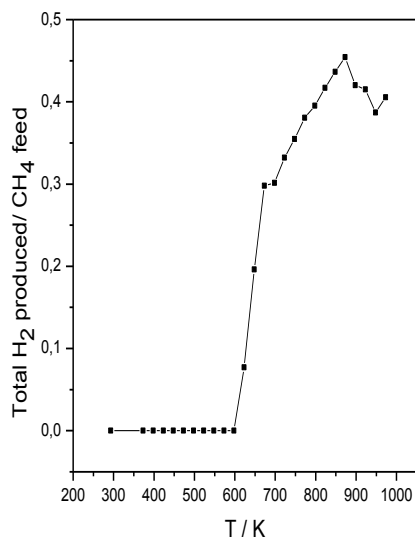


Figure 8.13 H<sub>2</sub> yield of 0,5%RhCo(5)- SBA15 catalyst (incipient wetness impregnation method) as a function of temperature.

## CHAPTER 9

### CONCLUSIONS

In this study, first the catalysts samples containing Co and/or Pb were synthesized by using three different preparation method. The synthesized catalysts samples were characterized by using N<sub>2</sub> Adsorption, XRD, XPS, IR, TEM, Raman Characterization techniques.

The catalysts synthesized by sol-gel method were characterized by XRD, BET and TEM techniques. The high angle XRD results showed that no characteristic peaks of metal oxide was observed up to Co/Si ratio=0.1 in Co-SBA-15 sample, indicating that Co finely dispersed on the surface of the sample or incorporated in the pore walls of the sample. In Pb containing samples, addition of Pb results in crystallization at Pb/Si=0.15. The ordered mesoporous structure was preserved up to Pb/Si=0.15. BET and TEM results showed that mesoporous structure was fully destroyed in samples containing Co and Pb. The incorporation of cobalt and lead oxides to SBA-15 as metal oxides leads the long range order to disappear. It can be concluded that there are chemical interactions between host SBA-15 and the guest metal oxides.

XPS, TEM and Raman techniques were used to characterize the samples prepared by Incipient wetness impregnation and post grafting method. According to the BET results, a decrease in the surface areas was observed by increasing the loadings of metals in SBA-15 which may be due to the filling of pores with metal

atoms. All of the nitrogen adsorption/desorption isotherms showed type IV hysteresis loop which indicates the mesoporous structure. XPS results revealed that Co both metallic and bi-metallic catalysts samples contain  $\text{Co}_3\text{O}_4$  crystallites. Raman results also supported this information. Raman bands at 604, 808, 977  $\text{cm}^{-1}$  are attributed to cyclic trisiloxane, the symmetrical Si-O-Si stretching mode and Si-OH stretch of surface hydroxyl groups, respectively. Raman spectra of the Co and/or Pb-SBA-15 samples show five Raman peaks located at around 192, 475, 516, 615 and 680  $\text{cm}^{-1}$ , corresponding to all the five Raman-active modes ( $A_{1g}$ ,  $E_g$  and 3  $F_{2g}$ ) of  $\text{Co}_3\text{O}_4$ . The present results indicate that the spectrum of SBA-15 is characterized by a intense Raman band around 490  $\text{cm}^{-1}$  and three weaker band at 604, 808 and 977  $\text{cm}^{-1}$ . The 492  $\text{cm}^{-1}$  band can be assigned to cyclic tetrasiloxane rings of the silica support. Pb loaded samples Raman spectras did not show any Pb oxide Raman active modes. The TEM images of the Pb and Co loaded samples indicate that the catalysts possess the typical two-dimensional hexagonal structure of SBA-15. The results showed that the cobalt and lead oxides are highly dispersed in the silicon framework. There is no indication of crystalline metal oxide on the surface. TEM images of Co and Pb impregnated SBA-15 samples showed that there is a large cobalt and lead oxide jungles on the structure.

According to the reaction test results, the 0,5%Rh-Co-SBA15 catalyst shows the highest methane conversion (82%) and  $\text{H}_2$  selectivity due to the lack of oxygen at high conversions. The non-precious metal show lower reactivities, but it is clearly understood that using them at high amounts (i.e. lower space velocities) would increase the conversion and thus conversion related selectivities. Addition of Pb to the Co-SBA15 catalyst increases the catalytic activity. While the methane conversion was 20% over Co-SBA-15 catalyst, Co-Pb/SBA15 samples present higher catalytic activity (40%) for partial oxidation under same reaction conditions. Comparing only Co catalysts and bimetallic Co-Pb-SBA-15 catalysts, production of  $\text{H}_2$  starts at lower temperatures over bimetallic catalysts. Increasing



the lead amount also increased the methane conversion compared to Co-SBA15 catalyst.

## REFERENCES

Asami, K., Mitani, S., Fujimori, H., Ohnuma, S. and Masumoto, T., Characterization of Co-Al-O magnetic thin films by combined use of XPS, XRD and EPMA, *Surf. Interface Anal.*, 28 (1999) 250–253.

Asif, M., Muneer, T., Energy supply, its demand and security issues for developed and emerging economies, *Renewable and Sustainable Energy Reviews*, 11 (2007) 1388–1413.

Baerns, M., Ross, J.R.H., *Catalytic Chemistry of methane conversion, Perspectives in Catalysis*, Black Well, London, 1989.

Berggren, A., Palmqvist Anders E. C. and Holmberg, K., Surfactant-templated mesostructured materials from inorganic silica, *Soft Matter*, 1 (2005) 219–226.

Bhoware, S.S, Shylesh, S., Kamble, K. R., Singh, A. P. , Cobalt-containing hexagonal mesoporous molecular sieves (Co-HMS): Synthesis, characterization and catalytic activity in the oxidation reaction of ethylbenzene, *Journal of Molecular Catalysis A: Chemical*, 255 (2006) 123–130.

Brühwiler, D., Postsynthetic functionalization of mesoporous silica, *Nanoscale*, 2 (2010) 887–892.

Burke, N. R., Trimm, D. L., Co-generation of energy and synthesis gas by partial oxidation of methane, *Catalysis Today*, 117 (2006) 248-252.

Cattarin, S., Guerriero, P., Musiani, M., Preparation of anodes for oxygen evolution by electrodeposition of composite Pb and Co oxides, *Electrochimica Acta*, 46 (2001) 4229–4234.

Cesar, D. V., Pe´rez, C. A. C., Schmal, M., and Salim, V. M. M., Quantitative XPS Analysis of Bimetallic Cu–Co Catalysts, *Phys. stat. sol.*, 187 (2001) 321–326.

Chattopadhyay, S. and Vesper, G., Heterogeneous–Homogeneous Interactions in Catalytic Microchannel Reactors, *AIChE Journal*, 52(2006) 2217-2229.

Chew, T. L., Ahmad A. L., Bhatia S., Ordered mesoporous silica (OMS) as an adsorbent and membrane for separation of carbon dioxide (CO<sub>2</sub>) *Advances in Colloid and Interface Science*, 153 (2010) 43–57.

Chino, N., Okubo, T., Nitridation mechanism of mesoporous silica: SBA-15, *Microporous and Mesoporous Materials*, 87 (2005) 15–22.

Christoskova, S.G., Stoyanova, M., Georgieva, M., Mehandjiev, D., Preparation and characterization of a higher cobalt oxide, *Materials Chemistry and Physics*, 60 (1999) 39-43.

Choudhary, T.V., Goodman, D.W., Methane activation on Ni and Ru model catalysts *Journal of Molecular Catalysis A: Chemical*, 163 (2000) 9-18.

Connor, R. P. O, Klein, E.J. and Schmidt, L.D., High yields of synthesis gas by millisecond partial oxidation of higher hydrocarbons, *Catalysis Letters*, 70(2000) 99-107.

Doraiswamy, L.K., and Sharma, M.M., *Heterogeneous Reactions: Analysis, Examples, and Reactor Design*, Vol.1, Gas solid and Solid solid Reactions, vol.2,

Fluid –Fluid and Fluid-Fluid-Solid Reactions, Newyork, John Wiley and Sons, 1984.

Ernst, B., Bensaddik, A., Hilaire L., Chaumette, P., Kihennemann, A., Study on a cobalt silica catalyst during reduction and Fischer–Tropsch reaction: In situ EXAFS compared to XPS and XRD, *Catalysis Today*, 39 (1998) 329-341.

Fangli, S., Meiqing, S., Yanan, F., Jun, W., Duan, W., Influence of Supports on Catalytic Performance and Carbon Deposition of Palladium Catalyst for Methane Partial Oxidation, *Journal of Rare Earths*, 25 (2007) 316 – 320.

Fathi, M., Hofstad, K. H., Sperle, T., Rokstad, O.A., Holmen, A., Partial oxidation of methane to synthesis gas at very short contact times, *Catalysis Today*, 42, (1998) 205-209.

Ferreira A. C., Goncalves, A.P., Gasche, T. A., Ferraria, A.M., Botelho do Rego, A.M., Correia, M.R., Margarida Bola, A., Branco, J.B., Partial oxidation of methane over bimetallic copper- and nickel-actinideoxides (Th, U), *Journal of Alloys and Compounds*, 497 (2010) 249–258.

Fuell Cell Technology Review,

<http://www.sciencedirect.com/science/article/pii/B9781856173971500058>, ( last accessed 20<sup>th</sup> May, 2011).

Gao, X.X., Huang, C.J. , Zhang, N.W., Li, J.H., Weng, W.Z., Wan, H.L., Partial oxidation of methane to synthesis gas over Co/Ca/Al<sub>2</sub>O<sub>3</sub> catalysts, *Catalysis Today*, 131 (2008) 211–218.

Giraldo, L. F., Lo'pez, B. L., Perez, L., Urrego, S., Sierra, L., Mesa, M., Mesoporous Silica Applications, *Macromol. Symp.*, 258 (2007) 129–141.

Golay, S., Wolfrath, O., Doepper, R., & Renken, A., Model discrimination for reactions with stop-effect, *Studies in Surface Science and Catalysis*, 109 (1997) 295-304.

Golay, S., Doepper, R., Renken, A., In-situ characterisation of the surface intermediates for the ethanol dehydration reaction over  $\gamma$ -alumina under dynamic conditions, *Applied Catalysis A: General* 172 (1998) 97-106.

Golay S., Doepper, R., Renken, A., Reactor performance enhancement under periodic operation for the ethanol dehydration over  $\gamma$ -alumina, a reaction with a stop-effect *Chemical Engineering Science*, 54 (1999) 4469-4474.

Gorshkov, S. V., Kurkin, V. I., Slivinskii, E. V., and Rozovskii, A. Y., High-Temperature Oxidation of Methane by Supported Lead Oxide, *Kinetics and Catalysis*, 42 (2001) 442-447.

Green Car Congress, Hydro Invests in Solid-Acid Fuel Cell Company for Auto Applications, [http://www.greencarcongress.com/2005/09/hydro\\_invests\\_i.html](http://www.greencarcongress.com/2005/09/hydro_invests_i.html), (last accessed 5<sup>th</sup> May, 2011).

GRI 3.0 Mechanism Parameters, <http://www.me.berkeley.edu/gri-mech/>, (last accessed 19<sup>th</sup> June, 2011).

Han, M., Yin, H., Miao, W., Zhou, S., Fabrication and properties of anode-supported solid oxide fuel cell, *Solid State Ionics*, 179 (2008) 1545–1548.

Hess, C., Tzolova-Müller, G., Herbert, R., The Influence of Water on the Dispersion of Vanadia Supported on Silica SBA-15: A combined XPS and Raman Study, *J. Phys. Chem. C*, 111 (2007) 9471-9479.

Hess, C., Hoefelmeyer, J.D., Tilley, T.D., Spectroscopic Characterization of Highly Dispersed Vanadia Supported on SBA-15, *J.Phys. Chem. B.*, 108 (2004) 9703-9709.

Hickman D.A. and Schmidt L.D., Production of syngas by direct catalytic oxidation of methane, *Science*, 259 (1993) 343-346.

Hoffmann, F., Cornelius M., Morell J., Fröba, M., Silica-Based Mesoporous Organic-Inorganic Hybrid Materials, *Angew.Chem.Int.Ed.*, 45(2006) 3216-3251.

Hohn, K.L., Schmidt, L.D., Partial oxidation of methane to syngas at high space velocities over Rh-coated spheres, *Applied Catalysis A: General*, 211(2001) 53-68.

Holmen, A., Direct conversion of methane to fuels and chemicals, *Catalysis Today*, 142 (2009) 2–8.

Huo Q., Margolese D. I., Ciesla U., . Demuth D. G, Feng P.,Gier T. E., Sieger P., Firouzi A., Chmelka B. F., Schuth F. AndStucky G. D., Organization of Organic Molecules with InorganicMolecular Species into Nanocomposite Biphase Arrays *Chem. Mater.*, 6(1994) 1176–1191.

Jana, S. K., Nishida, R., Shindo, K., Kugita, T., Namba, S., Pore size control of mesoporous molecular sieves using different organic auxiliary chemicals, *Microporous and Mesoporous Materials*, 68 (2004) 133–142.

Jayakumar, A., Vohs, J. M., and Gorte, R. J., Molten-Metal Electrodes for Solid Oxide Fuel Cells, *Ind. Eng. Chem. Res.*, 49(2010)10237–10241.

Joensen, F., Rostrup-Nielsen, J. R., Methane activation on Ni and Ru model catalysts, *Journal of Power Sources*, 105 (2002) 195- 201.

Joshi, J.B., Doraiswamy, L.K., Chemical Reaction Engineering, Albright's Chemical Engineering Handbook, CRC Press, 2010.

Jung, H. , Yoon ,W. L., Lee, H., Park , J. S., Shin, J. S., La, H., Lee, J. D., Fast start-up reactor for partial oxidation of methane with electrically-heated metallic monolith catalyst, Journal Of Power Source, 124 (2003) 76-80.

Khodakov, J A.Y., Constant, A.,Bechara, R.,and Zholobenko, V. L., Pore Size Effects in Fischer Tropsch Synthesis over Cobalt-Supported Mesoporous Silicas, Journal of Catalysis, 206 (2002) 230–241.

Kim, M.H., Surface chemical structures of  $\text{CoO}_x/\text{TiO}_2$  catalysts for continuous wet trichloroethylene oxidation, Korean J. Chem. Eng., 22 (2005) 839-843.

Kim P., Kim Y., Kim H., Song, I. K., Jongheop Y., Synthesis and characterization of mesoporous alumina with nickel incorporated for use in the partial oxidation of methane into synthesis gas, Applied Catalysis A: General, 272 (2004) 157–166.

Kirubakaran, A., Jain, S., Nema, R.K., A review on fuel cell technologies and power electronic interface, Renewable and Sustainable Energy Reviews, 13 (2009) 2430–2440.

Koh, A.C.W., Chen, L.,Leong, W. K., Johnson B. F.G., Tetyana Khimyak, Jianyi Lin, Hydrogen or synthesis gas production via the partial oxidation of methane over supported nickel–cobalt catalysts, International Journal of Hydrogen Energy, 32 (2007) 725 – 730.

Kongzhai, L., Hua, W., Yonggang, W., Mingchun, L., Catalytic performance of cerium iron complex oxides for partial oxidation of methane to synthesis gas, Journal of Rare Earths, 26 (2008) 705-710.

Koros, R.M., Novak, E.J., A diagnostic test of kinetic regime in a packed bed reactor, *Chem.Eng Sci.*, 22(1967) 470.

Krummenacher, J. J., West, K. N., Schmidt, L.D., Catalytic partial oxidation of higher hydrocarbons at millisecond contact times: decane, hexadecane, and diesel fuel, *Journal of Catalysis*, 215(2003) 332-343.

Larentis, A.L., Resende, N.S., Salim, V.M.M., Pinto, J.C., Modeling and optimization of the combined CO<sub>2</sub> reforming and partial oxidation of natural gas, *Applied Catalysis A: General*, 215(2001) 211-224.

Laugel, G., Arichi, J., Moliere, M., Kiennemann, A., Garin, F., Louis, B., Metal oxides nanoparticles on SBA-15: Efficient catalyst for methane combustion, *Catalysis Today*, 138 (2008) 38–42.

Li, Z., Hoflund, G.B., Catalytic oxidation of methane over Pd/Co<sub>3</sub>O<sub>4</sub>, *React.Kinet.Catal.Lett.*, 66 (1999) 367-374.

Li, K., Wang, H., Wei, Y., Yan, D., Direct conversion of methane to synthesis gas using lattice oxygen of CeO<sub>2</sub>-Fe<sub>2</sub>O<sub>3</sub> complex oxides, *Chemical Engineering Journal*, 156 (2010) 512–518.

Lin, Y., Beale, S.B., Performance predictions in solid oxide fuel cells, *Applied Mathematical Modelling*, 30 (2006) 1485–1496.

Llorca, J., Homs, N., Rossell, O., Seco, M., Luis, J., Fierro, G., Piscina, P., Highly dispersed cobalt in CuCo/SiO<sub>2</sub> cluster-derived catalyst, *Journal of Molecular Catalysis A: Chemical*, 149 (1999) 225–232.

Lu, Y., Surfactant-Templated Mesoporous Materials: From Inorganic to Hybrid to Organic, *Angew. Chem. Int. Ed.*, 45 (2006) 7664 – 7667.



Lunsford, J. H., Catalytic conversion of methane to more useful chemicals and fuels: a challenge for the 21<sup>st</sup> century, *Catalysis Today*, 63 (2000) 165–174.

Luo N., Zhao X., Cao F., Xiao T., and Fang, D., Thermodynamic Study on Hydrogen Generation from Different Glycerol Reforming Processes, *Energy & Fuels*, 21(2007) 3505–3512.

Lyubovsky, M., Roychoudhury, S., and LaPierre R., Catalytic partial “oxidation of methane to syngas” at elevated pressures, *Catalysis Letters*, 99 (2005) 113-117.

Madon, J.R., Boudart, M., Experimental Criterion for the Absence of Artifacts in the Measurement of Rates of Heterogeneous Catalytic Reactions, *Ind. Eng. Chem. Fundam.*, 21(1982) 438-447.

Mears, D.E., Tests for Transport Limitations in Experimental Catalytic Reactions, *Ind.Eng.Chem.Process.Des.Develop.*, 10 (1971) 541-547.

Marschall, K.J. and Mleczko, L., Short-Contact-Time Reactor for Catalytic Partial Oxidation of Methane, *Industrial & Engineering Chemistry Research*, 38 (1999), 1813-1821.

Marquez-Alvarez, C., Zilkova N., Perez-Pariente, J., and Cejka, J., Synthesis, characterization and catalytic applications of organized mesoporous aluminas, *Catalysis Reviews*, 50 (2008) 222–286.

Martin-Aranda, R. M., Cejka, J., Recent advances in catalysis over mesoporous molecular sieves, *Top. Catal.* 53 (2010) 141–153. bak

Martínez, A.,López, C., Márquez, F., and Díaz, I., Fischer–Tropsch synthesis of hydrocarbons over mesoporous Co/SBA-15 catalysts: the influence of metal

loading, cobalt precursor, and promoters, *Journal of Catalysis*, 220 (2003) 486–499.

Mendes, F. M. T., Perez, C. A. C., Noronha, F. B., Souza, C. D. D., Cesar, D. V., Freund, H.J., and Schmal, M., Fischer-Tropsch synthesis on anchored Co/Nb<sub>2</sub>O<sub>5</sub>/Al<sub>2</sub>O<sub>3</sub> catalysts: the nature of the surface and the effect on chain growth, *J. Phys. Chem. B*, 110 (2006) 9155-9163.

Meynen, V., Cool, P., Vansant, E.F., Verified syntheses of mesoporous materials, *Microporous and Mesoporous Materials*, 125 (2009) 170–223.

Meynen, V., Cool, P., Vansant, E.F., Kortunov, P., Grinberg, F., Karger, J., Mertens, M., Lebedev, O.I., Van, G., Tendeloo, Deposition of vanadium silicalite-1 nanoparticles on SBA-15 materials. Structural and transport characteristics of SBA-VS-15, *Microporous and Mesoporous Materials* 99 (2007) 14–22.

Moon, D.J., Hydrogen Production by Catalytic Reforming of Gaseous Hydrocarbons (Methane & LPG), *Catal Surv Asia*, 12 (2008) 188–202.

Mureseanu, M. , Reiss A., Stefanescu I., David, E., Parvulescu V., Renard G., Hulea, V., Modified SBA-15 mesoporous silica for heavy metal ions remediation, *Chemosphere*, 73 (2008) 1499–1504.

Nikoloski, A. N. and Nikol, M.J., Addition of cobalt to lead anodes used for oxygen evolution-A literature review, *Mineral Processing and Extractive Metall. Rev.*, 30(2010) 30-57. bak

Nobuntu, A., Mnqanqeni, N. M., Coville, N. J., The preparation and study of sol-gel synthesized Co/Zn/TiO<sub>2</sub> Fischer-Tropsch catalysts, *Applied Catalysis A: General*, 317 (2007) 195–203.

Nozaki ,T., Hashimoto, S., Omata, K., and Fujimoto, K., Oxidative Coupling of Methane with Membrane Reactors Containing Lead Oxide, *Ind. Eng. Chem. Res.* 32 (1993) 1174-1179.

Oye, G., Sjoblom, J., Stöcker, M., Synthesis, characterization and potential applications of new materials in the mesoporous range, *Advances in Colloid and Interface Science*, 89-90 (2001) 439-466.

Otsuka, K., Wang, Y., Sunada, E., Yamanaka, I., Direct Partial Oxidation of Methane to Synthesis Gas by Cerium Oxide, *Journal of Catalysis*, 175(1998)152–160.

Pavlova, S., Sazonova, N., Sadykov, V., Pokrovskaya, S., Kuzmin, V., Alikina, G., Lukashevich, A., Gubanova, E., Partial oxidation of methane to synthesis gas over corundum supported mixed oxides: One channel studies, *Catalysis Today*, 105(2005) 367-371.

Perkas, N., Zhong, Z., Chen, L., Besson, M., Gedanken, A., Sonochemically Prepared high Dispersed Ru/TiO<sub>2</sub> Mesoporous Catalyst for Partial Oxidation of Methane to Syngas, *Catalysis Letters*, 103(2005) 9- 14.

Ponvel, K. M., Kim Y. H., Lee C., Incorporation of nano-sized magnetite particles into mesoporous materials via –COOH groups, *Materials Chemistry and Physics* 122 (2010) 397–401.

Rashkov, S., Dobrev, T., Noncheva, Z., Stefanov, Y., Rashkova, B., Petrova, M., Preparation of anodes for oxygen evolution by electrodeposition of composite Pb and Co oxides, *Hydrometallurgy*, 52 (1999) 223–230.

Requies, J., Cabrero, M.A., Barrio, V.L., Güemez, M.B., Cambra, J.F., Arias, P.L., Alonso, F.J., Ojeda M., Pena, M.A., Fierro, J.L.G., Partial oxidation of

methane to syngas over Ni/MgO and Ni/La<sub>2</sub>O<sub>3</sub> catalysts, *Applied Catalysis A:General*, 289(2005) 214-223.

Rostrup-Nielsen, J.R., New aspects of syngas production and use, *Catalysis Today*, 63 (2000) 159-164.

Salazar-Villalpando, M. D., Berry, D. A., Gardner T. H., Partial oxidation of methane over Rh/supported-ceria catalysts: Effect of catalyst reducibility and redox cycles, *International Journal of Hydrogen Energy*, 33 ( 2008 ) 2695–2703.

Salogni, A., Colonna, P., Modeling of solid oxide fuel cells for dynamic simulations of integrated systems, *Applied Thermal Engineering*, 30(2010) 464–477.

Sayari, A., Yang, Y., SBA-15 Templated Mesoporous Carbon: New Insights into the SBA-15 Pore Structure, *Chem. Mater.*, 17 (2005) 6108-6113.

Schmidt, L.D., Klein, E.J., Leclere, C.A., Krummenacher, J.J., West, K.N., Syngas in millisecond reactors: higher alkanes and fast lightoff, *Chemical Engineering Science*, 58 (2003) 1037-1041.

Shan, W., Fleys, M., Lopicque, F., Swierezynski, D., Kiennemann, A., Simon, Y., Marquaire, P., Syngas production from partial oxidation of methane over Ce<sub>1-x</sub>Ni<sub>x</sub>O<sub>y</sub> catalysts prepared by complexation–combustion method, *Applied Catalysis A:General*, 311 (2006) 24-33.

Shylesh, S. Samuel, P. P., Sisodiya, S., Singh, A. P., Periodic Mesoporous Silicas and Organosilicas: An Overview Towards Catalysis, *Catal Surv Asia*, 12 (2008) 266–282.

Silberova, B., Venvik, H.J., Holmen, A., Production of hydrogen by short contact time partial oxidation and oxidative steam reforming of propane, *Catalysis Today*, 99(2005) 69-76.

Song, X., Guo Z., Technologies for direct production of flexible H<sub>2</sub>/CO synthesis gas, *Energy Conversion and Management*, 47 (2006) 560–569.

Sun, W., Jin, G., Guo, X., Partial oxidation of methane to syngas over Ni/SiC catalysts, *Catalysis Communications*, 6(2005) 135-139.

Taguchi, A., Schüth, F., Ordered mesoporous materials in catalysis, *Microporous and Mesoporous Materials*, 77 (2005) 1–45.

Trong On, D., Desplandier-Giscard, D., Danumah, C., Kaliaguine, S., Perspectives in catalytic applications of mesostructured materials, *Applied Catalysis A: General*, 222 (2001) 299–357.

Tsai, C. and Hsieh, T., New Approach for Methane Conversion Using a Discharge Reactor. 1. Influences of Operating Conditions on Syngas Production, *Industrial & Engineering Chemistry Research*, 43 (2004) 4043-4047.

Uner D., and Uner M., Adsorption calorimetry in supported catalyst characterization: Adsorption structure sensitivity on Pt/ $\gamma$ -Al<sub>2</sub>O<sub>3</sub>, *Thermochimica Acta*, 434 (2005) 107–112.

Vansant, E., Van der Voort, P., and Vranken, K., Characterization and Chemical Modification of the Silica Surface, in *Studies in Surface Science and Catalysis*, B. Delmon and J.T.Yates, eds., vol. 93, Elsevier, 1995, ch. 3.

Vinu, A., Mori, T., Ariga K., Review: New families of mesoporous materials, *Science and Technology of Advanced Materials* 7 (2006) 753–77.

Wang Y. M., Wu Z. Y., Zhu J. H., Surface functionalization of SBA-15 by the solvent-free method, *Journal of Solid State Chemistry*, 177 (2004) 3815–3823.

Wang, X., Lin, K. S. K., Chan, J. C. C., and Cheng, S., Direct Synthesis and Catalytic Applications of Ordered Large Pore Aminopropyl Functionalized SBA-15 Mesoporous Materials, *J. Phys. Chem. B*, 109 (2005) 1763-1769.

Wang P., Lu, Q., Li J., In situ Formation of Palladium Nanoparticles Inside the Pore Channels of Ordered Mesoporous Silica, *Catal Lett.*, 131 (2009) 444–450.

Wang K., Hissel, D., Pe'ra, M.C., Steiner, N., Marra, D., Sorrentino, M., Pianese C., Monteverde, M., Cardone, P., Saarinen, J., A Review on solid oxide fuel cell models, *International Journal of Hydrogen Energy* 36 (2011) 7212-7228.

Xi, J., Tang, X., Novel composite polymer electrolyte comprising poly(ethylene oxide) and triblock copolymer/mesostructured silica hybrid used for lithium polymer battery, *Electrochimica Acta*, 50 (2005) 5293–5304.

Xia Y., and M., A study of the behaviour of mesoporous silicas in OH/CTABr/H<sub>2</sub>O systems: phase dependent stabilisation, dissolution or semipseudomorphic transformation, *J. Mater. Chem.*, 13 (2003) 3112–3121.

Xiong, J.H., Zhang, Y., Liew, K., Li, J., Catalytic performance of zirconium-modified Co/Al<sub>2</sub>O<sub>3</sub> for Fischer–Tropsch synthesis, *Journal of Molecular Catalysis A: Chemical*, 231 (2005) 145–151.

Xiong, H., Zhang, Y., Liew K., Li, J., Fischer–Tropsch synthesis: The role of pore size for Co/SBA-15 catalysts, *Journal of Molecular Catalysis A: Chemical* 2008, 295, 68.

Yamawaki, M., Nishihara, T., Inagaki, Yoshiyuki., Minato, K., Oigawa H., Onuki, K., Hino R., Ogawa, M., Application of nuclear energy for environmentally friendly hydrogen generation, *International Journal of Hydrogen Energy*, 32 (2007) 2719 – 2725.

Yang Z., Lu, Y., and Yang, Z., Mesoporous materials: tunable structure, morphology and composition, *Chem. Commun.*, (2009) 2270–2277.

Yang, H., and Zhao D., Synthesis of replica mesostructures by the nanocasting strategy, *J. Mater. Chem.*, 15 (2005) 1217–1231.

Yokoi, T., Yoshitake, H., Tatsumi, T., Synthesis of amino-functionalized MCM-41 via direct co-condensation and post-synthesis grafting methods using mono-, di- and tri-amino-organoalkoxysilane, *J. Mater. Chem.*, 14 (2004) 951–957.

Yung, M.M., Holmgren, E.M., Ozkan U. S., Low-temperature Oxidation of carbon Monoxide on Co/ZrO<sub>2</sub>, *Catal. Letter.*, 118 (2007) 180-186.

Yuranov, I., Kiwi-Minsker, L., Buffat, P., and Renken, A., Selective Synthesis of Pd Nanoparticles in Complementary Micropores of SBA-15, *Chem. Mater.*, 16 (2004) 760-761.

Zhang, W., Zhang, L., Xiu, J., Shen, Z., Li, Y., Ying, P., Li, C., Pore size design of ordered mesoporous silicas by controlling micellar properties of triblock copolymer EO<sub>20</sub>PO<sub>70</sub>EO<sub>20</sub>, *Microporous and Mesoporous Materials*, 89 (2006) 179–185.

Zhao, D., Huo, Q., Feng J., Chmelka B. F., and Stucky G. D., Nonionic Triblock and Star Diblock Copolymer and Oligomeric Surfactant Syntheses of Highly Ordered, Hydrothermally Stable, Mesoporous Silica Structures, *J. Am. Chem. Soc.*, 120 (1998-a) 6024-6036.

Zhao, D., Feng J., and Stucky G., Triblock Copolymer Syntheses of Mesoporous Silica with Periodic 50 to 300 Angstrom Pores, *Science*, 279 (1998-b) 548-552.

Zhou, W., Chen, J., Fang, K., Sun, Y., The deactivation of Co/SiO<sub>2</sub> catalyst for Fischer–Tropsch synthesis at different ratios of H<sub>2</sub> to CO, *Fuel Processing Technology*, 87 (2006) 609–616.

Zhou, H., Chen, L., Malik, V., Knies, C., Hofmann, M. D., Bhatti, K.P., Chaudhary S., Klar P.J., Heimbrodt W., Klingshirn C., Kalt, H., Raman studies of ZnO:Co thin films, *Phys.Stat.Sol.*, 1 (2007) 112-117.

Zhu, J., Zhang, D., King, K.D., Reforming of CH<sub>4</sub> by partial oxidation: thermodynamic and kinetic analyses, *Fuel*, 80 (2001) 899-905.

Zhu, K., Wang, D., and Liu, J., Self-Assembled Materials for Catalysis, *Nano Res.*, 2 (2009) 1-29.



# APPENDIX A

## CHEMKIN GRI 3.0 MECHANISM PARAMETERS

No	Reaction	Rate Coefficient $A T^n \exp(-E/RT)$			Served as Optimization Variable in GRI-Mech Releases
		A (mol.cm <sup>3</sup> .s)	n (T in K)	E (cal/mol)	
<u>1</u>	O + O + M -> O2 + M	1.20E+17	-1		
<u>2</u>	O + H + M -> OH + M	5.00E+17	-1		
<u>3</u>	O + H2 -> H + OH	3.87E+04	2,7	6260	3
<u>4</u>	O + HO2 -> OH + O2	2.00E+13			
<u>5</u>	O + H2O2 -> OH + HO2	9.63E+06	2	4000	
<u>6</u>	O + CH -> H + CO	5.70E+13			
<u>7</u>	O + CH2 -> H + HCO	8.00E+13			
<u>8</u>	O + CH2(S) -> H2 + CO	1.50E+13			
<u>9</u>	O + CH2(S) -> H + HCO	1.50E+13			
<u>10</u>	O + CH3 -> H + CH2O	5.06E+13			1.1; 1.2; 2.1; 3.0
<u>11</u>	O + CH4 -> OH + CH3	1.02E+09	1,5	8600	1.2; 2.1; 3.0
<u>12</u>	O + CO + M -> CO2 + M	1.80E+10		2385	
<u>13</u>	O + HCO -> OH + CO	3.00E+13			
<u>14</u>	O + HCO -> H + CO2	3.00E+13			
<u>15</u>	O + CH2O -> OH + HCO	3.90E+13		3540	3
<u>16</u>	O + CH2OH -> OH + CH2O	1.00E+13			
<u>17</u>	O + CH3O -> OH + CH2O	1.00E+13			
<u>18</u>	O + CH3OH -> OH + CH2OH	3.88E+05	2,5	3100	
<u>19</u>	O + CH3OH -> OH + CH3O	1.30E+05	2,5	5000	
<u>20</u>	O + C2H -> CH + CO	5.00E+13			
<u>21</u>	O + C2H2 -> H + HCCO	1.35E+07	2	1900	3
<u>22</u>	O + C2H2 -> OH + C2H	4.60E+19	-1,4	28950	
<u>23</u>	O + C2H2 -> CO + CH2	6.94E+06	2	1900	
<u>24</u>	O + C2H3 -> H + CH2CO	3.00E+13			

<u>25</u>	O + C2H4 -> CH3 + HCO	1.25E+07	1,8	220	
<u>26</u>	O + C2H5 -> CH3 + CH2O	2.24E+13			
<u>27</u>	O + C2H6 -> OH + C2H5	8.98E+07	1,9	5690	3
<u>28</u>	O + HCCO -> H + CO + CO	1.00E+14			
<u>29</u>	O + CH2CO -> OH + HCCO	1.00E+13		8000	
<u>30</u>	O + CH2CO -> CH2 + CO2	1.75E+12		1350	
<u>31</u>	O2 + CO -> O + CO2	2.50E+12		47800	
<u>32</u>	O2 + CH2O -> HO2 + HCO	1.00E+14		40000	1.2; 2.1; 3.0
<u>33</u>	H + O2 + M -> HO2 + M	2.80E+18	-0,9		2.1; 3.0
<u>34</u>	H + O2 + O2 -> HO2 + O2	2.08E+19	-1,2		3
<u>35</u>	H + O2 + H2O -> HO2 + H2O	1.13E+19	-0,8		1.1; 1.2; 2.1; 3.0
<u>36</u>	H + O2 + N2 -> HO2 + N2	2.60E+19	-1,2		2.1; 3.0
<u>37</u>	H + O2 + AR -> HO2 + AR	7.00E+17	-0,8		1.2; 2.1; 3.0
<u>38</u>	H + O2 -> O + OH	2.65E+16	-0,7	17041	1.1; 1.2; 2.1; 3.0
<u>39</u>	H + H + M -> H2 + M	1.00E+18	-1		
<u>40</u>	H + H + H2 -> H2 + H2	9.00E+16	-0,6		
<u>41</u>	H + H + H2O -> H2 + H2O	6.00E+19	-1,2		3
<u>42</u>	H + H + CO2 -> H2 + CO2	5.50E+20	-2		
<u>43</u>	H + OH + M -> H2O + M	2.20E+22	-2		1.1;1.2;2.1; 3.0
<u>44</u>	H + HO2 -> O + H2O	3.97E+12		671	
<u>45</u>	H + HO2 -> O2 + H2	4.48E+13		1068	3
<u>46</u>	H + HO2 -> OH + OH	8.40E+13		635	3
<u>47</u>	H + H2O2 -> HO2 + H2	1.21E+07	2	5200	
<u>48</u>	H + H2O2 -> OH + H2O	1.00E+13		3600	
<u>49</u>	H + CH -> C + H2	1.65E+14			1.2; 2.1; 3.0
<u>50</u>	H + CH2 (+M) -> CH3 (+M)	pressure dependent			3
<u>51</u>	H + CH2(S) -> CH + H2	3.00E+13			
<u>52</u>	H + CH3 (+M) -> CH4 (+M)	pressure dependent			3
<u>53</u>	H + CH4 -> CH3 + H2	6.60E+08	1,6	10840	1.1; 1.2; 2.1; 3.0
<u>54</u>	H + HCO (+M) -> CH2O (+M)	pressure dependent			3
<u>55</u>	H + HCO -> H2 + CO	7.34E+13			1.1; 1.2; 2.1; 3.0
<u>56</u>	H + CH2O (+M) -> CH2OH (+M)	pressure dependent			
<u>57</u>	H + CH2O (+M) -> CH3O (+M)	pressure dependent			3
<u>58</u>	H + CH2O -> HCO + H2	5.74E+07	1,9	2742	3
<u>59</u>	H + CH2OH (+M) -> CH3OH (+M)	pressure dependent			
<u>60</u>	H + CH2OH -> H2 + CH2O	2.00E+13			
<u>61</u>	H + CH2OH -> OH + CH3	1.65E+11	0,7	-284	3
<u>62</u>	H + CH2OH -> CH2(S) + H2O	3.28E+13	-0,1	610	
<u>63</u>	H + CH3O (+M) -> CH3OH (+M)	pressure dependent			
<u>64</u>	H + CH3O -> H + CH2OH	4.15E+07	1,6	1924	
<u>65</u>	H + CH3O -> H2 + CH2O	2.00E+13			
<u>66</u>	H + CH3O -> OH + CH3	1.50E+12	0,5	-110	

<u>67</u>	H + CH3O -> CH2(S) + H2O	2.62E+14	-0,2	1070	
<u>68</u>	H + CH3OH -> CH2OH + H2	1.70E+07	2,1	4870	
<u>69</u>	H + CH3OH -> CH3O + H2	4.20E+06	2,1	4870	
<u>70</u>	H + C2H (+M) -> C2H2 (+M)	pressure dependent			
<u>71</u>	H + C2H2 (+M) -> C2H3 (+M)	pressure dependent			
<u>72</u>	H + C2H3 (+M) -> C2H4 (+M)	pressure dependent			
<u>73</u>	H + C2H3 -> H2 + C2H2	3.00E+13			
<u>74</u>	H + C2H4 (+M) -> C2H5 (+M)	pressure dependent			3
<u>75</u>	H + C2H4 -> C2H3 + H2	1.32E+06	2,5	12240	
<u>76</u>	H + C2H5 (+M) -> C2H6 (+M)	pressure dependent			3
<u>77</u>	H + C2H5 -> H2 + C2H4	2.00E+12			3
<u>78</u>	H + C2H6 -> C2H5 + H2	1.15E+08	1,9	7530	1.2; 2.1; 3.0
<u>79</u>	H + HCCO -> CH2(S) + CO	1.00E+14			
<u>80</u>	H + CH2CO -> HCCO + H2	5.00E+13		8000	
<u>81</u>	H + CH2CO -> CH3 + CO	1.13E+13		3428	
<u>82</u>	H + HCCOH -> H + CH2CO	1.00E+13			
<u>83</u>	H2 + CO (+M) -> CH2O (+M)	pressure dependent			3
<u>84</u>	OH + H2 -> H + H2O	2.16E+08	1,5	3430	3
<u>85</u>	OH + OH (+M) -> H2O2 (+M)	pressure dependent			3
<u>86</u>	OH + OH -> O + H2O	3.57E+04	2,4	-2110	3
<u>87</u>	OH + HO2 -> O2 + H2O	1.45E+13		-500	1.2; 2.1; 3.0
<u>88</u>	OH + H2O2 -> HO2 + H2O	2.00E+12		427	
<u>89</u>	OH + H2O2 -> HO2 + H2O	1.70E+18		29410	
<u>90</u>	OH + C -> H + CO	5.00E+13			
<u>91</u>	OH + CH -> H + HCO	3.00E+13			
<u>92</u>	OH + CH2 -> H + CH2O	2.00E+13			
<u>93</u>	OH + CH2 -> CH + H2O	1.13E+07	2	3000	
<u>94</u>	OH + CH2(S) -> H + CH2O	3.00E+13			
<u>95</u>	OH + CH3 (+M) -> CH3OH (+M)	pressure dependent			
<u>96</u>	OH + CH3 -> CH2 + H2O	5.60E+07	1,6	5420	3
<u>97</u>	OH + CH3 -> CH2(S) + H2O	6.44E+17	-1,3	1417	1.1; 1.2; 2.1; 3.0
<u>98</u>	OH + CH4 -> CH3 + H2O	1.00E+08	1,6	3120	1.1; 1.2; 2.1; 3.0
<u>99</u>	OH + CO -> H + CO2	4.76E+07	1,2	70	1.1; 1.2; 2.1; 3.0
<u>100</u>	OH + HCO -> H2O + CO	5.00E+13			
<u>101</u>	OH + CH2O -> HCO + H2O	3.43E+09	1,2	-447	3
<u>102</u>	OH + CH2OH -> H2O + CH2O	5.00E+12			
<u>103</u>	OH + CH3O -> H2O + CH2O	5.00E+12			
<u>104</u>	OH + CH3OH -> CH2OH + H2O	1.44E+06	2	-840	
<u>105</u>	OH + CH3OH -> CH3O + H2O	6.30E+06	2	1500	
<u>106</u>	OH + C2H -> H + HCCO	2.00E+13			
<u>107</u>	OH + C2H2 -> H + CH2CO	2.18E-04	4,5	-1000	

<u>108</u>	OH + C2H2 -> H + HCCOH	5.04E+05	2,3	13500	
<u>109</u>	OH + C2H2 -> C2H + H2O	3.37E+07	2	14000	
<u>110</u>	OH + C2H2 -> CH3 + CO	4.83E-04	4	-2000	
<u>111</u>	OH + C2H3 -> H2O + C2H2	5.00E+12			
<u>112</u>	OH + C2H4 -> C2H3 + H2O	3.60E+06	2	2500	3
<u>113</u>	OH + C2H6 -> C2H5 + H2O	3.54E+06	2,1	870	
<u>114</u>	OH + CH2CO -> HCCO + H2O	7.50E+12		2000	
<u>115</u>	HO2 + HO2 -> O2 + H2O2	1.30E+11		-1630	
<u>116</u>	HO2 + HO2 -> O2 + H2O2	4.20E+14		12000	3
<u>117</u>	HO2 + CH2 -> OH + CH2O	2.00E+13			
<u>118</u>	HO2 + CH3 -> O2 + CH4	1.00E+12			1.1; 1.2; 2.1; 3.0
<u>119</u>	HO2 + CH3 -> OH + CH3O	3.78E+13			1.1; 1.2; 2.1; 3.0
<u>120</u>	HO2 + CO -> OH + CO2	1.50E+14		23600	
<u>121</u>	HO2 + CH2O -> HCO + H2O2	5.60E+06	2	12000	3
<u>122</u>	C + O2 -> O + CO	5.80E+13		576	
<u>123</u>	C + CH2 -> H + C2H	5.00E+13			
<u>124</u>	C + CH3 -> H + C2H2	5.00E+13			
<u>125</u>	CH + O2 -> O + HCO	6.71E+13			2.1; 3.0
<u>126</u>	CH + H2 -> H + CH2	1.08E+14		3110	1.2; 2.1; 3.0
<u>127</u>	CH + H2O -> H + CH2O	5.71E+12		-755	2.1; 3.0
<u>128</u>	CH + CH2 -> H + C2H2	4.00E+13			
<u>129</u>	CH + CH3 -> H + C2H3	3.00E+13			3
<u>130</u>	CH + CH4 -> H + C2H4	6.00E+13			
<u>131</u>	CH + CO (+M) -> HCCO (+M)	pressure dependent			
<u>132</u>	CH + CO2 -> HCO + CO	1.90E+14		15792	
<u>133</u>	CH + CH2O -> H + CH2CO	9.46E+13		-515	
<u>134</u>	CH + HCCO -> CO + C2H2	5.00E+13			
<u>135</u>	CH2 + O2 -> OH + H + CO	5.00E+12		1500	1.1; 1.2; 2.1; 3.0
<u>136</u>	CH2 + H2 -> H + CH3	5.00E+05	2	7230	3
<u>137</u>	CH2 + CH2 -> H2 + C2H2	1.60E+15		11944	
<u>138</u>	CH2 + CH3 -> H + C2H4	4.00E+13			3
<u>139</u>	CH2 + CH4 -> CH3 + CH3	2.46E+06	2	8270	3
<u>140</u>	CH2 + CO (+M) -> CH2CO (+M)	pressure dependent			
<u>141</u>	CH2 + HCCO -> C2H3 + CO	3.00E+13			
<u>142</u>	CH2(S) + N2 -> CH2 + N2	1.50E+13		600	3
<u>143</u>	CH2(S) + AR -> CH2 + AR	9.00E+12		600	3
<u>144</u>	CH2(S) + O2 -> H + OH + CO	2.80E+13			3
<u>145</u>	CH2(S) + O2 -> CO + H2O	1.20E+13			3
<u>146</u>	CH2(S) + H2 -> CH3 + H	7.00E+13			1.1; 1.2; 2.1; 3.0
<u>147</u>	CH2(S) + H2O (+M) -> CH3OH (+M)	pressure dependent			
<u>148</u>	CH2(S) + H2O -> CH2 + H2O	3.00E+13			3
<u>149</u>	CH2(S) + CH3 -> H + C2H4	1.20E+13		-570	
<u>150</u>	CH2(S) + CH4 -> CH3 + CH3	1.60E+13		-570	3

<u>151</u>	CH2(S) + CO -> CH2 + CO	9.00E+12			
<u>152</u>	CH2(S) + CO2 -> CH2 + CO2	7.00E+12			
<u>153</u>	CH2(S) + CO2 -> CO + CH2O	1.40E+13			
<u>154</u>	CH2(S) + C2H6 -> CH3 + C2H5	4.00E+13		-550	
<u>155</u>	CH3 + O2 -> O + CH3O	3.56E+13		30480	1.1; 1.2; 2.1; 3.0
<u>156</u>	CH3 + O2 -> OH + CH2O	2.31E+12		20315	1.1; 1.2; 2.1; 3.0
<u>157</u>	CH3 + H2O2 -> HO2 + CH4	2.45E+04	2,5	5180	
<u>158</u>	CH3 + CH3 (+M) -> C2H6 (+M)	pressure dependent			3
<u>159</u>	CH3 + CH3 -> H + C2H5	6.84E+12	0,1	10600	1.1; 1.2; 2.1; 3.0
<u>160</u>	CH3 + HCO -> CH4 + CO	2.65E+13			1.1; 1.2; 2.1
<u>161</u>	CH3 + CH2O -> HCO + CH4	3.32E+03	2,8	5860	
<u>162</u>	CH3 + CH3OH -> CH2OH + CH4	3.00E+07	1,5	9940	
<u>163</u>	CH3 + CH3OH -> CH3O + CH4	1.00E+07	1,5	9940	
<u>164</u>	CH3 + C2H4 -> C2H3 + CH4	2.27E+05	2	9200	
<u>165</u>	CH3 + C2H6 -> C2H5 + CH4	6.14E+06	1,7	10450	3
<u>166</u>	HCO + H2O -> H + CO + H2O	1.50E+18	-1	17000	1.1; 1.2; 2.1; 3.0
<u>167</u>	HCO + M -> H + CO + M	1.87E+17	-1	17000	1.1; 1.2; 2.1; 3.0
<u>168</u>	HCO + O2 -> HO2 + CO	1.35E+13		400	1.2; 2.1; 3.0
<u>169</u>	CH2OH + O2 -> HO2 + CH2O	1.80E+13		900	
<u>170</u>	CH3O + O2 -> HO2 + CH2O	4.28E-13	7,6	-3530	3
<u>171</u>	C2H + O2 -> HCO + CO	1.00E+13		-755	
<u>172</u>	C2H + H2 -> H + C2H2	5.68E+10	0,9	1993	
<u>173</u>	C2H3 + O2 -> HCO + CH2O	4.58E+16	-1,4	1015	
<u>174</u>	C2H4 (+M) -> H2 + C2H2 (+M)	pressure dependent			
<u>175</u>	C2H5 + O2 -> HO2 + C2H4	8.40E+11		3875	3
<u>176</u>	HCCO + O2 -> OH + CO + CO	3.20E+12		854	3
<u>177</u>	HCCO + HCCO -> CO + CO + C2H2	1.00E+13			
<u>178</u>	N + NO -> N2 + O	2.70E+13		355	2.1; 3.0
<u>179</u>	N + O2 -> NO + O	9.00E+09	1	6500	3
<u>180</u>	N + OH -> NO + H	3.36E+13		385	2.1; 3.0
<u>181</u>	N2O + O -> N2 + O2	1.40E+12		10810	
<u>182</u>	N2O + O -> NO + NO	2.90E+13		23150	
<u>183</u>	N2O + H -> N2 + OH	3.87E+14		18880	2.1; 3.0
<u>184</u>	N2O + OH -> N2 + HO2	2.00E+12		21060	
<u>185</u>	N2O (+M) -> N2 + O (+M)	pressure dependent			
<u>186</u>	HO2 + NO -> NO2 + OH	2.11E+12		-480	
<u>187</u>	NO + O + M -> NO2 + M	1.06E+20	-1,4		
<u>188</u>	NO2 + O -> NO + O2	3.90E+12		-240	
<u>189</u>	NO2 + H -> NO + OH	1.32E+14		360	
<u>190</u>	NH + O -> NO + H	4.00E+13			2.1; 3.0
<u>191</u>	NH + H -> N + H2	3.20E+13		330	3
<u>192</u>	NH + OH -> HNO + H	2.00E+13			

<u>193</u>	NH + OH -> N + H2O	2.00E+09	1,2		
<u>194</u>	NH + O2 -> HNO + O	4.61E+05	2	6500	
<u>195</u>	NH + O2 -> NO + OH	1.28E+06	1,5	100	
<u>196</u>	NH + N -> N2 + H	1.50E+13			
<u>197</u>	NH + H2O -> HNO + H2	2.00E+13		13850	
<u>198</u>	NH + NO -> N2 + OH	2.16E+13	-0,2		
<u>199</u>	NH + NO -> N2O + H	3.65E+14	-0,5		2.1; 3.0
<u>200</u>	NH2 + O -> OH + NH	3.00E+12			
<u>201</u>	NH2 + O -> H + HNO	3.90E+13			3
<u>202</u>	NH2 + H -> NH + H2	4.00E+13		3650	3
<u>203</u>	NH2 + OH -> NH + H2O	9.00E+07	1,5	-460	
<u>204</u>	NNH -> N2 + H	3.30E+08			
<u>205</u>	NNH + M -> N2 + H + M	1.30E+14	-0,1	4980	
<u>206</u>	NNH + O2 -> HO2 + N2	5.00E+12			
<u>207</u>	NNH + O -> OH + N2	2.50E+13			
<u>208</u>	NNH + O -> NH + NO	7.00E+13			
<u>209</u>	NNH + H -> H2 + N2	5.00E+13			
<u>210</u>	NNH + OH -> H2O + N2	2.00E+13			
<u>211</u>	NNH + CH3 -> CH4 + N2	2.50E+13			
<u>212</u>	H + NO + M -> HNO + M	4.48E+19	-1,3	740	3
<u>213</u>	HNO + O -> NO + OH	2.50E+13			
<u>214</u>	HNO + H -> H2 + NO	9.00E+11	0,7	660	3
<u>215</u>	HNO + OH -> NO + H2O	1.30E+07	1,9	-950	
<u>216</u>	HNO + O2 -> HO2 + NO	1.00E+13		13000	
<u>217</u>	CN + O -> CO + N	7.70E+13			
<u>218</u>	CN + OH -> NCO + H	4.00E+13			2.1; 3.0
<u>219</u>	CN + H2O -> HCN + OH	8.00E+12		7460	2.1; 3.0
<u>220</u>	CN + O2 -> NCO + O	6.14E+12		-440	
<u>221</u>	CN + H2 -> HCN + H	2.95E+05	2,5	2240	2.1; 3.0
<u>222</u>	NCO + O -> NO + CO	2.35E+13			2.1; 3.0
<u>223</u>	NCO + H -> NH + CO	5.40E+13			
<u>224</u>	NCO + OH -> NO + H + CO	2.50E+12			2.1; 3.0
<u>225</u>	NCO + N -> N2 + CO	2.00E+13			
<u>226</u>	NCO + O2 -> NO + CO2	2.00E+12		20000	
<u>227</u>	NCO + M -> N + CO + M	3.10E+14		54050	
<u>228</u>	NCO + NO -> N2O + CO	1.90E+17	-1,5	740	2.1; 3.0
<u>229</u>	NCO + NO -> N2 + CO2	3.80E+18	-2	800	2.1; 3.0
<u>230</u>	HCN + M -> H + CN + M	1.04E+29	-3,3	126600	
<u>231</u>	HCN + O -> NCO + H	2.03E+04	2,6	4980	2.1; 3.0
<u>232</u>	HCN + O -> NH + CO	5.07E+03	2,6	4980	2.1; 3.0
<u>233</u>	HCN + O -> CN + OH	3.91E+09	1,6	26600	2.1; 3.0
<u>234</u>	HCN + OH -> HOCN + H	1.10E+06	2	13370	3
<u>235</u>	HCN + OH -> HNCO + H	4.40E+03	2,3	6400	

<u>236</u>	HCN + OH -> NH2 + CO	1.60E+02	2,6	9000	
<u>237</u>	H + HCN (+M) -> H2CN (+M)	pressure dependent			
<u>238</u>	H2CN + N -> N2 + CH2	6.00E+13		400	
<u>239</u>	C + N2 -> CN + N	6.30E+13		46020	
<u>240</u>	CH + N2 -> HCN + N	3.12E+09	0,9	20130	2.1; 3.0
<u>241</u>	CH + N2 (+M) -> HCNN (+M)	pressure dependent			
<u>242</u>	CH2 + N2 -> HCN + NH	1.00E+13		74000	
<u>243</u>	CH2(S) + N2 -> NH + HCN	1.00E+11		65000	
<u>244</u>	C + NO -> CN + O	1.90E+13			
<u>245</u>	C + NO -> CO + N	2.90E+13			
<u>246</u>	CH + NO -> HCN + O	4.10E+13			2.1; 3.0
<u>247</u>	CH + NO -> H + NCO	1.62E+13			2.1; 3.0
<u>248</u>	CH + NO -> N + HCO	2.46E+13			2.1; 3.0
<u>249</u>	CH2 + NO -> H + HNCO	3.10E+17	-1,4	1270	3
<u>250</u>	CH2 + NO -> OH + HCN	2.90E+14	-0,7	760	3
<u>251</u>	CH2 + NO -> H + HCNO	3.80E+13	-0,4	580	
<u>252</u>	CH2(S) + NO -> H + HNCO	3.10E+17	-1,4	1270	
<u>253</u>	CH2(S) + NO -> OH + HCN	2.90E+14	-0,7	760	
<u>254</u>	CH2(S) + NO -> H + HCNO	3.80E+13	-0,4	580	
<u>255</u>	CH3 + NO -> HCN + H2O	9.60E+13		28800	3
<u>256</u>	CH3 + NO -> H2CN + OH	1.00E+12		21750	
<u>257</u>	HCNN + O -> CO + H + N2	2.20E+13			
<u>258</u>	HCNN + O -> HCN + NO	2.00E+12			
<u>259</u>	HCNN + O2 -> O + HCO + N2	1.20E+13			
<u>260</u>	HCNN + OH -> H + HCO + N2	1.20E+13			
<u>261</u>	HCNN + H -> CH2 + N2	1.00E+14			
<u>262</u>	HNCO + O -> NH + CO2	9.80E+07	1,4	8500	
<u>263</u>	HNCO + O -> HNO + CO	1.50E+08	1,6	44000	
<u>264</u>	HNCO + O -> NCO + OH	2.20E+06	2,1	11400	
<u>265</u>	HNCO + H -> NH2 + CO	2.25E+07	1,7	3800	
<u>266</u>	HNCO + H -> H2 + NCO	1.05E+05	2,5	13300	
<u>267</u>	HNCO + OH -> NCO + H2O	3.30E+07	1,5	3600	
<u>268</u>	HNCO + OH -> NH2 + CO2	3.30E+06	1,5	3600	
<u>269</u>	HNCO + M -> NH + CO + M	1.18E+16		84720	
<u>270</u>	HCNO + H -> H + HNCO	2.10E+15	-0,7	2850	3
<u>271</u>	HCNO + H -> OH + HCN	2.70E+11	0,2	2120	3
<u>272</u>	HCNO + H -> NH2 + CO	1.70E+14	-0,8	2890	
<u>273</u>	HOCN + H -> H + HNCO	2.00E+07	2	2000	
<u>274</u>	HCCO + NO -> HCNO + CO	9.00E+12			3
<u>275</u>	CH3 + N -> H2CN + H	6.10E+14	-0,3	290	3
<u>276</u>	CH3 + N -> HCN + H2	3.70E+12	0,1	-90	3
<u>277</u>	NH3 + H -> NH2 + H2	5.40E+05	2,4	9915	
<u>278</u>	NH3 + OH -> NH2 + H2O	5.00E+07	1,6	955	

<u>279</u>	NH <sub>3</sub> + O -> NH <sub>2</sub> + OH	9.40E+06	1,9	6460	
<u>280</u>	NH + CO <sub>2</sub> -> HNO + CO	1.00E+13		14350	
<u>281</u>	CN + NO <sub>2</sub> -> NCO + NO	6.16E+15	-0,8	345	
<u>282</u>	NCO + NO <sub>2</sub> -> N <sub>2</sub> O + CO <sub>2</sub>	3.25E+12		-705	
<u>283</u>	N + CO <sub>2</sub> -> NO + CO	3.00E+12		11300	
<u>284</u>	O + CH <sub>3</sub> -> H + H <sub>2</sub> + CO	3.37E+13			3
<u>285</u>	O + C <sub>2</sub> H <sub>4</sub> -> H + CH <sub>2</sub> CHO	6.70E+06	1,8	220	
<u>286</u>	O + C <sub>2</sub> H <sub>5</sub> -> H + CH <sub>3</sub> CHO	1.10E+14			
<u>287</u>	OH + HO <sub>2</sub> -> O <sub>2</sub> + H <sub>2</sub> O	5.00E+15		17330	3
<u>288</u>	OH + CH <sub>3</sub> -> H <sub>2</sub> + CH <sub>2</sub> O	8.00E+09	0,5	-1755	
<u>289</u>	CH + H <sub>2</sub> (+M) -> CH <sub>3</sub> (+M)	pressure dependent			3
<u>290</u>	CH <sub>2</sub> + O <sub>2</sub> -> H + H + CO <sub>2</sub>	5.80E+12		1500	3
<u>291</u>	CH <sub>2</sub> + O <sub>2</sub> -> O + CH <sub>2</sub> O	2.40E+12		1500	
<u>292</u>	CH <sub>2</sub> + CH <sub>2</sub> -> H + H + C <sub>2</sub> H <sub>2</sub>	2.00E+14		10989	
<u>293</u>	CH <sub>2</sub> (S) + H <sub>2</sub> O -> H <sub>2</sub> + CH <sub>2</sub> O	6.82E+10	0,2	-935	
<u>294</u>	C <sub>2</sub> H <sub>3</sub> + O <sub>2</sub> -> O + CH <sub>2</sub> CHO	3.03E+11	0,3	11	
<u>295</u>	C <sub>2</sub> H <sub>3</sub> + O <sub>2</sub> -> HO <sub>2</sub> + C <sub>2</sub> H <sub>2</sub>	1.34E+06	1,6	-384	
<u>296</u>	O + CH <sub>3</sub> CHO -> OH + CH <sub>2</sub> CHO	2.92E+12		1808	
<u>297</u>	O + CH <sub>3</sub> CHO -> OH + CH <sub>3</sub> + CO	2.92E+12		1808	
<u>298</u>	O <sub>2</sub> + CH <sub>3</sub> CHO -> HO <sub>2</sub> + CH <sub>3</sub> + CO	3.01E+13		39150	
<u>299</u>	H + CH <sub>3</sub> CHO -> CH <sub>2</sub> CHO + H <sub>2</sub>	2.05E+09	1,2	2405	
<u>300</u>	H + CH <sub>3</sub> CHO -> CH <sub>3</sub> + H <sub>2</sub> + CO	2.05E+09	1,2	2405	
<u>301</u>	OH + CH <sub>3</sub> CHO -> CH <sub>3</sub> + H <sub>2</sub> O + CO	2.34E+10	0,7	-1113	
<u>302</u>	HO <sub>2</sub> + CH <sub>3</sub> CHO -> CH <sub>3</sub> + H <sub>2</sub> O <sub>2</sub> + CO	3.01E+12		11923	
<u>303</u>	CH <sub>3</sub> + CH <sub>3</sub> CHO -> CH <sub>3</sub> + CH <sub>4</sub> + CO	2.72E+06	1,8	5920	
<u>304</u>	H + CH <sub>2</sub> CO (+M) -> CH <sub>2</sub> CHO (+M)	pressure dependent			
<u>305</u>	O + CH <sub>2</sub> CHO -> H + CH <sub>2</sub> + CO <sub>2</sub>	1.50E+14			
<u>306</u>	O <sub>2</sub> + CH <sub>2</sub> CHO -> OH + CO + CH <sub>2</sub> O	1.81E+10			
<u>307</u>	O <sub>2</sub> + CH <sub>2</sub> CHO -> OH + HCO + HCO	2.35E+10			
<u>308</u>	H + CH <sub>2</sub> CHO -> CH <sub>3</sub> + HCO	2.20E+13			
<u>309</u>	H + CH <sub>2</sub> CHO -> CH <sub>2</sub> CO + H <sub>2</sub>	1.10E+13			
<u>310</u>	OH + CH <sub>2</sub> CHO -> H <sub>2</sub> O + CH <sub>2</sub> CO	1.20E+13			
<u>311</u>	OH + CH <sub>2</sub> CHO -> HCO + CH <sub>2</sub> OH	3.01E+13			
<u>312</u>	CH <sub>3</sub> + C <sub>2</sub> H <sub>5</sub> (+M) -> C <sub>3</sub> H <sub>8</sub> (+M)	pressure dependent			3
<u>313</u>	O + C <sub>3</sub> H <sub>8</sub> -> OH + C <sub>3</sub> H <sub>7</sub>	1.93E+05	2,7	3716	
<u>314</u>	H + C <sub>3</sub> H <sub>8</sub> -> C <sub>3</sub> H <sub>7</sub> + H <sub>2</sub>	1.32E+06	2,5	6756	3
<u>315</u>	OH + C <sub>3</sub> H <sub>8</sub> -> C <sub>3</sub> H <sub>7</sub> + H <sub>2</sub> O	3.16E+07	1,8	934	
<u>316</u>	C <sub>3</sub> H <sub>7</sub> + H <sub>2</sub> O <sub>2</sub> -> HO <sub>2</sub> + C <sub>3</sub> H <sub>8</sub>	3.78E+02	2,7	1500	
<u>317</u>	CH <sub>3</sub> + C <sub>3</sub> H <sub>8</sub> -> C <sub>3</sub> H <sub>7</sub> + CH <sub>4</sub>	9.03E-01	3,6	7154	
<u>318</u>	CH <sub>3</sub> + C <sub>2</sub> H <sub>4</sub> (+M) -> C <sub>3</sub> H <sub>7</sub> (+M)	pressure dependent			



<u>319</u>	$O + C_3H_7 \rightarrow C_2H_5 + CH_2O$	9.64E+13			
<u>320</u>	$H + C_3H_7 (+M) \rightarrow C_3H_8 (+M)$	pressure dependent			
<u>321</u>	$H + C_3H_7 \rightarrow CH_3 + C_2H_5$	4.06E+06	2,2	890	
<u>322</u>	$OH + C_3H_7 \rightarrow C_2H_5 + CH_2OH$	2.41E+13			
<u>323</u>	$HO_2 + C_3H_7 \rightarrow O_2 + C_3H_8$	2.55E+10	0,3	-943	
<u>324</u>	$HO_2 + C_3H_7 \rightarrow OH + C_2H_5 + CH_2O$	2.41E+13			
<u>325</u>	$CH_3 + C_3H_7 \rightarrow C_2H_5 + C_2H_5$	1.93E+13	-0,3		

## APPENDIX B

### XPS AND RAMAN FIGURES

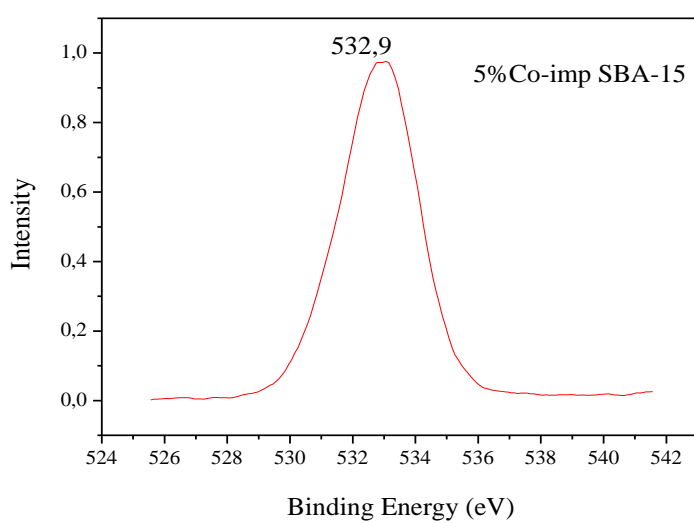


Figure B.1 XPS spectra of the O 1s level for Co impregnated mesoporous silica sample

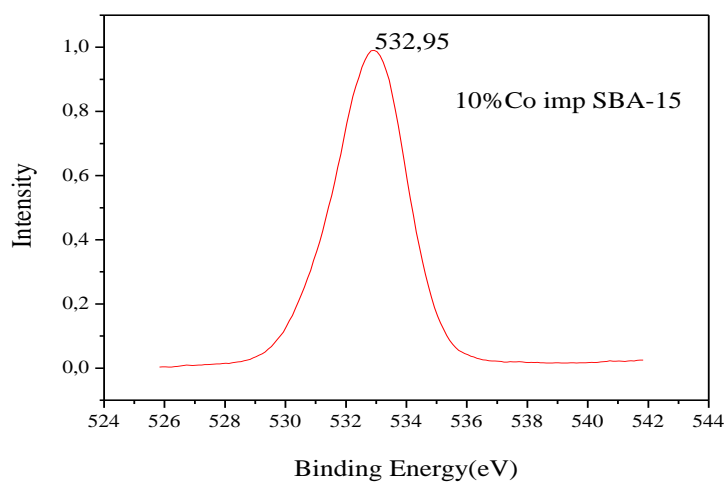


Figure B.2 XPS spectra of the O 1s level for Co impregnated mesoporous silica sample

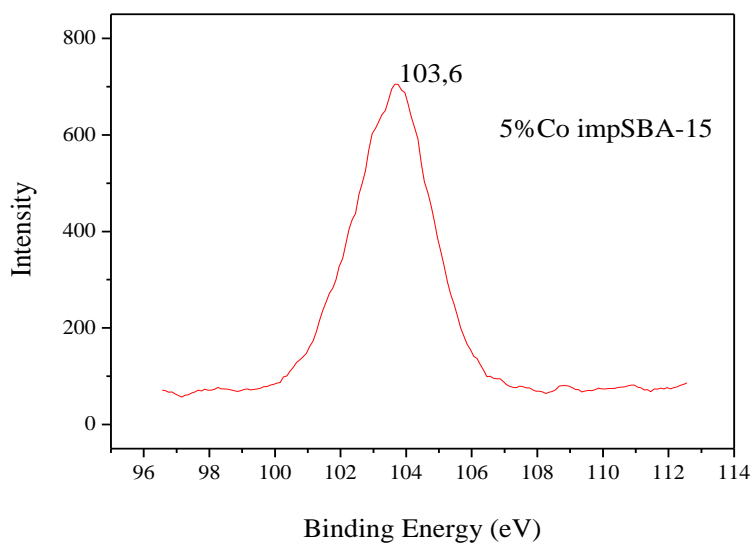


Figure B.3 XPS spectra of the Si 2p level for Co impregnated mesoporous silica sample

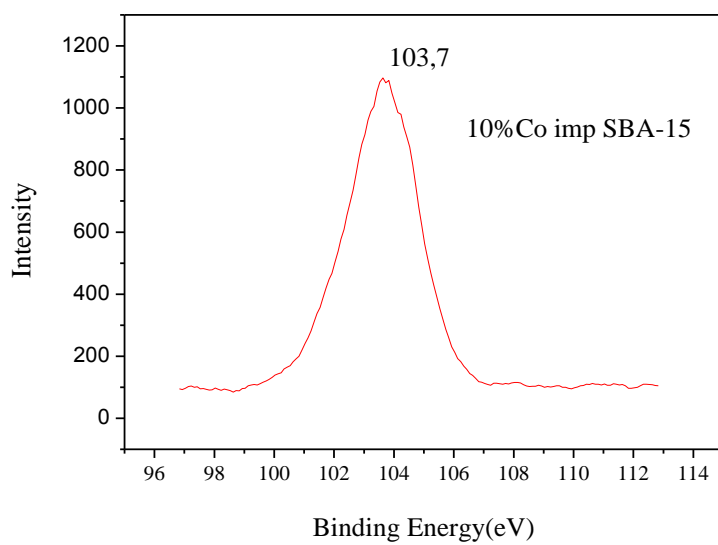


Figure B.4 XPS spectra of the Si 2p level for Co impregnated mesoporous silica sampl

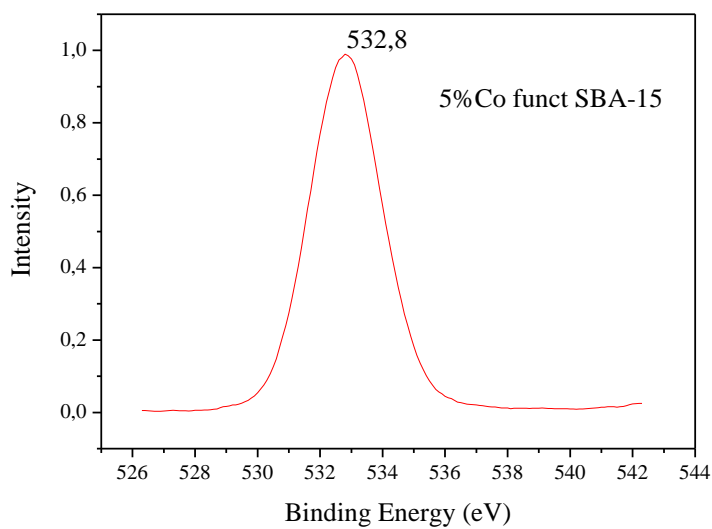


Figure B.5 XPS spectra of the O 1s level for Co functionalized mesoporous silica sample

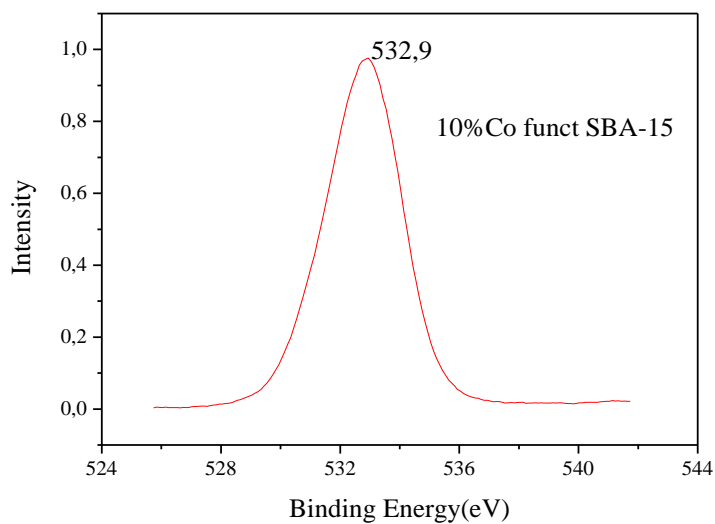


Figure B.6 XPS spectra of the O 1s level for Co functionalized mesoporous silica sample.

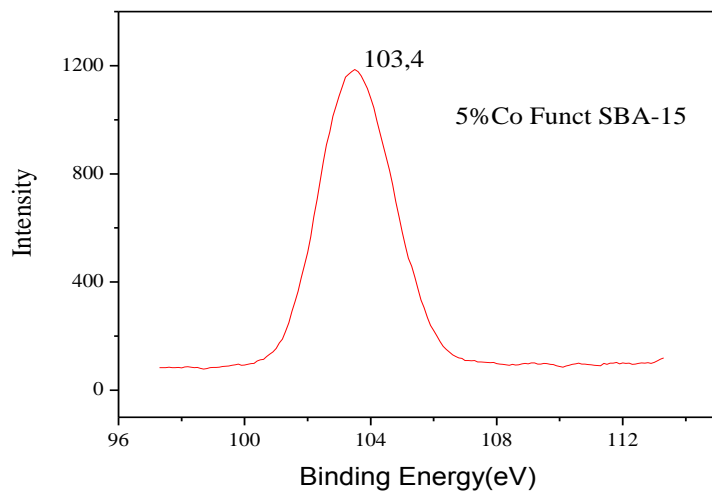


Figure B.7 XPS spectra of the Si 2p level for Co functionalized mesoporous silica sample

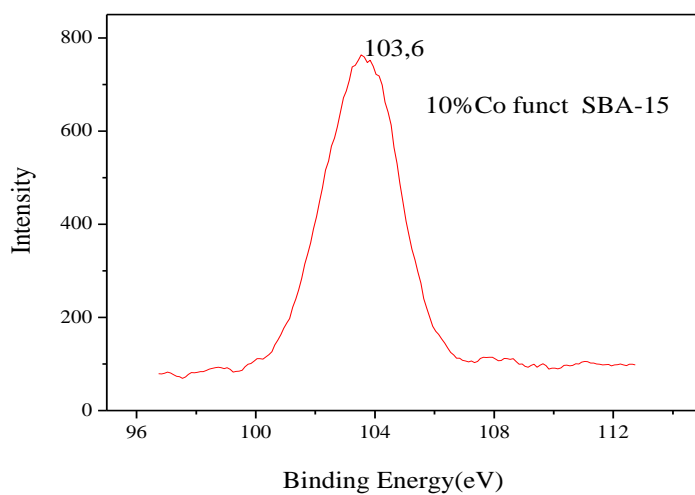


Figure B.8 XPS spectra of the Si 2p level for Co functionalized mesoporous silica sample.

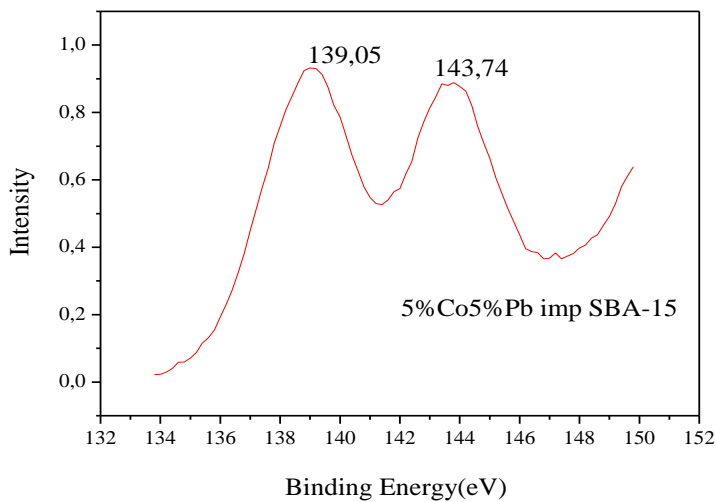


Figure B.9 XPS spectra of the Pb 4f level for Co and Pb impregnated mesoporous silica sample.

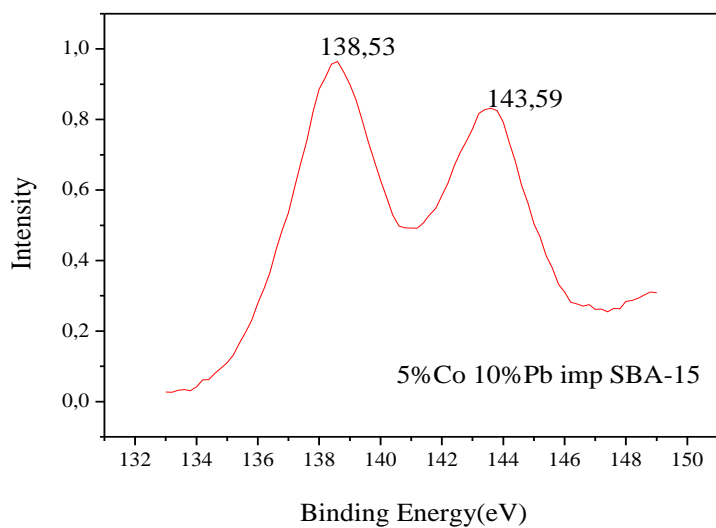


Figure B.10 XPS spectra of the Pb 4f level for Co and Pb impregnated mesoporous silica sample.

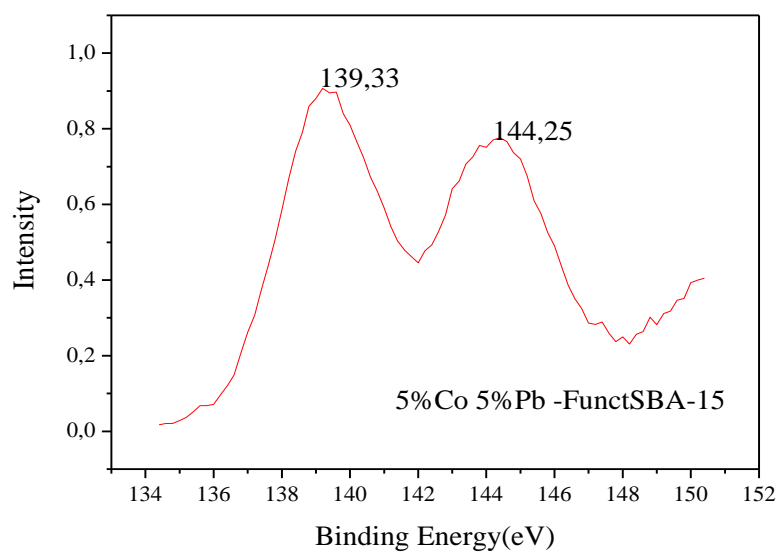


Figure B.11 XPS spectra of the Pb 4f level for Co and Pb impregnated mesoporous silica sample.

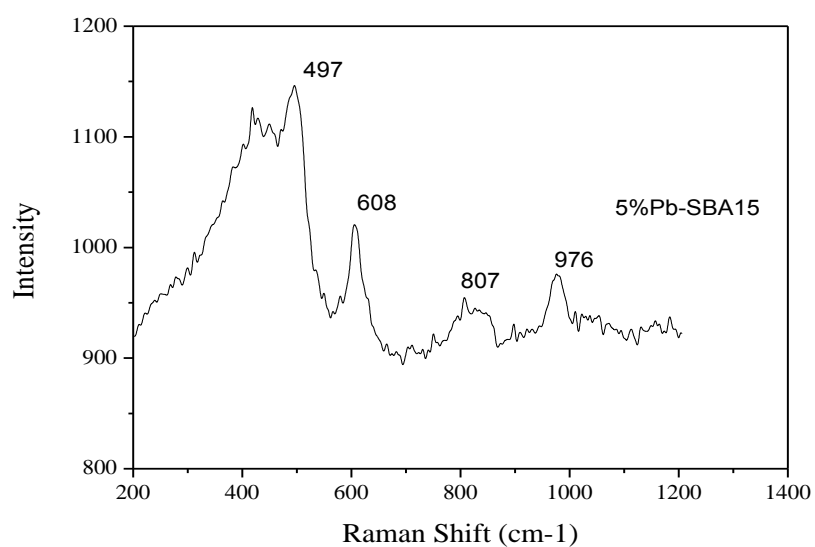


Figure B.12 Raman spectra of 5%Pb-SBA-15 catalyst

# APPENDIX C

## BET FIGURES

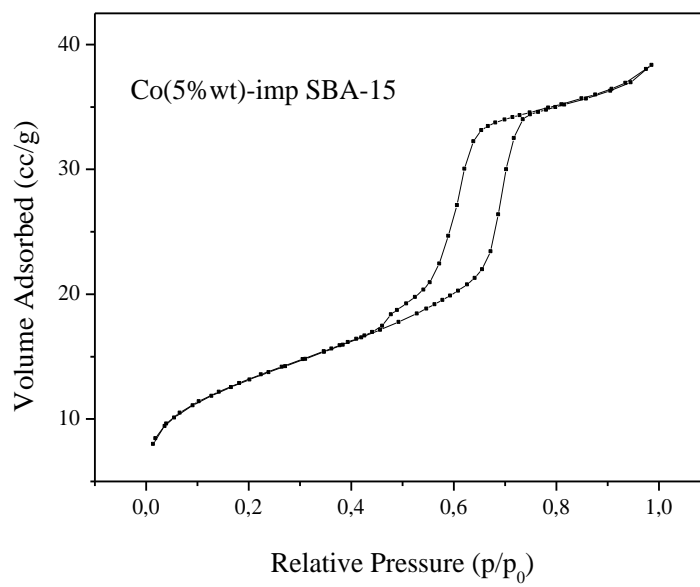


Figure C.1 Nitrogen adsorption isotherm of Co(5% wt)-impregnated SBA-15



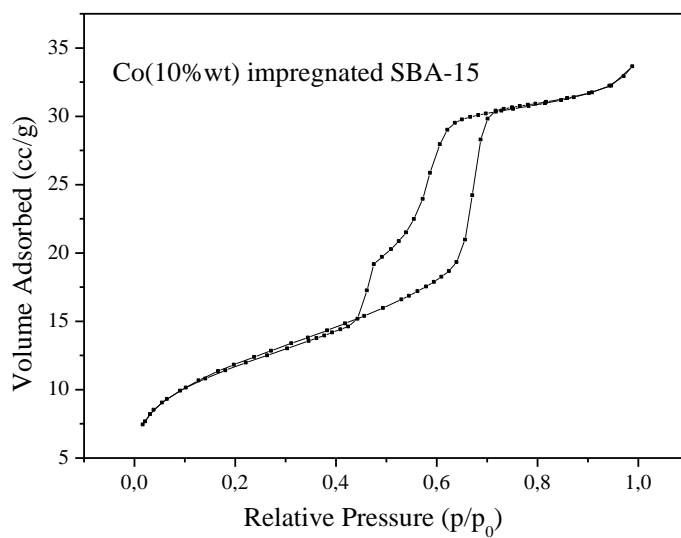


Figure C.2 Nitrogen adsorption isotherm of Co(10% wt) impregnated SBA-15

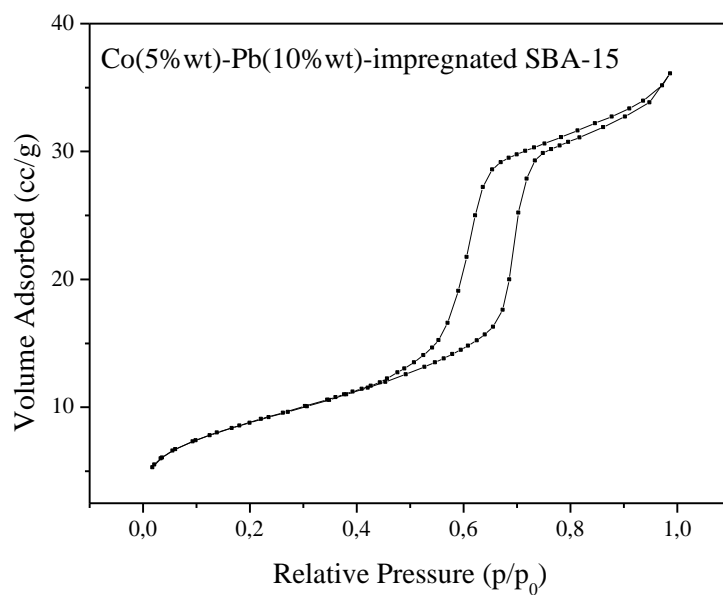


Figure C.3 Nitrogen adsorption isotherm of Co(5% wt)-Pb(10% wt)-impregnated SBA-15

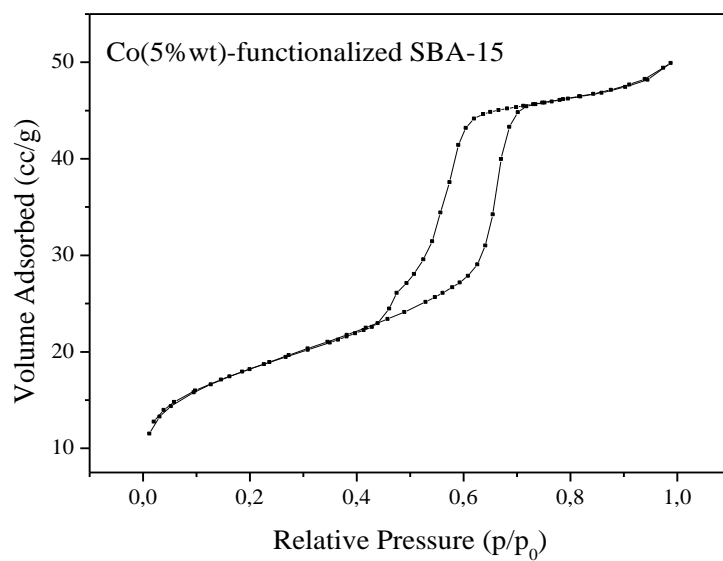


Figure C.4 Nitrogen adsorption isotherm of Co(5% wt)-functionalized SBA-15

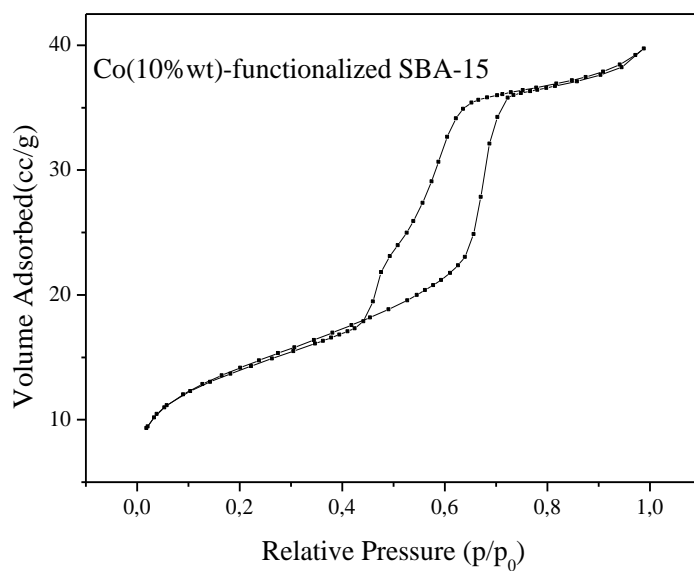


Figure C.5 Nitrogen adsorption isotherm of Co(10% wt)-functionalized SBA-15

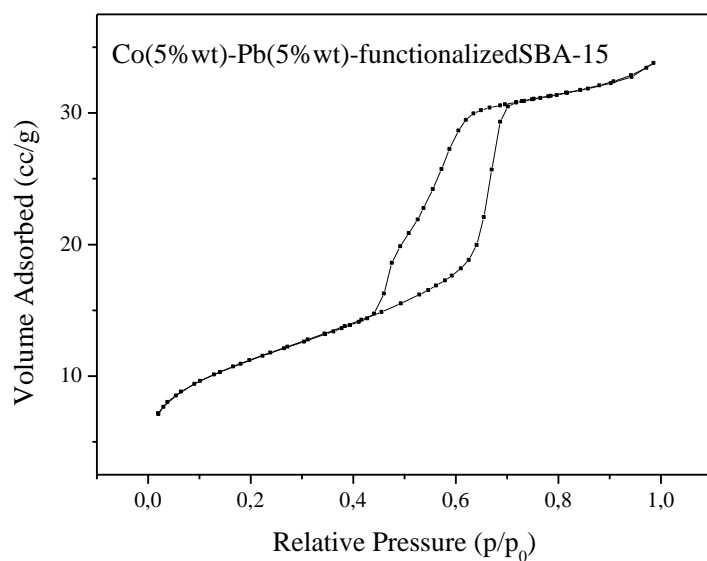


Figure C.6 Nitrogen adsorption isotherm of Co(5% wt)-Pb(5% wt)-functionalized SBA-15

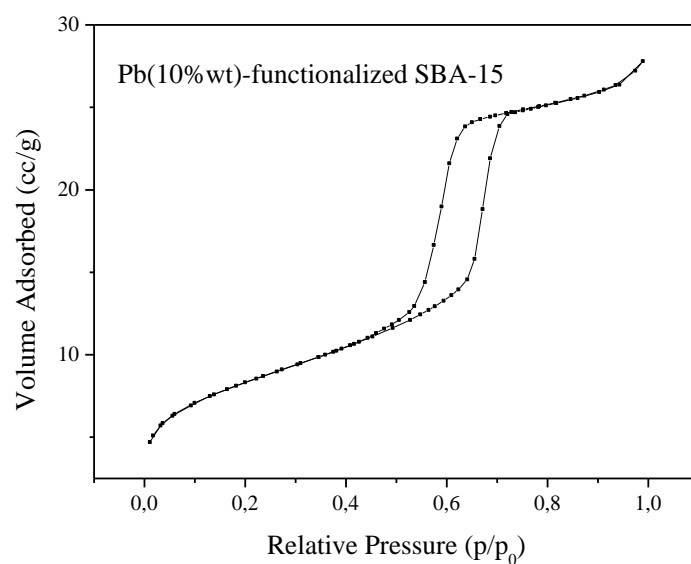


Figure C.7 Nitrogen adsorption isotherm of Pb (10% wt)-functionalized SBA-15

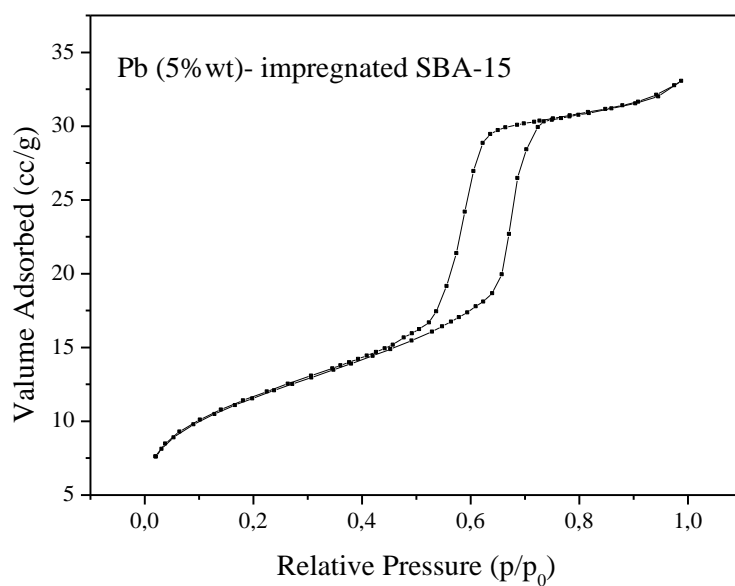


Figure C.8 Nitrogen adsorption isotherm of Pb (5% wt)- impregnated SBA-15

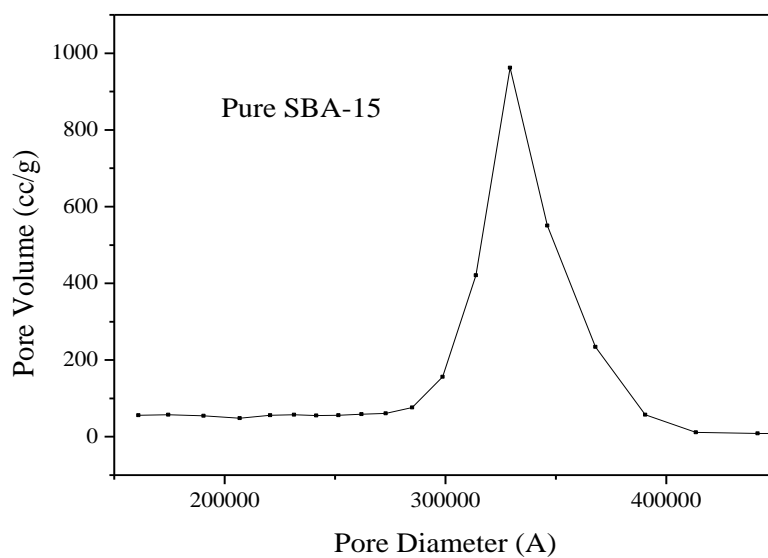


Figure C.9 BJH adsorption pore size distribution of Pure SBA-15

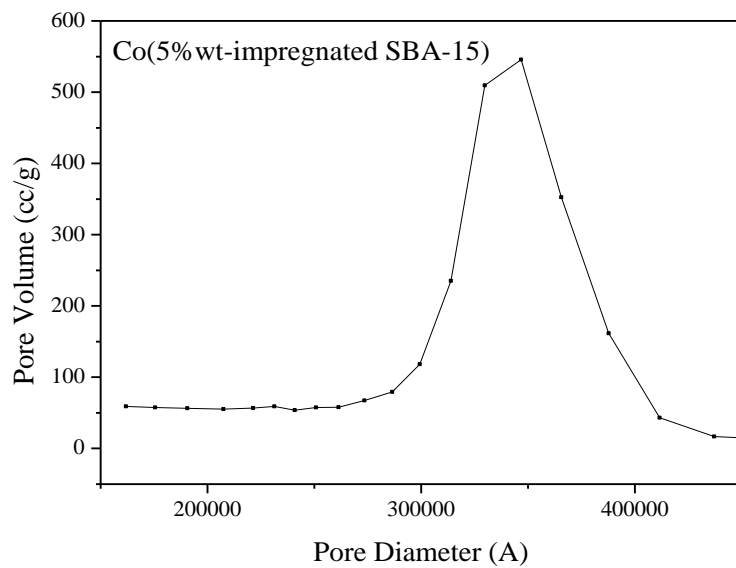


Figure C.10 BJH adsorption pore size distribution of Co(5%wt-impregnated SBA-15)

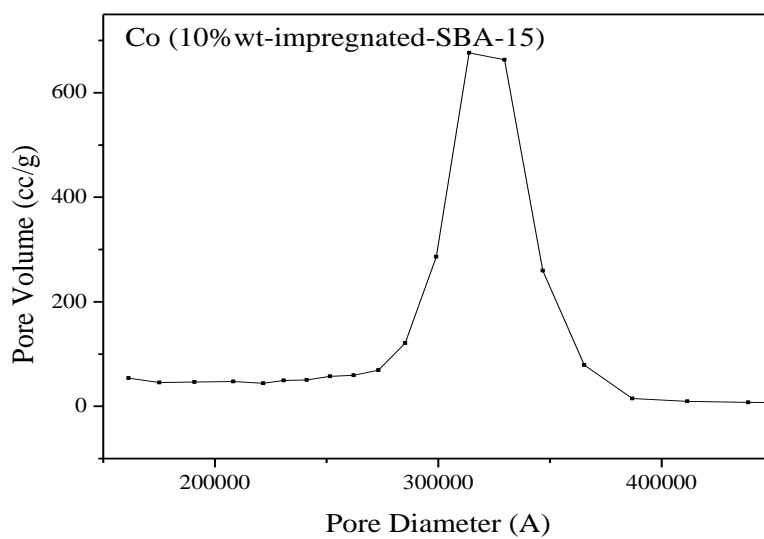


Figure C.11 BJH adsorption pore size distribution of Co (10%wt-impregnated-SBA-15)

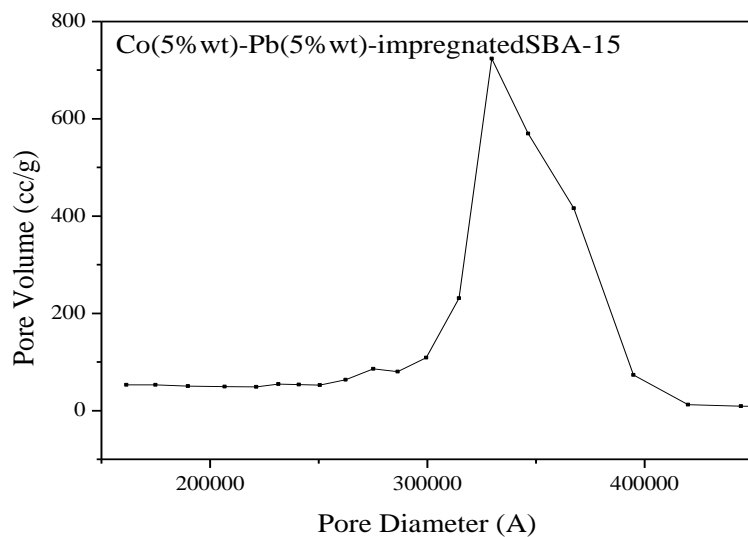


Figure C.12 BJH adsorption pore size distribution of Co(5% wt)-Pb(5% wt)-impregnated SBA-15

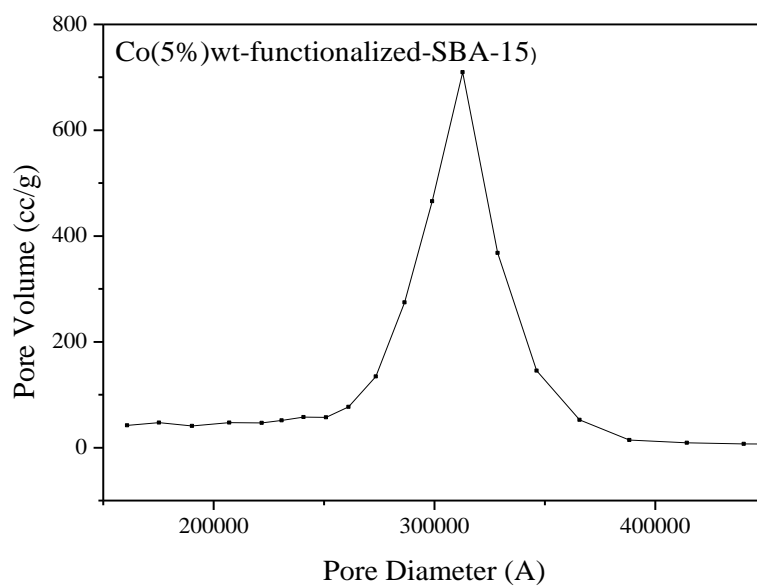


Figure C.13 BJH adsorption pore size distribution of Co(5% wt)-functionalized SBA-15

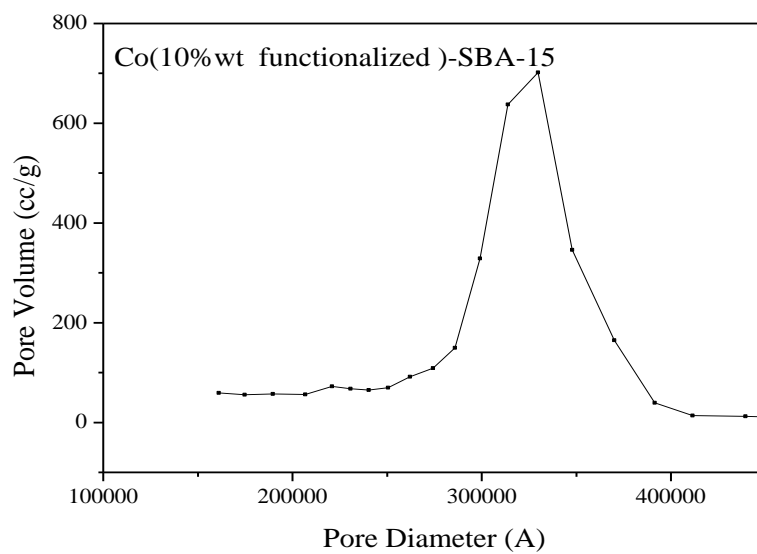


Figure C.14 BJH adsorption pore size distribution of Co(10%wt functionalized)-SBA-15

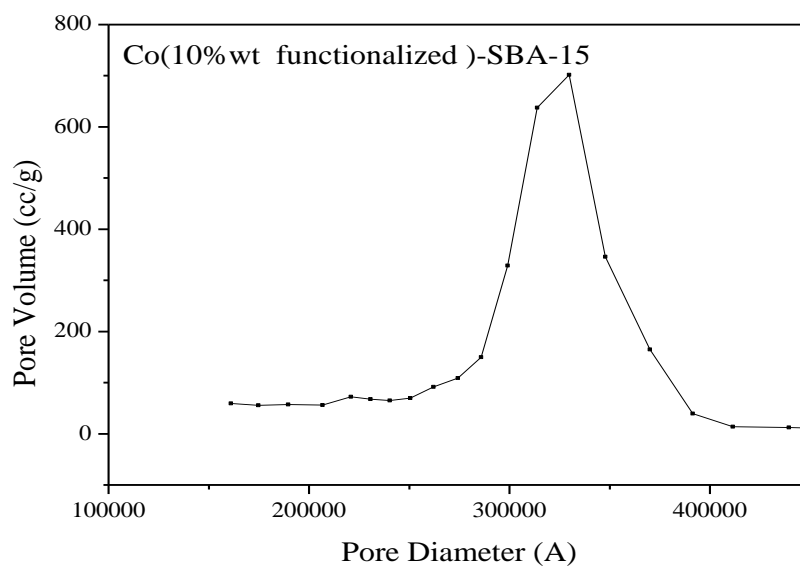


Figure C.15 BJH adsorption pore size distribution of Co(10%wt functionalized)-SBA-15

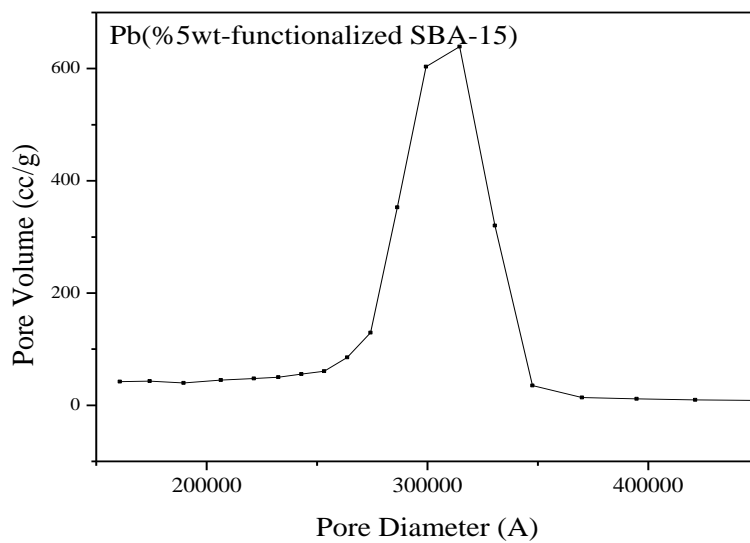


Figure C.16 BJH adsorption pore size distribution of Pb(5wt-functionalized SBA-15)

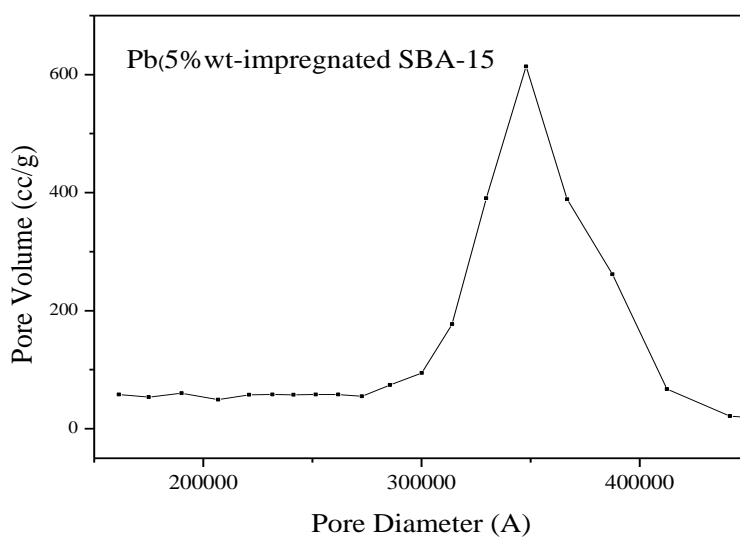


Figure C.17 BJH adsorption pore size distribution of Pb(5wt-impregnated SBA-15)



# CURRICULUM VITAE

Mukaddes Can  
Middle East Technical University  
Department of Chemical Engineering  
06531 Ankara/Turkey

Phone: +90 312 210 43 86

Fax: +90 312 210 26 00

E-mail: mcan@metu.edu.tr

## PERSONAL INFORMATION

Nationality: Turkish (TC)

Gender: Female

Date and Place of Birth: 23th August 1976, Eskişehir

## EDUCATION

Degree	Institution	Year of Graduation
Ph. D.	METU Chemical Engineering	2011
M.Sc.	Eskisehir Osmangazi University Chemical Engineering	2001
B. Sc.	Eskisehir Osmangazi University Chemical Engineering	1998
High School	Eskişehir Cumhuriyet High School	1993

## WORK EXPERIENCE

Year	Place	Enrollment
1995 July	Eskişehir ETI Food	Internship
1995 August	EskisehirPlamat Plastic	Internship
1996 July	Eskişehir ETI Food	Internship

## **MEMBERSHIPS**

2006 - Catalysis Society of Turkey

## **FOREIGN LANGUAGES**

Advanced English

## **PROFESSIONAL**

### **Year**

2009 April –2010 February, Visiting Scientist;  
Technical University of Darmstadt, Eduard-Zintl-Institut, Darmstadt, Germany,  
Synthesis and Characterization of Co-Pb-SBA-15 catalysts by using Raman and XPS techniques”

2002- 2011, Research Assistant;  
Middle East Technical University (METU), Department of Chemical Engineering,  
Ankara, Turkey. Making PhD in METU in the name of Selcuk University.

## **PUBLICATIONS**

### **Refereed Journals:**

1. S. Şensöz, M. Can, "Pyrolysis of pine (*Pinus Brutia* Ten.) chips:1. Effect of pyrolysis temperature and heating rate on the product yields", *Energy Sources*, 24 (2002), 347-355.
2. S. Şensöz, M. Can, "Pyrolysis of pine (*Pinus Brutia* Ten.) chips: 2. Structural analysis of biooil", *Energy Sources*, 24(2002), 357-364.
3. M. Can, B. Akça, A. Yılmaz, D. Uner, Synthesis and characterization of mesoporous Co-Pb/SBA-15”, *Turkish Journal of Physics*, 29 (2005) 287-293.
4. B. Akca, M. Can, V. Degirmenci, A. Yilmaz, D. Uner, “Single step synthesis of mesoporous Co-Pb/SBA-15 catalysts”, *Studies in Surface Science and Catalysis*, 172 (2007) 317.

5. B. Akca, O. Güner, M. Can, A.Yılmaz, D. Uner, "Oxidation States and the Acidity of Ordered Arrays of Co-Pb Mixed Oxide Nanoparticles Templated in SBA-15", Topics in Catalysis, 4 (2008) 187-192.
6. M. Can, D. Uner, "Methane Partial Oxidation over Co and/or Pb-SBA-15 mesoporous mixed oxide catalysts" in preparation.

### **National and International Conference Presentations:**

1. Angın, D., M. Can, S. Şensöz, "Pyrolysis of Pine (*Pinus Brutia* Ten)woods in fix bed reactor", III. National Clean Energy Symposium, İstanbul, 2000, Oral Presentation.
2. M. Can, B. Akça, A. Yılmaz, D. Uner, "Synthesis and characterization of mesoporous Co-Pb/SBA-15", EuropaCAT VII, Sofia/ BULGARIA, 2005. Poster Presentation.
3. M. Can, B. Akça, A. Yılmaz, D. Uner, " Synthesis and characterization of mesoporous Co-Pb/SBA-15", NANO-TRI, Bilkent University, ANKARA, 2005, Poster Presentation.
4. M. Can, B. Akça, A. Yılmaz, D.Uner, "What is the limiting of loading of Co and/ or in SBA-15?? ", NANO-TR 2, METU, ANKARA, 2006, Poster Presentation.
5. M. Can, B. Akça, A. Yılmaz, D.Uner, "Synthesis and characterization of mesoporous Co-Pb/SBA-15", UKMK 7, ESKİŞEHİR, 2006, Poster Presentation.
6. M. Can, B.Akça, A. Yılmaz, D. Uner,"Synthesis and characterization of mesoporous Co-Pb/SBA-15", TOCAT 5, Tokyo/JAPAN, 2006. Oral Presentation.
7. B. Akça, M. Can, A. Yılmaz, D. Uner., "What is the limiting of loading of Co and/ or in SBA-15? ", European Materials Research Society Fall meeting (MRS), POLAND, 2006. Poster Presentation.
8. M.Can, A.Yılmaz, D.Üner, "Synthesis of Pt /Co-Pb/SBA15 mesoporous catalysts and characterization of the samples with TPR technique" 2<sup>nd</sup> National Catalysis Congress (NCC-2), Erzurum, Turkey, June 2008, Poster Presentation.

9. M. Can, A. Yılmaz, D. Uner, "Methane Partial Oxidation over Rh-Co and/or Pb/SBA-15 Mesoporous Catalysts" EuropaCATIX, Salamanca/SPAIN, August 30-September 4, 2009, Poster Presentation.
  
10. M. Can, C. Hess, A. Yılmaz, D. Üner, "Characterization of the Co and/or Pb-SBA-15 mesoporous materials synthesized by two different methods", 6<sup>th</sup>EFCATS Summer School, "Catalysis and Surface Science for Renewables and Energy", Izmir-Turkey, September 2010, Poster Presentation.

**Summer Schools:**

1. 6<sup>th</sup> EFCATS Summer School, "Catalysis and Surface Science for Renewables and Energy", September 13-19, 2010, Izmir, Turkey.
  
2. "Solid State NMR and Recent Developments", 30 October-1 November, 2007, Middle East Technical University Central Laboratory, Ankara, Turkey.
  
3. First Anatolian School on Catalysis (ASC-I), September 25-October 6, 2006, Middle East Technical University, Ankara, Turkey, (Workshop I: Master class Catalysis. Workshop II: Computational Catalysis.)